# SEDIMENTOLOGICAL AND PETROPHYSICAL CHARACTERIZATION OF SARAH FORMATION WITH THE AID OF GIS, CENTRAL SAUDI ARABIA

BY

**WASEEM RAZZAQ**

A Thesis Presented to the

DEANSHIP OF GRADUATE STUDIES

**KING FAHD UNIVERSITY OF PETROLEUM & MINERALS**

DHAHRAN, SAUDI ARABIA

In Partial Fulfillment of the
Requirements for the Degree of

## MASTER OF SCIENCE

In

## GEOLOGY

**December, 2013**

KING FAHD UNIVERSITY OF PETROLEUM & MINERALS

DHAHRAN- 31261, SAUDI ARABIA

**DEANSHIP OF GRADUATE STUDIES**

This thesis, written by **Waseem Razzaq** under the direction of his thesis advisor and approved by his thesis committee, has been presented and accepted by the Dean of Graduate Studies, in partial fulfillment of the requirements for the degree of **MASTER OF SCIENCE IN GEOLOGY.**

Dr. Abdul-Aziz Al Shaibani
Department Chairman

Dr. Osman Abdullatif
(Advisor)

Dr. Salam A. Zummo
Dean of Graduate Studies

Dr. Ali Sahin
(Member)

9/3/14
Date

Dr. Mustafa Hariri
(Member)

© Waseem Razzaq

2013

*Dedicated to My Beloved Parents Brothers, Sisters*

*And*

*Martyrs of 2005 Earthquake (Pakistan)*

# Acknowledgements

"Al-Hamdu Lillahi Rabbil Aalameen" All praise and glory be to Almighty Allah (SWT) for his limitless blessings and guidance. May Allah bestow his peace on the Prophet (PBHUH).

I sincerely acknowledge the support and facilities provided by King Fahd University of Petroleum & Minerals, Dhahran, Saudi Arabia and special thanks to DSR (RCRG project-1114), for providing support and environment for research.

I would like to express my deepest appreciation to my thesis advisor Dr. Osman Abdullatif for his moral support and words of encouragement; he continually and persuasively conveyed a spirit of adventure in regard to research. I am thankful to Dr. Ali Sahin and Dr. Mustafa Hariri for their valuable contributions, guidance and sincere advice throughout my thesis research. In addition special thanks are due to Dr. Dogan, Dr. Babalola, and Dr. Hassan, for their guidance and support.

I would also like to express my deepest gratitude to the faculty members of Earth Sciences Department and special thanks to Chairman Dr. Abdul-Aziz Al Shaibani. I am deeply indebted to Mr. Azizullah Khan for the preparation of thin-sections and coring, Mr. Musa Ali for petrophysical studies, Mr. Mushabab Asiri for SEM-EDX micrographs studies and Mr. Shahul Hameed for logistics. Special are due to thanks to Mr. Luqman and Dr. Abbas (CENT-RI) for their help in XRD and CT-scan studies.

Above all, I would also like to thank my parents for their endless love and support, who although far away from me, always close to my thoughts and heart. I would also like to thank my sisters and brothers for their moral support and encouragement.

I would also like to express my sincere appreciation to ESD colleagues and special thanks to Assad and Mutasim for helping in the field part. I would like to acknowledge my friends Muhammad Osman, Waleed, Owais, Luqman, Umer, Nasir, Ali, Saad Khan, Hassan and Uneb.

# Table of Contents

# List of Figures

# List of Tables

# Thesis Abstract

**Name:** Waseem Razzaq

**Title:** Sedimentological and Petrophysical Characterization of Sarah Formation with the Aid of GIS, Central Saudi Arabia.

**Major:** Geology

**Date of Degree:** December 2013.

This research was conducted to characterize the sedimentological and petrophysical heterogeneity of the Late Ordovician Sarah Formation at proximal, medial and distal part of Al-Ilb paleochannel and to construct the GIS based smart map. The method of study includes sedimentological field and laboratory investigation; the field investigation is followed by facies analysis and construction of vertical and lateral profile while laboratory investigation is followed by thins-section petrography and SEM-EDX, CT-scan and XRD analysis.

The Sarah Formation of Late Ordovician age shows six lithofacies in dominantly glacio-fluvio and braided river environment. Massive gravels (Gm) facies are observed at different parts of channel and give indication of glacial retreat. The presence of fine to medium grained and sometimes coarse to very coarse grained trough cross bedded, planer and horizontal cross bedded sandstone facies is observed throughout the channel, the channel cutting, sandy bed from and lateral accretion are prominent in almost all the sections, so on the basis of mentioned architectural elements (sandy bedform, channels

and lateral accretion) the environment is interpreted as glacial outwash braided river deposits.

The Sarah Formation sandstone is moderately to poorly sorted and in some cases well sorted. The sandstone is classified as quartz arenites (98% pure quartz on QFL classification). In addition to quartz, very low percentage (1%) feldspar is observed in some samples. Iron oxide and clay mineral are dominantly present in the pores. Kaolinite and smectite is found in most samples. The petrophysical studies revealed very good quality of porosity present in all parts. On the other hand, the permeability values are high and ranging between 53mD to 5D. The descriptive statistics clearly indicate the normal distribution of porosity values for proximal, medial and distal part of paleochannel and log-normal distribution of permeability values. The scatter plots of porosity versus horizontal and vertical permeability show very poor correlation for each part of paleochannel and the main controlling factors are clays, iron oxide, grain size, pore size, pore volume and connection of pore throat. These observations further prove that Sarah Formation is severely affected by shallow burial conditions during diagenesis.

Master of Science Degree

King Fahd University of petroleum & Minerals

Dhahran, Saudi Arabia

December, 2013

# Thesis Abstract (Arabic)

## الرسالة ملخص

رزاق وسيم :الكامل الاسم

نظم بمساعدة الصارة لتكوين والبترولية الرسوبية الصفات دراسة :الرسالة عنوان
.السعودية العربية المملكة وسط، الجغرافية المعلومات

الجيولوجيا :التخصص

.م2013ديسمبر :العلمية الدرجة تاريخ

لتكوين البترولية الرسوبية في الموجود جاندس الت عدم لتوصيف البحث هذا أجري
الثلوج مجاري من والبعيد والمتوسط، القريب الجزء في (المتأخر الأوردفيسي) الصارة
التي البحثية المنهجية الجغرافية المعلومات نظم بإستخدام ذكية خريطة وبناء، القديمة
شملت؛ المعملية الإختبارات وبعض قل الحفي الرسوبية الدراسات من كل تشمل إتباعها تم
، والأفقية الرأسية المقاطع بناء مع الرسوبية السحنات دراسة على الحقلية الدراسات
(thin-section) الدقيقة لشرائح المجهرية الدراسات من كل على المعملية الإختبارات شملت بينما
، (SEM-EDX) السينية الأشعة يافأطشتيت – الإلكتروني بالمجهر والدراسات ،(petrography)
.(XRD) السينية الأشعة حيود وتحاليل ،(CT-scan) المقطعي والتصوير

بيئات رسوبية يات تمثل رسوبية سحنات ست ة (المتأخر الأوردفيسي) الصارة تكوين يظهر
تم (Gm) المصمت الحصى سحنة .المجدولة الأنهار بيئة رسوبيات إلى نهرية-جليدية
ذات السحنة وجود .الجليد إنحسار على مؤشرا وتعطي القناة من مختلفة أجزاء في تسجيلها

الـ تط بق ذات جدا الـ خ شـ نة إلـ ى الـ خ شـ نة الـ حـ بـ ي بات وأحـ ياند ا الـ مـ تو سطة إلـ ى الـ نـ اعمة الـ حـ بـ ي بات ف ي تـ سجـ يلها تـ م الأف قي، الـ مـ تـ قاطع الـ تط بق ذو الـ رملي والـ حجر والـ مـ سـ توي الـ حـ و ضي الـ مـ تـ قاطع وا ضحة تـ عـ تـ بر الـ جاند بي والـ تراكم من الـ رملـ ية ةق بطلاو، قـ اطعةال والـ قـ ناة، الـ قـ ناة أذ حاء جمـ يع تـ م الـ مذكورة الـ مـ عماريـ ة الـ عـ نا صر ضوء وعـ لى، والأف قـ ية الـ رأ سـ ية الـ مـ قاطع كل ف ي تـ قريـ با (braided river). مجدول نـ هر روا سب أذها عـ لى الـ تر سـ ي بـ ية الـ بـ ي ئة تـ فـ سـ ير

الـ حالات بـ عض وف ي زال فـ رديـ ئة إلـ ى مـ تو سطة روا سب عـ لى يـ حـ توي الـ رملي الـ صارة تـ كويـ ن الـ نـ قي الـ كوارتـ ز من ٪ 98 ) (Quartz Arenites) أريـ نايـ ت كوارتـ ز إلـ ى الـ رملي الـ حجريـ صـ نف .الـ فرز جـ يدة من ( ٪ 1 ) جدا مـ نخ فـ ضة نـ سـ بة لـ وحظت الـ كوارتـ ز، إلـ ى بـ الإ ضافـ ة .(QFL) لـ تـ صـ نـ يف وف قا .الـ مـ سامات ف ي بـ كـ ثرة موجودة الـ طـ ينـ ية والـ معادن الـ حديـ د أكا سـ يد .الـ عـ ينات بـ عض ف ي الـ فـ لـ سـ بار كـ شـ فت .الـ عـ ينات معظم ف ي (Smectite) والإ سمـ كـ تـ يت (Kaolinite) الـ كولـ نـ يت معدنـ ي عـ لى الـ عـ ثور تـ م منـ طقة أجزاء جمـ يع ف ي موجودة جدا جـ يدة نـ وعـ ية ذات مـ سامات عـ لى الـ بـ تروف يزيـ ائـ ية الـ درا سات . سيدار ملي 5و 53 ماب ين وتـ تراوح مرتـ فعة كاند ت الـ نـ فاذيـ ة قـ يم ف إن أخرى، نـ احـ ية من .الـ درا سة الـ قريـ ب الـ جزء ف ي الـ مـ سامـ ية لـ قـ يم الـ طـ بـ يعي الـ توزيـ ع إلـ ى بـ و ضوح تـ شـ ير و صـ ف ية إحـ صاءات لـ قـ يم طـ بـ يعي تـ وزيـ ع أيـ ضا و سجلت، الـ قديـ مة الـ ثلوج مجاري من والـ بـ عيد والـ مـ تو سط، الأف قـ ية الـ نـ فاذيـ ة مع الـ مـ سامـ ية لـ قـ يم الـ تـ شـ تت مخططات أظهرت .الـ لوغرثـ مـ ية الـ نـ فاذيـ ة الـ عوامل وكاند ت، الـ قديـ م الـ مجرى أجزاء من جزء لـ كل اجد ضـ عـ يـ فة عـ لاقـ ة أظهرت والـ رأ سـ ية حجم، الـ حـ بـ ي بات حجم، الـ حديـ د أكـ سـ يد، الـ طـ ينـ ية الـ معادن :تـ ضم ذلك ف ي الـ مـ تحكمة الـ رئـ يـ سـ ية الـ صارة تـ كويـ ن أن تـ ثـ بت الـ نـ تائـ ج هذه .الـ مـ سامات مـ سارات وإتـ صال، الـ مـ سامات حجم، الـ مـ سامات (diagenesis). الـ مـ تأخرة الـ نـ شأة مـ لـ ياتـ ع أثـ ناء الـ ضحل الـ دفـ ن بـ ظروف كـ بـ يرة بـ درجة تـ أثـ ر

الـ عـ لوم ف ي الـ ماجـ سـ تـ ير درجة

والـ معادن لـ لـ بـ تروليف هد الـ مـ لك جامعة

الـ سـ عوديـ ة الـ عربـ ية الـ مـ مـ لكة ـ الـ ظهران

2013 ديـ سمـ بر

# Chapter 1

# Introduction

## 1.1 Introduction

The Sarah Formation of the Late Ordovician age includes glacial and preglacial sediments and has been interpreted as paleovalley infill. The structure and paleo topography caused by glacial erosion during the era proves the time of glaciation. Sarah Formation is exposed in the central Saudi Arabia and varies in thickness from hundred to several hundred meters. The Paleozoic glacial deposits have several equivalent Formations in Saudi Arabia and as well as in south Turkey, Algeria, and Mauritania (Figure 6). The Arabian Plate suffer glaciation phenomenon in two different time span (Figure 1); one in the Ordovician time and second in the Carboniferous time (D.P. Le Heron et al., 2009). Sarah Formation is considered as one of the important targets for unconventional natural gas resources.

This research work is expected to contribute to understanding of the sedimentological characteristics and reservoir quality of Sarah Formation based on outcrop observation and laboratory studies at Central Saudi Arabia. Outcrop analog can be used to reconstruct geological model that can help in better understanding of the reservoir and forecast the subsurface.

Geographic in Formation system (GIS) is a tool that works in multiple layers and helps in describing, analyzing and storing the spatial data. This spatial data is stored in the form of

attribute table and then link geographically to assigned position. In this research, GIS is used to comprehend the correlation of different parameters like porosity and permeability of proximal medial and distal part of paleovalley and link tabular and geographical data into intelligent maps.

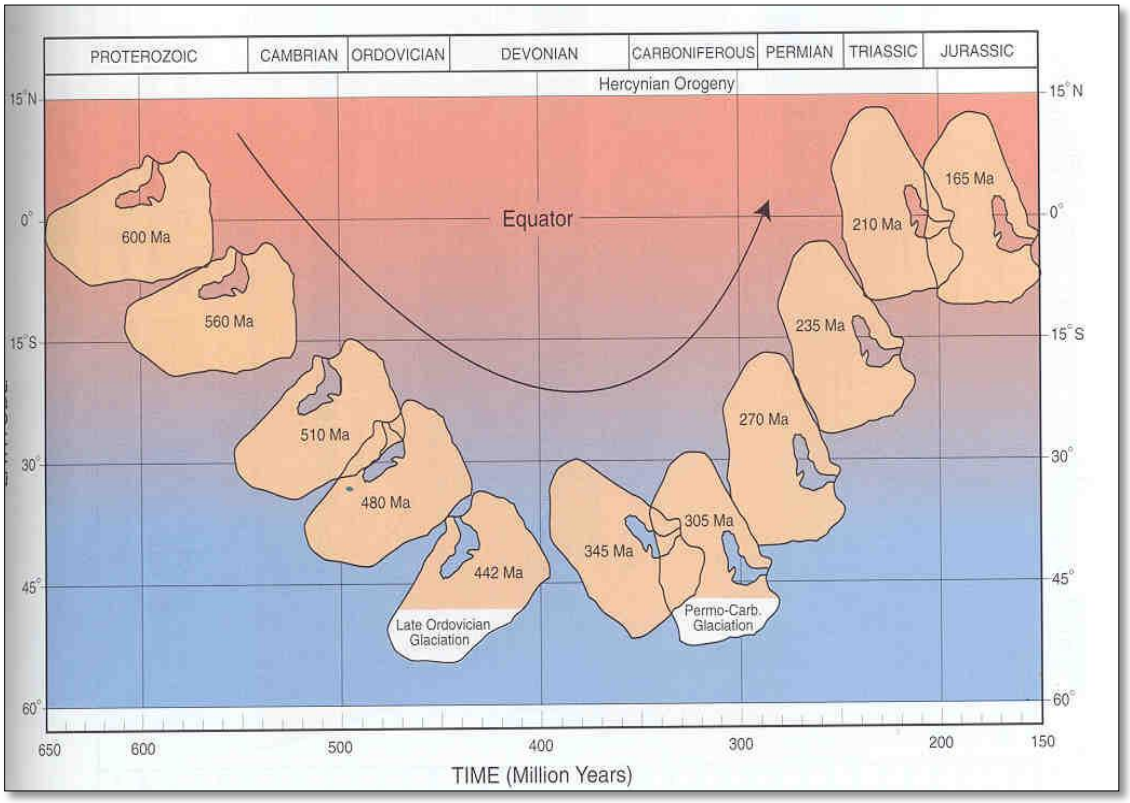


Figure 1: Position of Arabian Plate in Paleozoic and Early Mesozoic era (Konert et al., 2001)

## 1.2 Location of the Study Area

The study area lies in Hail province in central Saudi Arabia. The Sarah Formation crops out in central Saudi Arabia and is bounded by latitude 27º 00’ to 28 º 00’ North and 42 º 00’ to 43 º 30’ East (Figure 2). The Sarah Formation is considered as tight gas sandstone reservoir with mostly unexplored area of Paleozoic petroleum system (Millson et al., 1996, Schenk et al., 2000). The Sarah Formation is exposed in more than six main paleovalleys at Baqa area (Figure 3). The paleovalleys deeply incised into Saq Sandstone, Qasim Formation, and Zarqa Formation (Figure 7). The estimated thickness of Sarah Formation is about 150 m to 200 (?) m (Figure 7). The facies in outcrop vary from reddish heterogeneous medium grained sandstone with low angle trough cross bedding, ripple marks, laterally and vertically stacked fining upward fluvial and glacio-fluvial sandstone packages (Figure 7 and Figure 6). At Al Ilb (Hail) paleovalley tillite is persevered at the base of Sarah Formation with very heterogeneous lithology and clasts of Shield and cover rocks. As a result, the Sarah Formation is considered to be very heterogeneous Formation. The depositional and diagenetic controls affect the porosity and permeability patterns. The parameters that controlling porosity and permeability of Sarah Formation includes grain size, sorting, cement, and matrix pore size distribution and their connectivity.

## 1.3 Scope and Objective of the Study

The objective of the study is to investigate sedimentological characteristics and reservoir heterogeneity of glacio-fluvial deposits of Sarah Formation. This can enhance understanding and Prediction of reservoir rock property in the subsurface.


Figure 2: Location map of the study area; Central Saudi Arabia

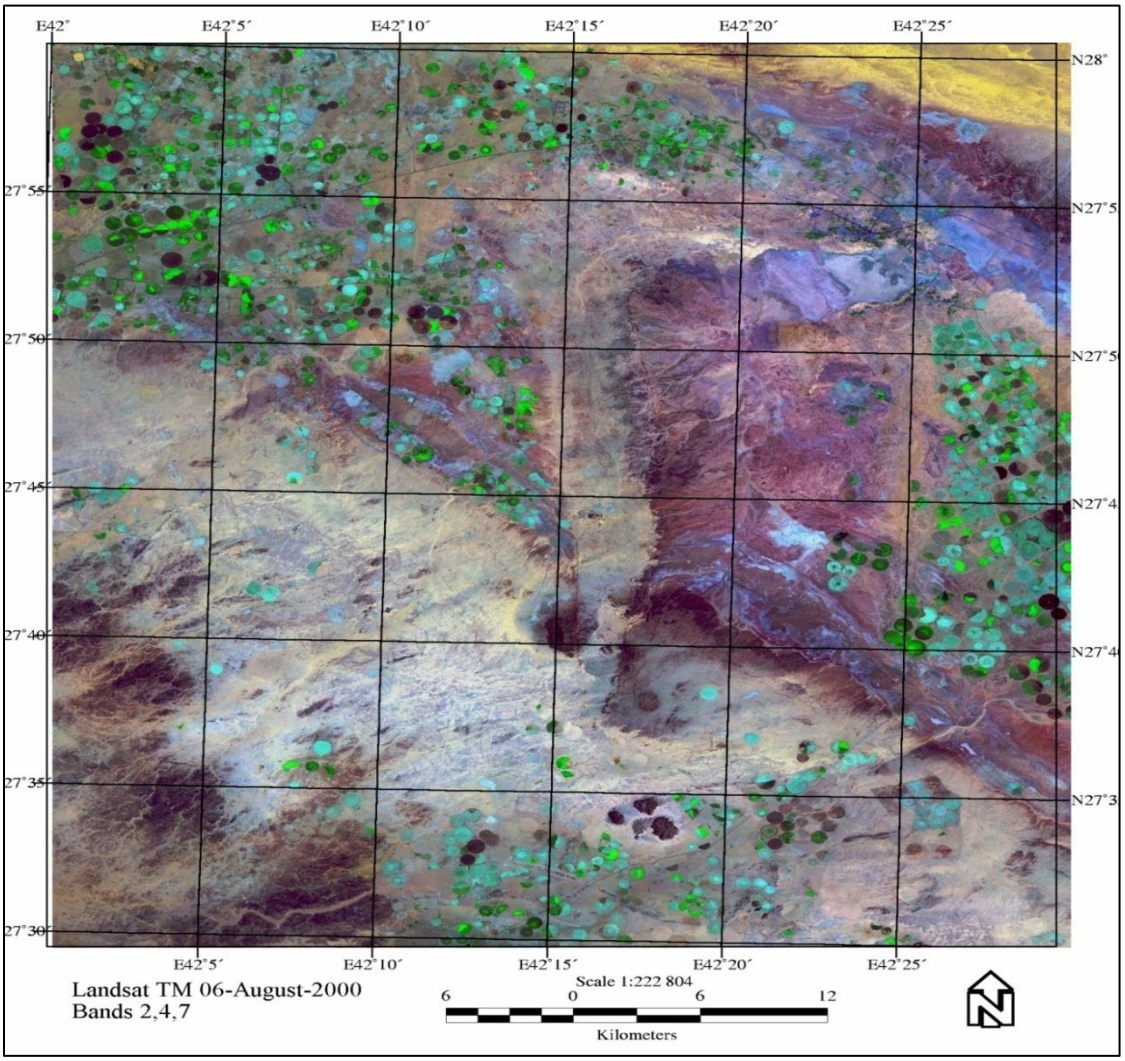


Figure 3: Landsat image of study area, Al Ilb Paleochannel

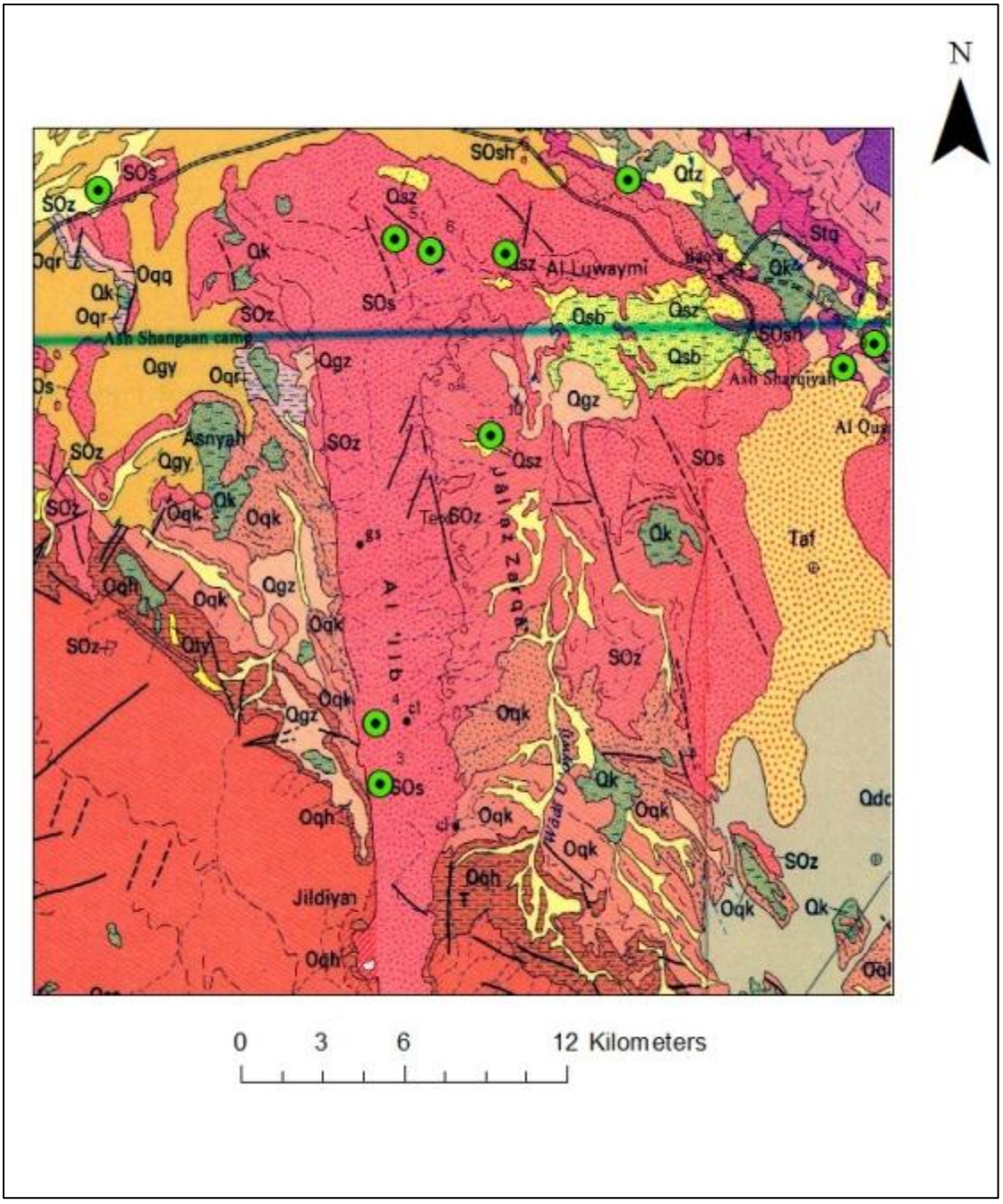


Figure 4: Geologic Map of the Baqa Quadrangle, Sheet 27 F, Kingdom of Saudi Arabia (Modified after Vaslet et al., 1987)

This study integrates the field and laboratory works.

The core objectives of the present study are as follow:

- Characterize the facies type, architectural element and the paleoenviroment
- Determine sedimentological characteristics and heterogeneity
- Investigate the porosity and permeability distribution
- Reconstructs the GIS based smart maps for glacio-fluvial Sarah Formation

## 1.4 Problem Statement

The study reveals the heterogeneity and complex architecture of facies distribution within the Sarah Formation. The facies show heterogeneous nature both in horizontal and vertical direction on outcrop scale. Along with the reservoir heterogeneity, the limited information from subsurface encourages outcrops study. Moreover, the outcrops provides different scale of heterogeneity (micro-macro) and outcrop studies help in understanding the spatial distribution of facies in term of dimensions size and orientation (Abdullatif and Makkawi 2004, 2010). High resolution outcrop model that forecast the distribution of facies is always essential in reservoir characterization. Sarah Formation is considered as unconventional tight gas reservoir in the subsurface (Al-Mahmoud and Al-Ghamdi, 2010). Briner et al., 2010 study indicates the complexity in term of paleoenviroment and

paleogeographic settings of glacial outwash deposits (Sarah Formation) make subsurface exploration difficult. More precise studies are required at different scales to generate a proxy for subsurface distribution. Although the Sarah Formation have good reservoir quality zones, but patchy geographical distribution and sedimentological heterogeneity make them challenging. Therefore, this study is devoted to understand the heterogeneity of Sarah Formation.

## 1.5 Previous Work

In 1978, McClure was the first scientist who identified and proved evidences of Late Ordovician glaciation in Saudi Arabia. The ice sheet covered the major part of Africa, eastern part of South America and most part of Arabia. The Late Ordovician glaciation resulted in glacially formed unconformities and glacio- marine and glacio-fluvial and glacial deposits that was influxes into deeply incised paleovalleys (Senalp and Al-Laboun 2000). The paleovalleys mapping were carried by Vaslet (1987, 1989, and 1990). Senalp and Al-Laboun (2000) conducted field trips to study the detailed sedimentological significance of Late Ordovician Zarqa and Sarah Formation in Qasim and Hail regions of Saudi Arabia. Besides sedimentological studies, Moscariello and others (2009) studied the paleogeography of Sarah Formation mainly based on well data and outcrop observations. Sarah Formation is important reservoir target in north western and Rub' Al-Khali Basin of Saudi Arabia (Vaslet, 2009; McGillivray and Hussein, 1992, Zhang et al., 2009). It is characterized by low porosity, very low permeability and moderately over pressurized nature (Abdullatif, 2011). Dabagh, 2013 work on Paleozoic succession of

Saudi Arabia, specifically focusing on provenance and tectonic growth of Arabian plat and there effect on Sarah Formation at northern and southern block. Recent work on petrophysical parameters of Sarah formation has been done by Al-Zayer et al., in 2013, this research concludes the high degree of horizontal and vertical heterogeneity of Sarah Formation is present with some sweet spot zones.

# Chapter 2

# Literature Review

## 2.1 Introduction

The Arabian and North African plates were subjected to glaciation and deglaciation phenomenon in Cryogenian and Hirnantian time period and in Carboniferous and Permian (Le Heron at al. 2009). The ice sheets extended from eastern part of North Africa (Figure 6), and spread over to Saudi Arabia (Vaslet 1990; Ghienne (2003); and Le Heron et al., 2004). The evidence of this glaciation is widespread in the rocks strata and easily identified in the fields. The identification criteria is the presence of soft sediment deformation structure, having soft sediment folds, meso to micro scale faults, striated pavements and Formation of other erosional surfaces (Danial et al., 2010). The ancient deposits of several ages across the region show some similarities and differences. Specifically talking about the Hirnantian age deposits, the glacially related deposits have significantly producing reservoir quality across North Africa and Middle East (Figure 8). Hamra and Illizi basins of Algeria and North and central Marzuq basins of Libya have 50 fields, some of which are classified as giant fields (Hallett, 2004). In Morocco, the Hirnantian ice sheets expanded northward and moved toward south and central part of Morocco and covered the entire region (Figure 6). The Late Ordovician deposits are exposed along 800 km long belt and outcropping in the Anti-Atlas mountain of south Morocco. These deposits differ from others in case of sediment deformation and

thickness. The thickness reflects the bathymetric break that baffle the continued northward advance of the ice masses (Le Heron et al. 2007).

The Proterozoic rocks are exposed along the north-eastern belt of Arabian basement. The Sarah Formation in Saudi Arabia was named by (McClure 1978). Pocock and Kopp (1949) depicted a clear unconformity between Ordovician Ra'an Shale of Qasim Formation and Silurian Qusaiba Shale in central Saudi Arabia. Pocock and Kopp (1949) define the Sarah Formation as light tan to brown, lenticular, cross-bedded sandstone and are slightly conglomeratic. They also observed that the Sarah Formation is distributed widely and scattered. They also measured and described this unit at Jabel Jildia in the Hail Quadrangle as well in Jabel Sarah in the Saq quadrangle. They also come up with the conclusion that the areal distribution of the aforementioned units indicate that the sandstone were deposited in paleovalleys which are almost identical to the Al-Ilb and the Sarah pale valleys. Bramkamp and others (1963) map the Wadi Ar-Rimah Quadrangle, recognized a similar unconformity within the Tabuk Formation (now Qasim Formation, which is brown to tan sandstone unit in the khanasir Sarah, Khashm Ar-Ran'an and Al-Ilb area). They mention that this sandstone unit is transgressive over the lower and middle parts of the Tabuk Formation. Bigot (1970) reported 1 m thick heterogeneous horizon containing igneous and metamorphic pebbles and boulders overlaying the Ra'an Shale Member at both Ri Al-Fuhah and Bir Himas outcrops. The convincing evidence about Late Ordovician glaciation in the central Saudi Arabia was given by McClure (1978). McClure's work clearly shows that the glacial striated grooved rounded, faceted

polished sandstone and granite boulders and tillite were deposited in the Paleozoic outcrops. McClure (1978) put the unconformity between tillite beds and the Sarah Formation. Jal Al Saqiyah is the only location where the glacial boulders and tillites were found (Senalp 2000). He also mentions in his paper about the McClure (1978) publication that it did not give any information about paleontological and lithological data to make precise correlation. Young (1981) also describe the similar tillite accumulations from the outcrops in the central Saudi Arabia and give support to the idea of Late Ordovician glaciation as documented by McClure (1978). Clark-Lowes (1980) performed sedimentological study at Khanasir Sarah (Sarah ridge) near Al-Quwarah in the Qasim region. He suggested that diamictites, sandstone, conglomerates, conglomeratic sandstone and shale horizons are unconformably onlap the lower and middle parts of Qasim Formation and he named it as Sarah Member. They also consider Sarah Member as paleovalley filled by fluvial and mudflow deposits. Al-Laboun (1982, 1986) agreed on McClure's (1978) glacial interpretation, with the elaboration on distribution of boulder beds both horizontally and vertically. Lithostratigraphic succession of Early Paleozoic rocks was revised by Vaslet and others, (1987). The Zarqa Formation is at the bottom and Sarah Formation is at the top and consists of mainly fine to coarse grained cross-bedded sandstone and at several localities, tillites preserved at the base of paleovalleys (Figure 6). The French geologists prepared the valley model which is then used by Vaslet (1987, 1989, and 1990) to map the Sarah paleovalleys.

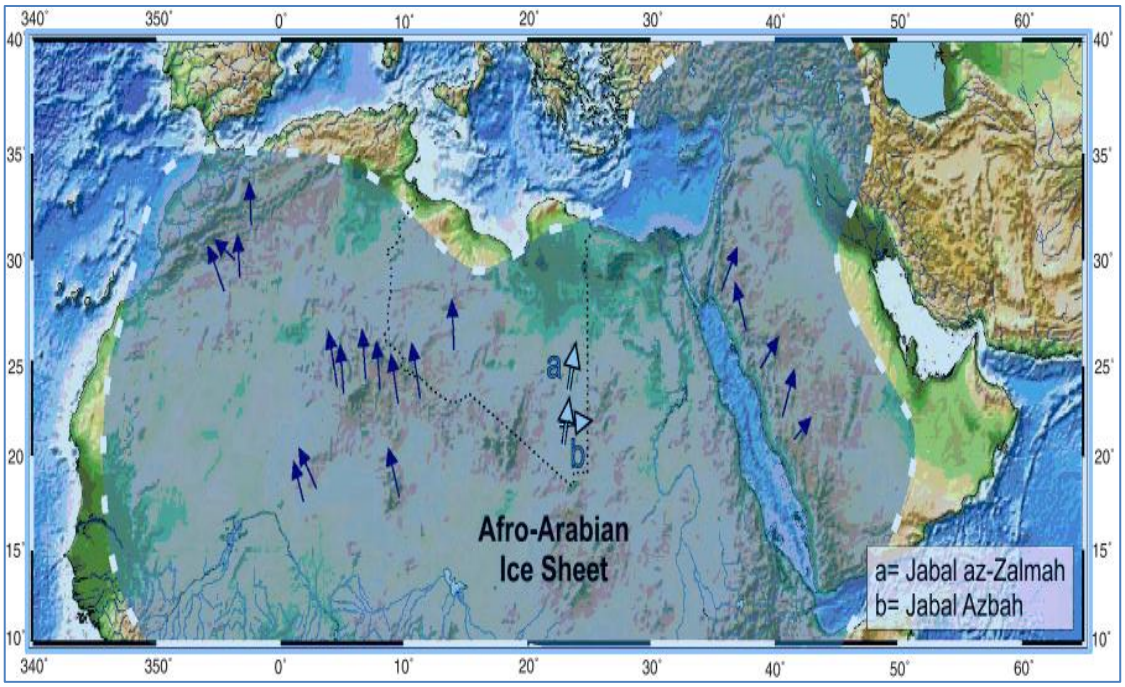


Figure 5: Late Ordovician ice sheets configuration in Saudi Arabia and North and West Africa. The arrows are indicating paleo ice flow direction (Le Heron et al. 2007).

Geographically, the paleovalleys are located along the early Paleozoic belt that onlap against the margin of Arabian Shield in (Figure 7). These paleovalleys are narrow near the starting point and become wider downstream, trending northward or northeastward. McGillivery and Husseini (1992) also agree with Vaslet (1987, 1989, and 1990) on the presence of deep incised glacial paleovalleys in outcrops that extend eastward into the deep basins. Al-Hajri (1995) documented Sarah Formation as Middle Ashgill age and stressed on the fluvio-marine character of this Formation. Al-Hajri (1995), omit Zarqa Formation from his proposed Paleozoic stratigraphic column because he did not find any correlation between field or subsurface. Senalp (2000) conducted several field trips to

study Sarah and Zarqa Formations to identify clear evidence of glaciation. These findings support the previous field work of Vaslet (1987, 1989, and 1990) and some other geologists. Senalp (2000) comes up with new findings that include: a) the glacial pavements in Al-Qara (Buraydah), Al-Luwayami and Jal Az-Zarqa (Baqa), Al-Bukayriyah and Al-Ilb paleovalleys were due to grounded ice-sheets. b) The ice movement on soft sediment resulted in deep grooves, continuous striations, chatter marks and solifluction structure. c) The northward movement of ice is indicated by overturned drag folds. d) Big polished granitic dropstone were found in the mudstone and wave rippled sandstone sequence of glacio-marine and glacio-lacustrine sedimentation. But these type of soft sedimentation deformation structures are missing in Al-Ilb paleovalley excepts centimeter size pebbles (diamictites) is present in one of the outcrop section of proposed study. Clark-Lowes (2005) interpreted the major glacioeustatic sea-level changes during Late Ordovician time. The sea-level fluctuations were not restricted to the Saudi Arabia, but extended up to Algeria and Libya and resulted in incised paleovalleys that are filled by glacial sediments. Clark-Lowes (2005) recommends changing the name of the new member of Tabuk Formation as Sarah Member. Senalp (2006) worked on some paleovalleys and interpreted as fluvial, estuarine and tide dominated lithofacies association consisting of fine to medium grains, trough and planar cross-bedded sandstone, with the thickness of about 70m.

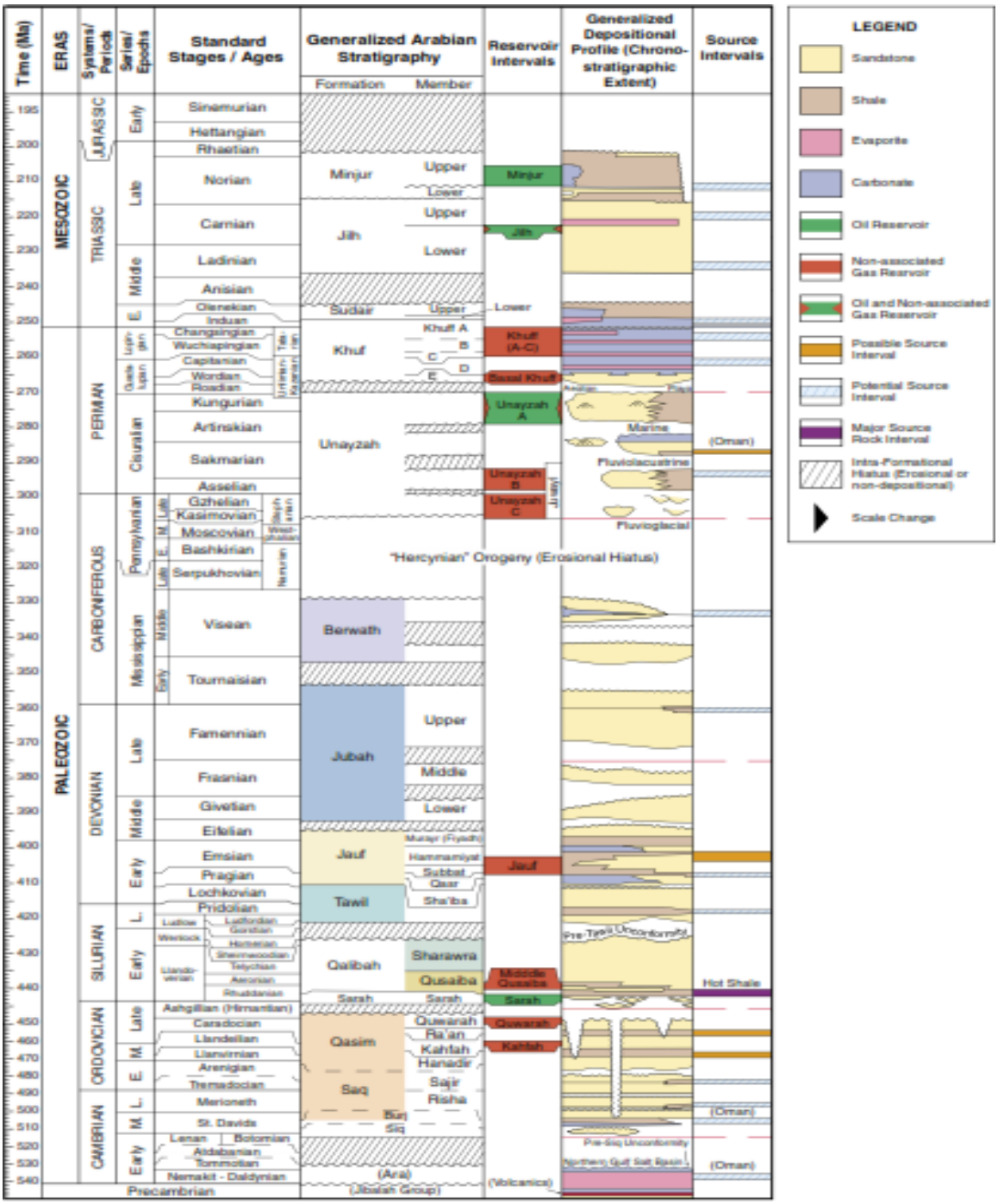


Figure 6: Paleozoic system of Saudi Arabia (Modified after Haq and Al Qahtani, 2005)

Al-Harbi and others (2011) conducted the research on petrographical and geochemical study on paleovalleys fill sediment provenance and their tectonic setting. He classified the Sarah sandstone as quartz arenites (i.e. 99% on average). The provenance study has led to the conclusion that the resultant mature sandstone belongs to the Arabian Basement rocks.

## 2.2 Geological Setting

Paleozoic sedimentary deposits outcrop in the Arabian Peninsula along the northeastern margin of Proterozoic Basement (Figure 7). The Paleozoic rocks are also exposed in southern part of Jordan, north and south of Saudi Arabia, and northern part of Yemen. Sandstone and Quaternary alkali-olivine basalt of the Harrat. The basal surface of Sarah Formation is rugged and consists of medium grains that are gritty and pebbly (Al-Harbi, 2011).

## 2.3 Stratigraphy of Sarah Formation

The Arabian Peninsula was the part of Gondwana during early Proterozoic times and laid at low to high latitude in the Southern hemisphere. The Arabian Peninsula's sedimentary record shows four distinct glacial events (Bell and Spaak 2006). Vaslet (1990) characterizes the glacier into phases i.e. Advance and Retreat. During the retreat time the glacier melt and outwash sediments led to the deposition of Sarah Formation. The lithological and geomorphological units of Sarah Formation show some distinction.

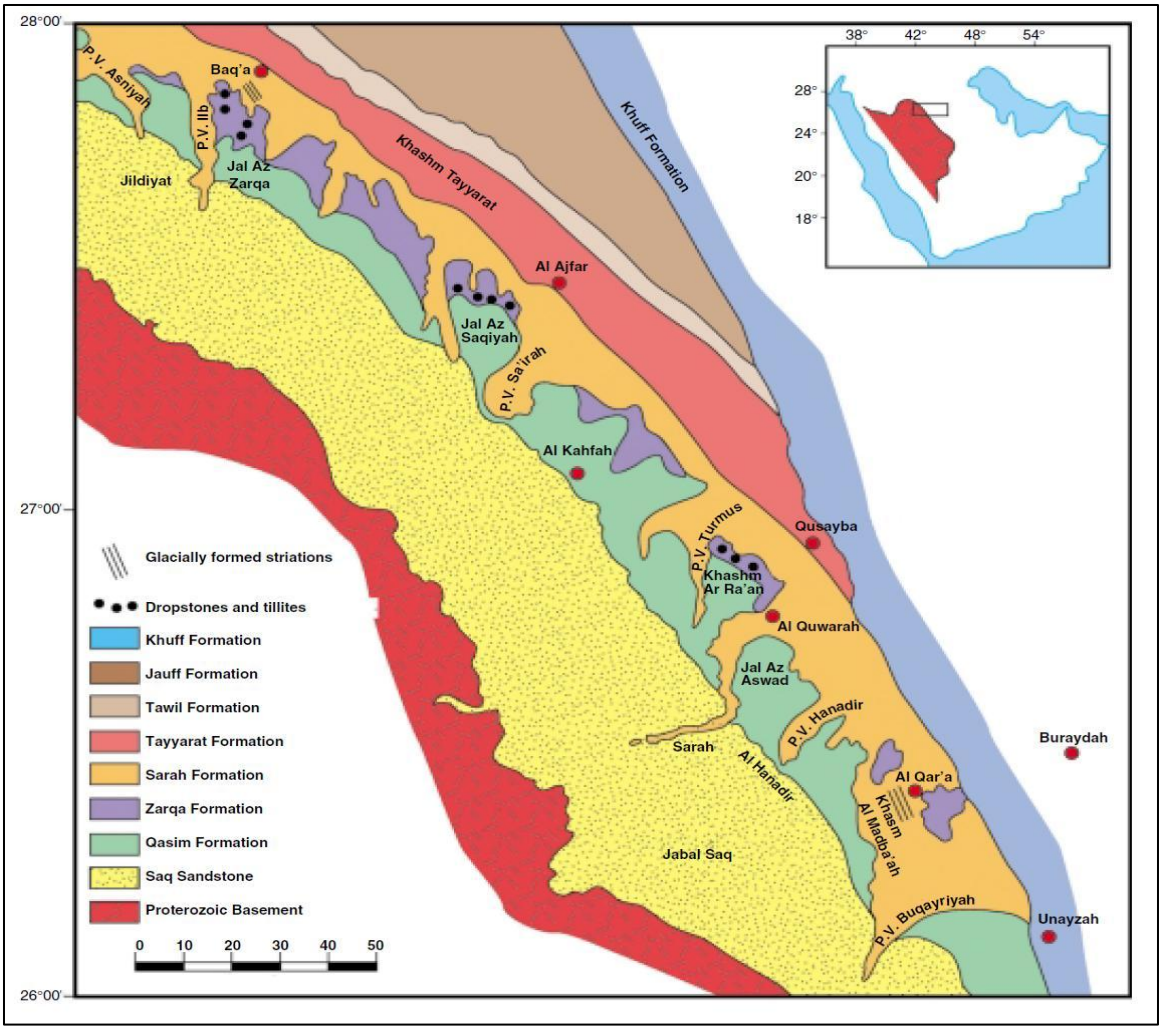


Figure 7: The distribution of Sarah Formation's Paleovalleys in Al- Qasim area, Saudi Arabia (Senalp and Al-Laboun, 2000)

The Sarah ridge sandstone is more resistant as compared to other sandstone deposits of Late Ordovician. The clastics of Middle Cambrian to Devonian age are most complete in the northern part of Saudi Arabia. The Proterozoic rocks are overlapped by Cambro-Ordovician Saq

The Sarah Formation was considered as fluvial and marine sediments as glacial paleovalleys by (Al Sharhan and Nairn 1997). The complication of the facies distribution, environment and paleogeography of the Formation in the subsurface makes the prediction of the reservoir quality difficult (Al-Mahmoud and Al- Ghamdi, 2010; Briner et al., 2010).

The following work flow has been designed by Aguilera et al. in (2008) to understand the reservoir quality. The outcrop analysis is the very first step and if it is proved as good quality, then reservoir models is prepared. The reservoir model contains structural, stratigraphical, petrophysical and sedimentological analysis. The outcrop models are usually used as proxy for subsurface reservoir distribution. The geological model increases the understanding of the reservoir heterogeneity and gives the foundation for creating rest of the reservoir model leading to simulation models. Moreover, the outcrop models provide valuable insight into understanding of the boundaries and internal facies distribution of high frequency cycle. The outcrop analog provide 2-D and 3-D views of facies with better details of diagenetic overprint then is found in the surface (Borer and Harris, 1991; Tyler and Finley 1991; Willis and White, 2000; Willis and Gabel, 2001). Porosity and permeability are modeled by using geostatistical methods (Aguilera et al. 2008).

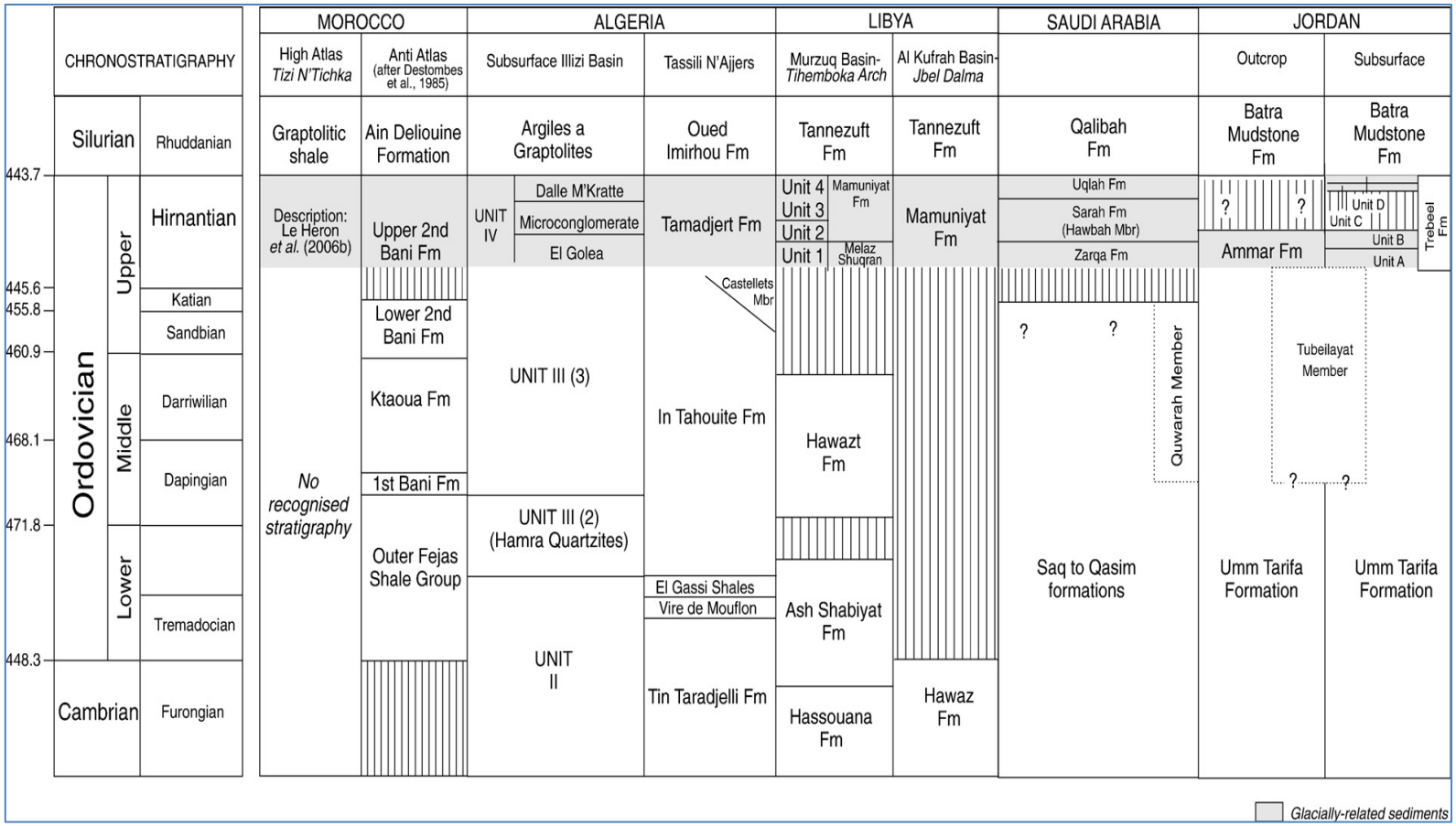


Figure 8: The Chronostratigraphy of Late Ordovician glacial deposits across North Africa and Middle East (after Le Heron et al., 2008)

The most crucial parameter is permeability because of having control on fluid flow and production capability. To determine smaller scale variability of permeability variograms, detailed equally spaced measurements can be made at selected outcrops (Sahin and Hassan 1998). The statistical distribution of porosity and permeability are linked with texture, mineralogy, depositional facies burial depth and post depositional processes (Weibel et al. 2012).

# Chapter 3

# Methods of Investigation

## 3.1 Introduction

The core objectives of the study are categorized into three main folds. These are geological field investigations, sedimentological and petro-physical studies, and reconstruction of outcrop analog. This chapter is mainly based on field investigation and laboratory analysis. In order to perform geological field study of Sarah Formation, Al-Ilb paleochannel in Hail area was selected. A summary of each investigation is explained in the following flow chart (Figure 9).

## 3.2 Field work

Ten outcrops of Sarah Formation were studied at different localities at Al-Ilb paleovalley (Figure 4). The dimension of Al-Ilb paleochannel is approximately 30 x 3 km. The outcrops of the Al-Ilb paleovalley were selected after detailed field survey. The field investigations include lithologic description obtained by measuring vertical and lateral profiles. Facies were identified based on texture grain size and sedimentary structures. The architectural elements were noticed on the outcrop. A total of one hundred and five (105) samples were collected from 10 outcrops. These samples were used for detailed petrographic and petrophysical analysis, as representative of each bed.

## 3.3 Laboratory Analysis

The laboratory investigations included: petrophysical measurements and sedimentological analysis. The former included porosity and permeability measurements and the later the petrography (thin-section) studies, SEM, XRD and CT-scan analysis. 226 core plugs were cut from 105 samples for porosity and permeability and 27 were chosen for detailed petrographical study. Among these 10 samples were analyzed using SEM. XRD, and CT scanning techniques.

### 3.3.1 Petrophysical Measurements

One hundred and five (105) samples were cored horizontally and vertically to prepare 226 plugs. For each sample porosity and permeability measurement were conducted. The samples were analyzed using Gas expansion and saturation method for porosity calculation. Gas permeability method is used for calculating permeability of the samples. Both the equipment require well defined core plug in term of length and diameter. The weight of the core plug is measured. All the aforementioned information is uploaded to the system to calculate the grain volume, pore volume and bulk volume. The result of this calculation makes possible the grain density calculation leading to percentage porosity measurement.

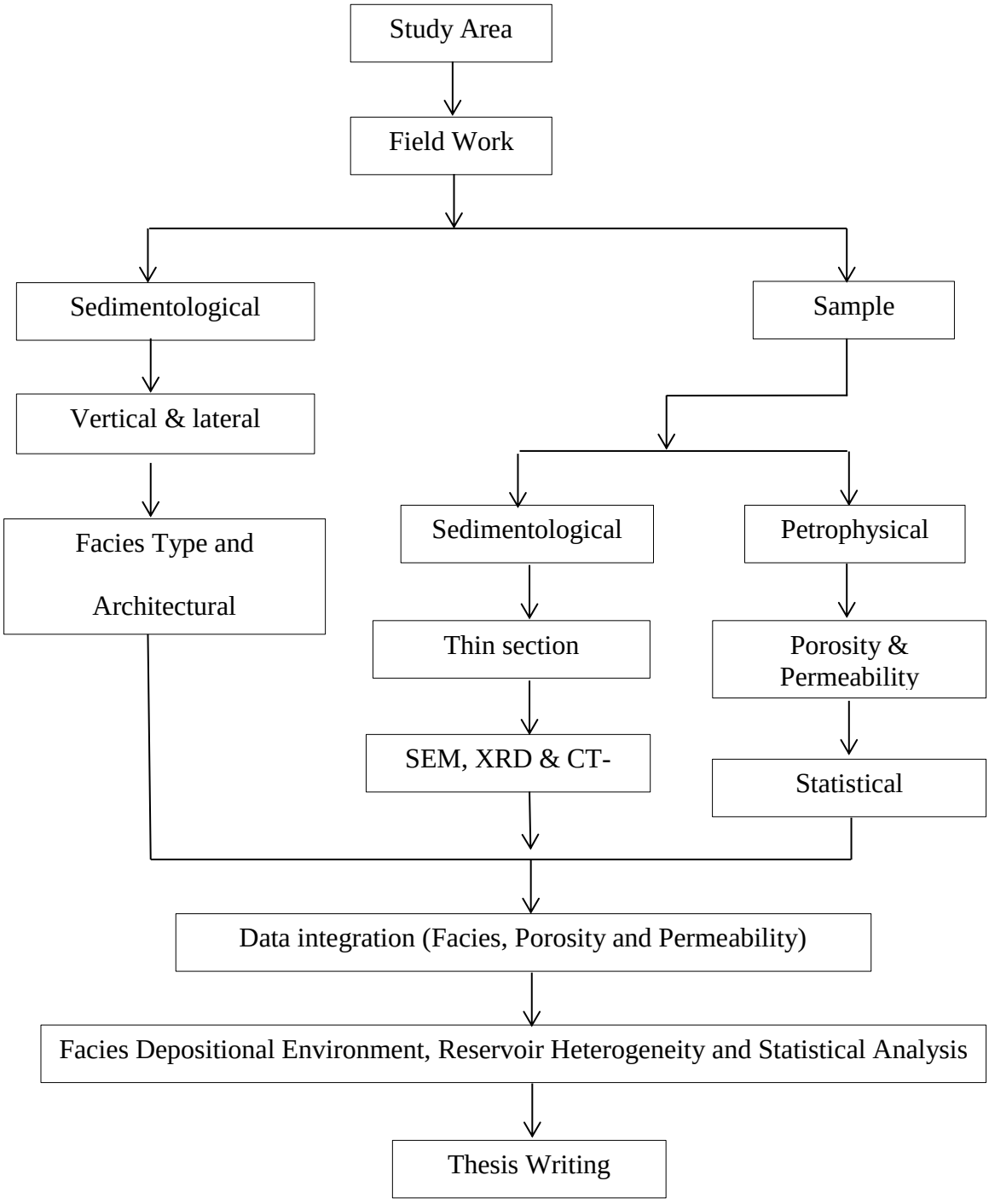


Figure 9: Flow chart showing the research procedure

### 3.3.2 Thin-section Petrography

Thin-section petrographic analyses were conducted for twenty seven (27) samples. The selected (27) sample for petrographical analysis were impregnated with blue epoxy pressurized incubator. After the impregnation, the sample is left over night for curing. Then the sample is glued to glass slides using Canada Balsam and kept under pressure to stick to the glass appropriately. The rock piece is cut from slides leaving the thin layer on the glass. Silicon carbide is used for grinding the glass mounted slab consequently to get polished and smooth surface. The thin-section is then analyzed visually by point count method under plain-polarized microscope (Solomon and Green 1966; Scholle 1979 and Krumbein and Pettijhon 1961).

### 3.3.3 X-Ray Diffraction (XRD)

Selected (10) samples from different parts of paleochannel are analyzed using XRD. Basically, X-Ray diffraction is a useful tool for mineralogical analysis; it works on a simple principal that the bombardment from X-Ray source (Copper) on specimen (sandstone) is diffracted at an angle Carroll and Dorothy 1970). This diffraction is then collected by detector as 2-theta. To get optimum result, solid rock sample was placed on smear mount which is then inserted into diffractometer. Then, from the distance of 10 mm X-Ray source was bombarded with a focal beam width of 1mm and power of 200 waat/$mm^2$. For better results, sample is kept at theta while detector is at angle of 2-theta with respect to the incident beam. The Scintag Inc. (Rigaku Miniflex) has been used for the analysis. The experimental procedure requires that the specimens is subjected to X-

Ray source at 40kv of accelerating voltage and 40 mA beam current using a divergent slit of1 degree, scatter slit of 1 degree and 0.2 mm nickel filter. The scanning speed and interval for data collection was 0.01 degree at 2 theta per second. The scanning angle of 10 degree to 70 degree has been selected (Hardy and Tucker, 1988).

### 3.3.4 Scanning Electron Microscopy (SEM) and EDS

The SEM gives a detailed high resolution qualitative analysis and helps in better understanding of the micro structure. The SEM is usually performed on the fresh surface of the sample that gives the real images. Some of the structures may be destroyed during thin-section preparation, and it may be not clear by plain polarized microscope. But SEM gives microscopic results of clays cementation, voids patterns, grain boundaries, elemental composition and pore structure. The elemental composition is analyzed using EDS.

Ten (10) samples were selected for SEM-EDS analysis. Joel JSM 5800 LV SEM was used to analyze microstructure. The sample of broken rock pieces were placed on the platinum core holder, held with carbon paint. The samples are coated with gold alloy to make it good electrical conductor (Goldstein and Yakowitz 1975)

### 3.3.5 Computed Tomography Scanning (CT scan)

The 3-D image of the object is obtained by applying the high resolution X-Ray CT (computed tomography) technique. This technique is non-destructive, and digitally cut the specimen into number of slices, the slices are then combined to get the complete

scanned images. The CT scanned images show very clear internal feature and helps in understanding of the pore pattern. The CT scan works on the simple principal; the high source of X-Ray from source is bombarded on sample to get the high resolution images. Two phenomena usually take place, either the X-Ray scatter or absorbed by the sample. The attenuation of energy takes place (during absorption) which is the function of density and atomic number of the material (Zatz, 1981).

# Chapter 4

# Field Lithofacies Analysis

## 4.1 Introduction

This chapter covers the field sedimentological description based on lithofacies. To conduct research, Al-Ilb paleochannel were selected (Figure 11). The Sarah Formation is well exposed in Al-Ilb paleochannel (Figure 3). Ten outcrop sections of Sarah Formation were examined laterally and vertically from top to bottom. The facies were described laterally and horizontally. The architectural elements were also identified and determined in all the outcrops.

The proximal, medial, and distal part of Al-Ilb paleochannel are represented by ten outcrops. The distribution of the outcrops is given in the (Figure 11) and the coordinates are listed in Table 1. These outcrops were selected on the basis of field observations and literature review. Each outcrop of the paleochannel was carefully studied with respect to sedimentological parameters along vertical and lateral direction from base to top. The facies description of each outcrop includes grain size classification, color identification, sorting, thickness of each unit, contact and sedimentary structures. Each section was measured from bottom to top and photographs were taken for lateral mosaics. Detailed samplings were performed at each outcrop; samples representing each lithofacies were used for further studies.

Table 1: Coordinates of the studied Sarah Formation outcrops at Al-Ilb paleochannel (Baqa, Hail area).

| Section No. | Northing | Easting |
|---|---|---|
| **S1** | N 27º 55.00' | E 042º 10.00' |
| **S2** | N 27º 55.207' | E 042º 20.537' |
| **S3** | N 27º 43.221' | E 042º 15.610' |
| **S4** | N 27º 44.713' | E 042º 15.530' |
| **S5** | N 27º 54.043' | E 042º 15.895' |
| **S6** | N 27º 53.804' | E 042º 116.613' |
| **S7** | N 27º 53.804' | E 042º 116.613' |
| **S8** | N 27º 51.945' | E 042º 25.433' |
| **S9** | N 27º 51.477' | E 042º 24.829' |
| **S10** | N 27º 5.141' | E 042º 17.818' |

## 4.2. Lithofacies Description

The outcrop of Sarah Formation representing proximal, medial and distal part of paleochannel were studied carefully along lateral and vertical profile and facies were described and interpreted to determine the depositional environment. Lateral and vertical

profiles of each outcrop are carefully prepared in the field. They help to understand the lithofacies association leading to towards the interpretation of depositional environment. Field observations were recorded made by using the geology of fluvial deposits facies codes (Mail 1995). The lithofacies description was based on primary depositional attribute, mainly grain size, color, texture, sedimentary structure and bedding plane. Major lithofacies that have been identified within proximal, medial and distal part of Al-Ilb paleochannel are described as follows.

### 4.3 Proximal Part of Paleochannel

The proximal part of the Al-Ilb paleochannel contains two stratigraphic profiles (S3), and S4) as illustrated in Figure 13. The S3 is 4.75m high and consisted of 4 units. The lower unit (1m from the base) is medium grained light brown planar cross bedded sandstone. The second unit is 2.5m thick trough cross bedded sandstone and laterally changes to planar cross bedding with scouring surfaces. The third unit is 0.5m thick, coarse grained trough cross bedded sandstone with scouring at the base. The S3 ends up with 2.5m thick unit of medium to coarse grain trough cross bedded sandstone, the coarser grains are recorded at the bottom and finer at top. In general the S1 starts with planar cross bedding and vertically shift to trough cross bedding with a grain size ranging from medium to coarse with consistent color (light brown) (Figure 13).

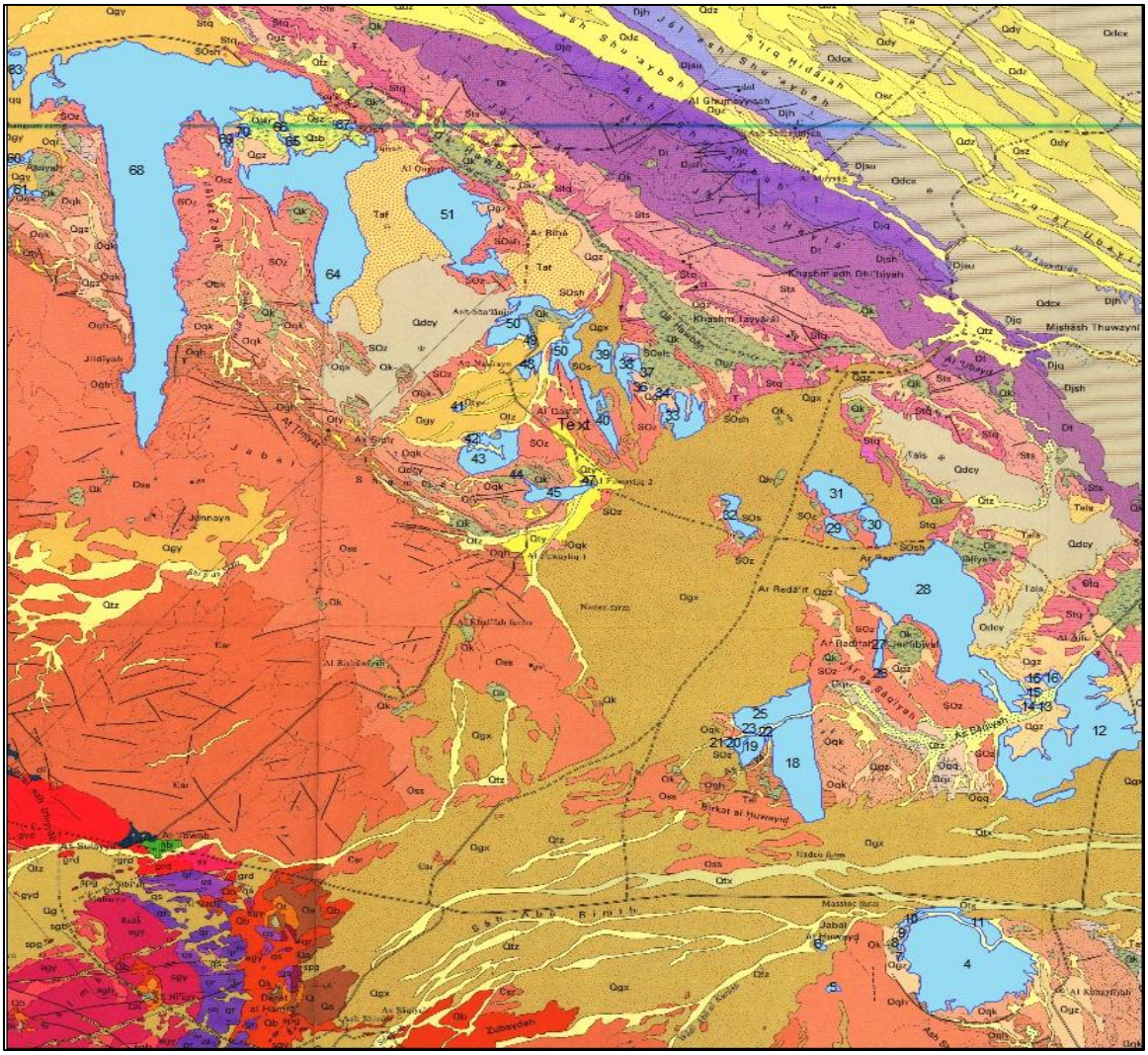

Figure 10: Distribution of Late Ordovician Sarah Formation in Baqa Quadrangle, Sheet 27, Kingdom of Saudi Arabia (Vaslet et al, 1987).

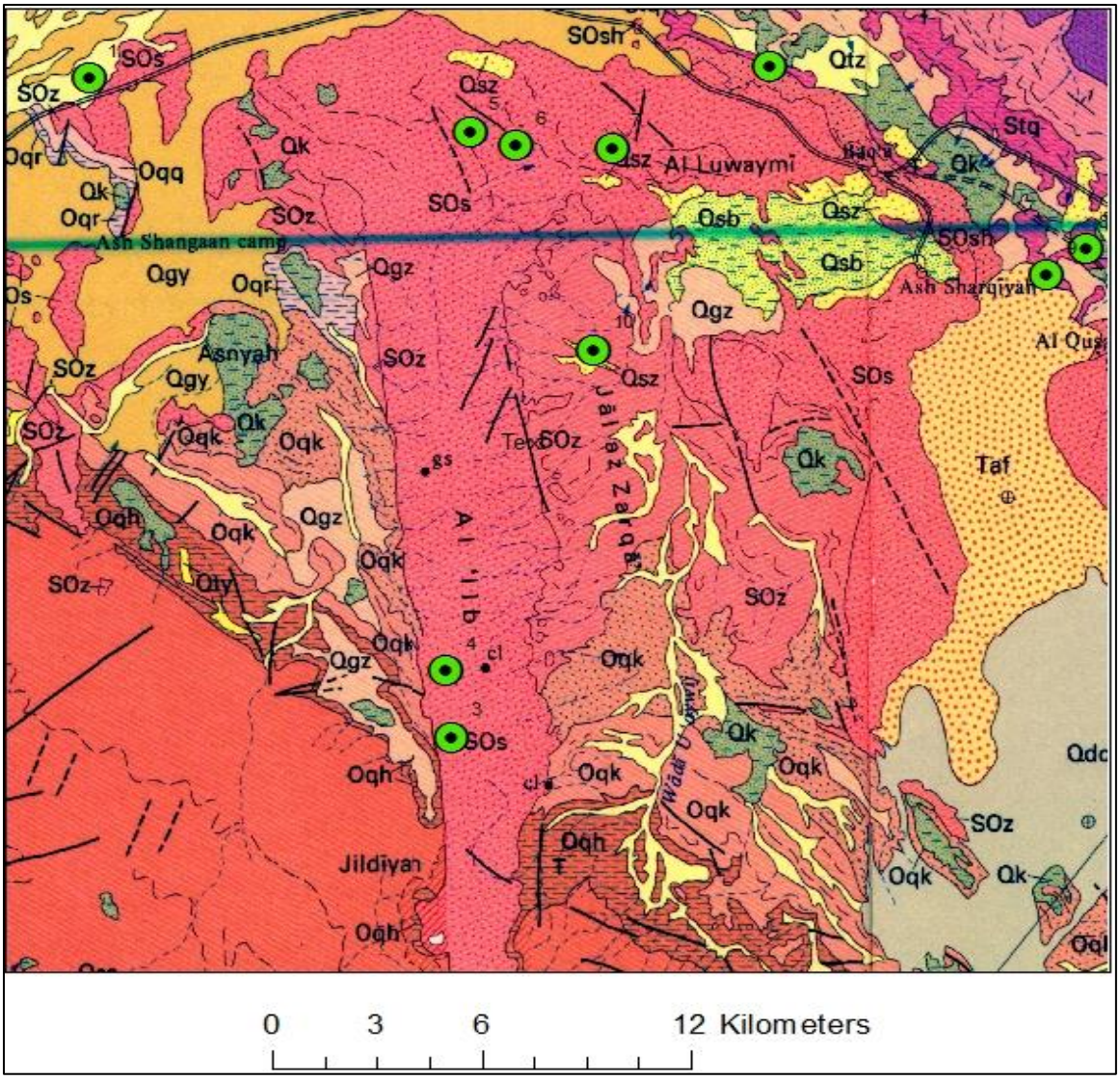


Figure 11: Map showing the distribution of outcrops in the Al-Ilb paleochannel, Baqa Quadrangle (Vaslet et al, 1987).

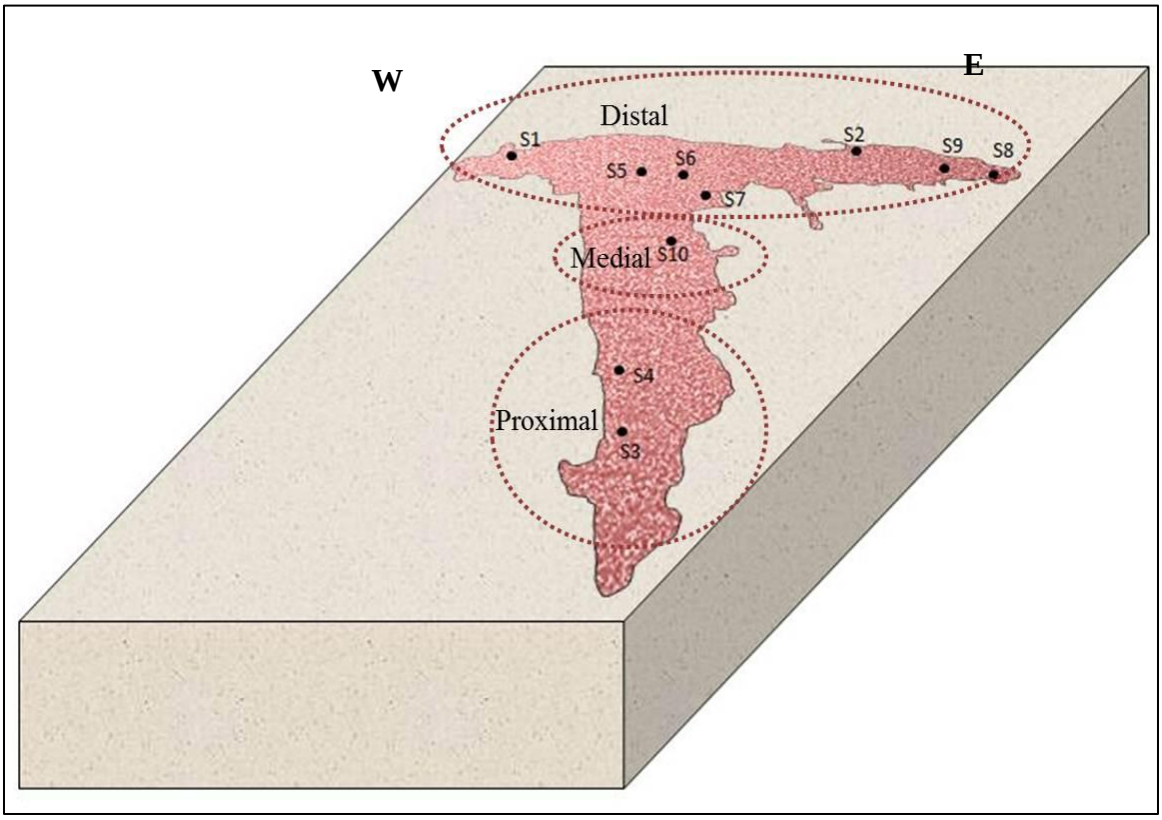


Figure 12: Conceptual block diagram showing the Proximal, Medial and Distal parts of Sarah Formation and location of outcrops at Al-Ilb paleochannel.

The Section S4 is 17m high. Starting with fine to medium grain light brown trough cross bedded sandstone at the base (first 2m) (Figure 16, Figure 14). Second unit is 4m thick medium to fine grain light brown unit, small scale trough cross beds and laterally changes to horizontal stratification. The remaining units consist of fine to medium grain trough cross-bedded sandstone (Figure 13).

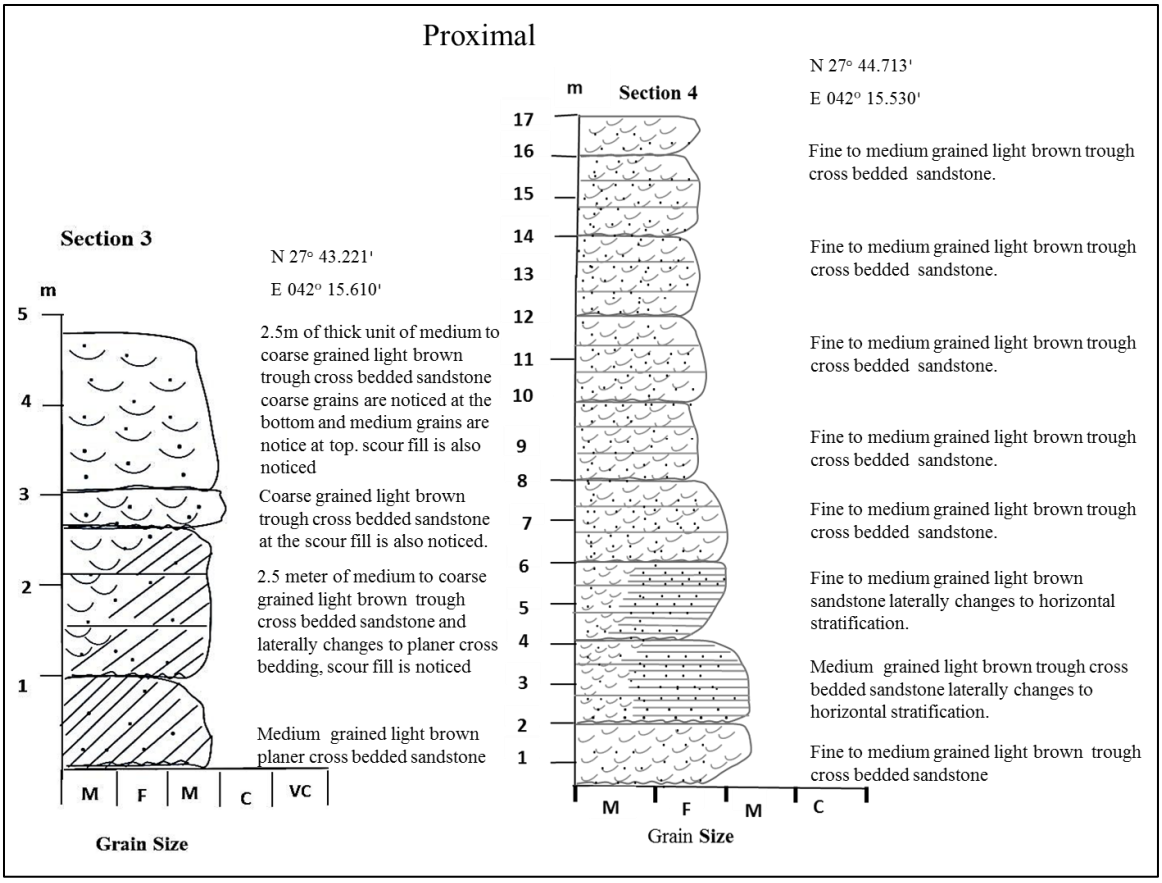


Figure 13: Vertical facies sections representing proximal part of Sarah Formation, Al-Ilb paleochannel.

Figure 14: Field photo of S3 representing Sarah Formation, Al-Ilb Paleovalley.

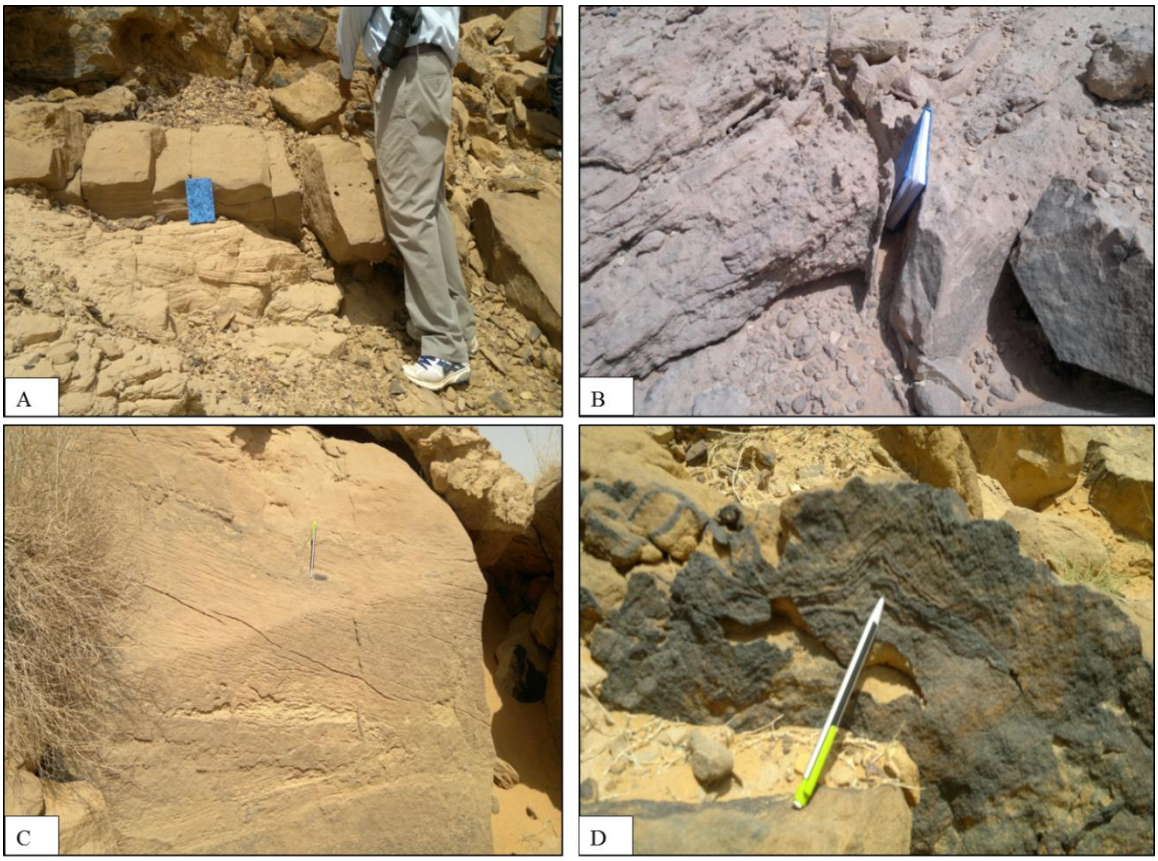


Figure 15: Different facies of Sarah Formation at S3, (A) Planar cross bedded sand stone facies (Sp). (B) Trough cross bedded sandstone facies (St). (C) Planar cross bedded sandstone facies (at closer look) (Sp). (D) Ferruginised sandstone.

## 4.4 Medial Part of Paleochannel

Section S10 represents the medial part of the Al-Ilb paleochannel. It is approximately 8.5m high and consists of 6 units (Figure 17). The facies observed in this profile is horizontally stratified fine to medium and coarse grained sandstone (Sh). The base of the section is fine to medium grained reddish brown horizontally stratified, sandstone (1m). The 2m thick unit of medium grain horizontally stratified sandstone conformably overlies

the unit 1 with scouring at the base. This sequence ends with fine to medium grained horizontally stratified sandstone. Then another sequence starts with high energy, coarse grained reddish brown horizontally stratified sandstone with scoured at the base. Dropstone is also observed in this 1.5m thick unit. The rest of the profile consists of 2 units with 2m and 1m thickness, consisting of fine to medium grained horizontally stratified sandstone.

### 4.5 Distal Part of Paleochannel

The distal part of Al-Ilb paleochannel consists of 7 sections covering this part appropriately (Figure 20). These sections include S1, S2, S5, S6, S7, S8, and S9 (Figure 20). The facies observed in distal part are dominantly medium to fine, trough cross bedded (St) and planar cross bedded (Sp) except some of the beds with very coarse to gravel size. The vertical profile of each section represents wide range of grains sizes and sedimentary structure representing the complex paleogeography of the paleochannel.

The thickness of the medium to fine grained trough cross bedded sandstone varies from 1m to 2.5m, dominantly ferruginised sandstone. The coarse to very coarse grains trough cross bedded sandstone is also noticed in some of the profile (S1, S8, S9) (Figure 28). The thickness of coarse to very coarse grained units are pretty much consistent with about 2.5m. In such type of beds, the base is scoured or has erosive contact to the lower unit and grain size is coarser at the bottom and becomes finer towards the top. Poorly sorted matrix supported diamictites is noticed at S9. The lower contact is scoured and ferruginous (Figure 28).

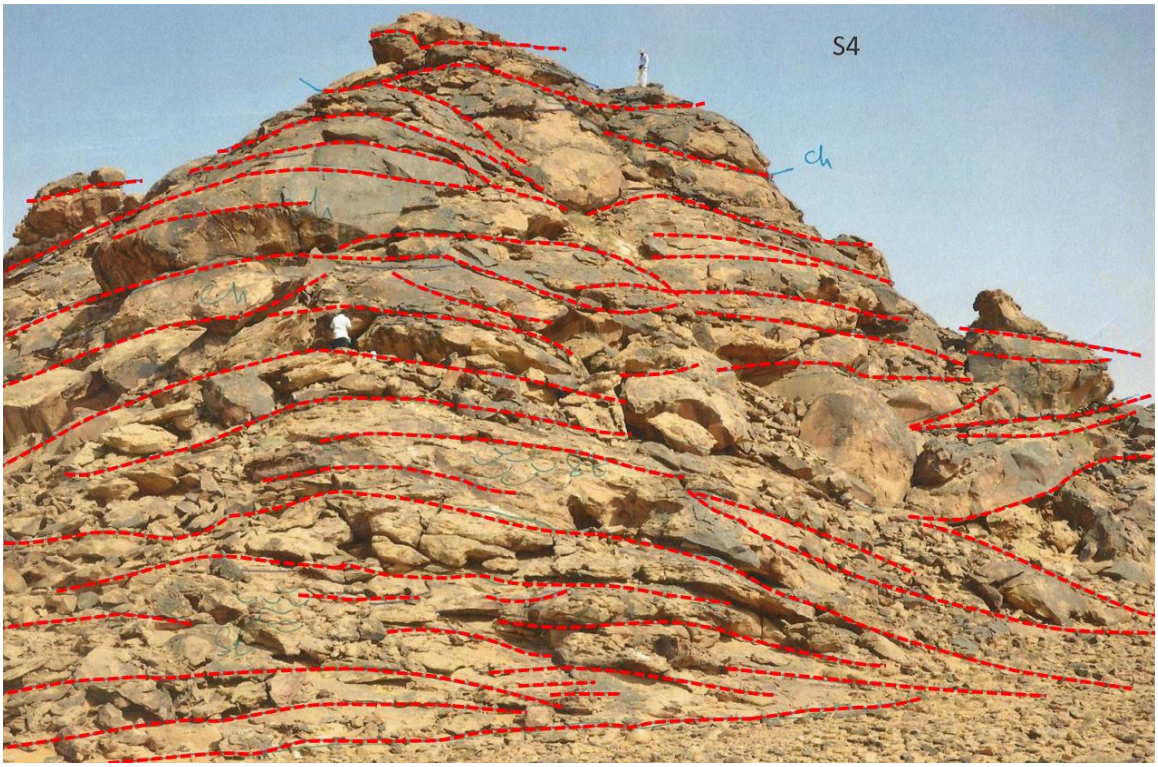


Figure 16: Photograph showing a lateral outcrop S4 dominated by trough cross bedded sandstone facies, showing sandy bedform, channels and lateral accretion.

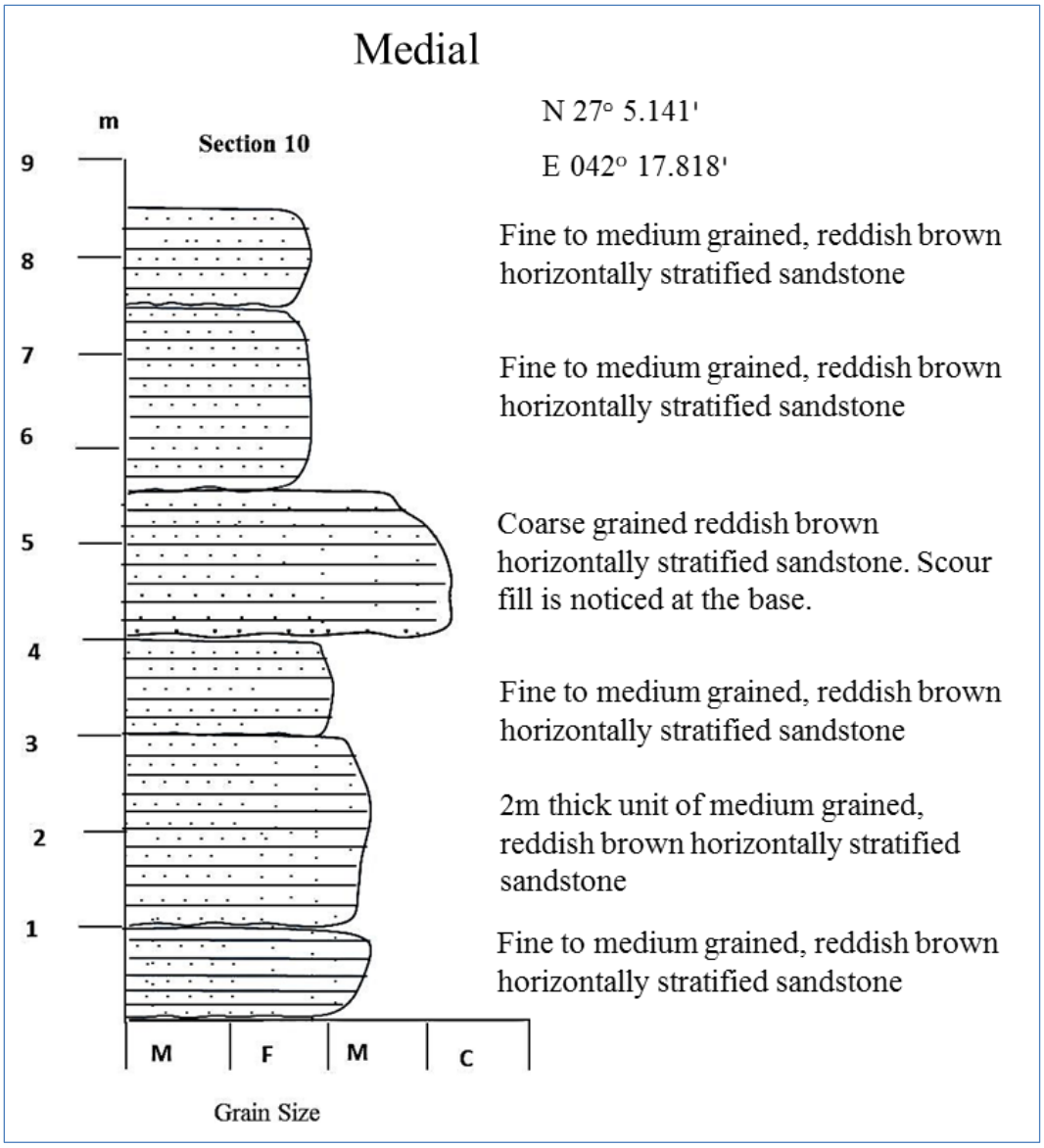


Figure 17: Vertical S10 of Sarah Formation at Al-Ilb paleochannel, representing horizontally stratified sandstone facies.

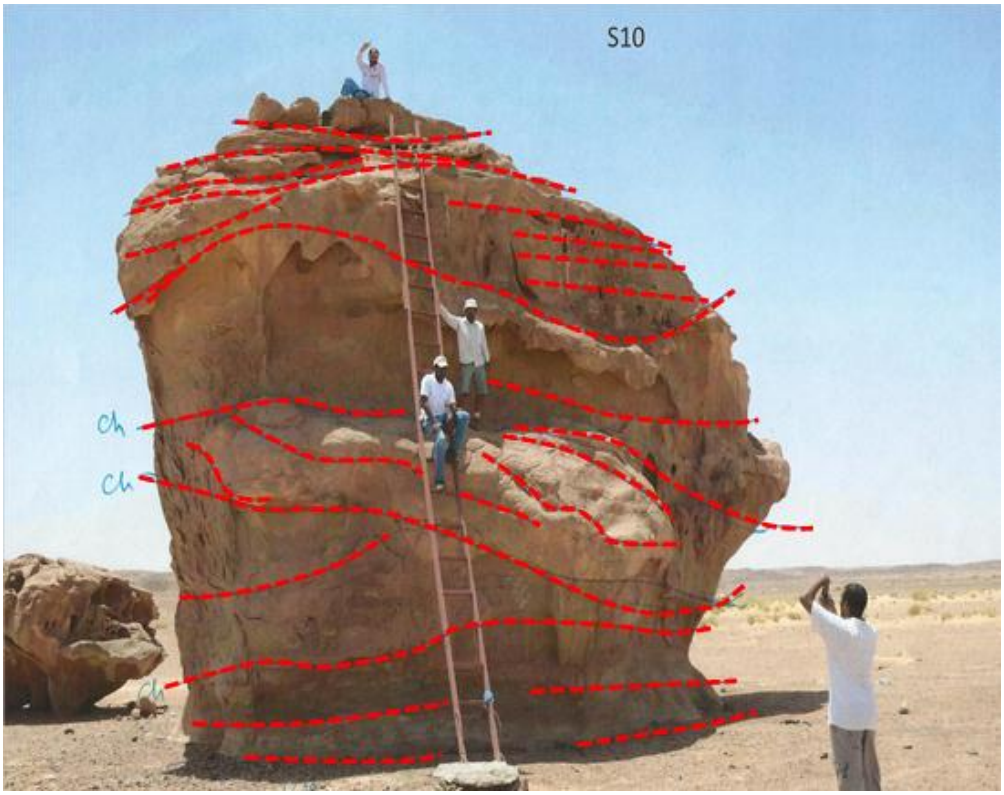


Figure 18: Photograph showing the vertical and lateral extent of Sarah Formation, Al-Ilb Paleochannel (S10)

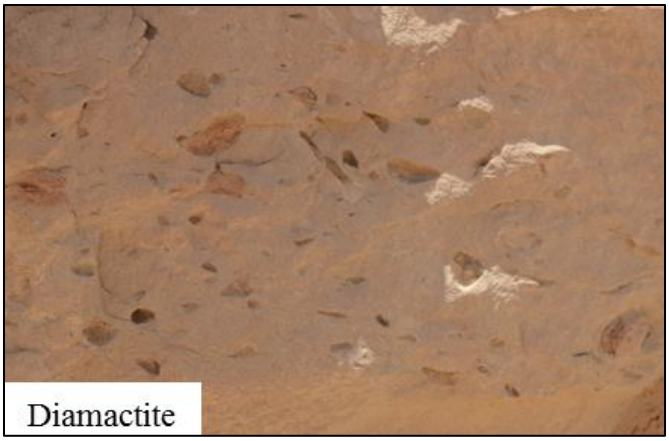


Figure 19: Photograph showing diamactite at Al-Ilb paleochannel (S10).

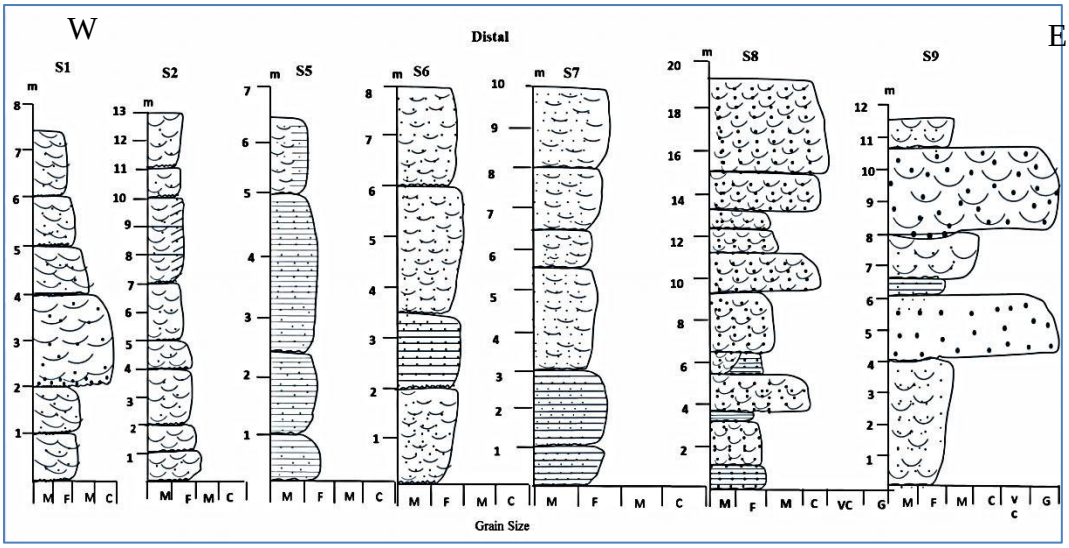


Figure 20: Vertical facies sections of outcrops, representing the distal part of Sarah Formation at Al-Ilb Paleochannel

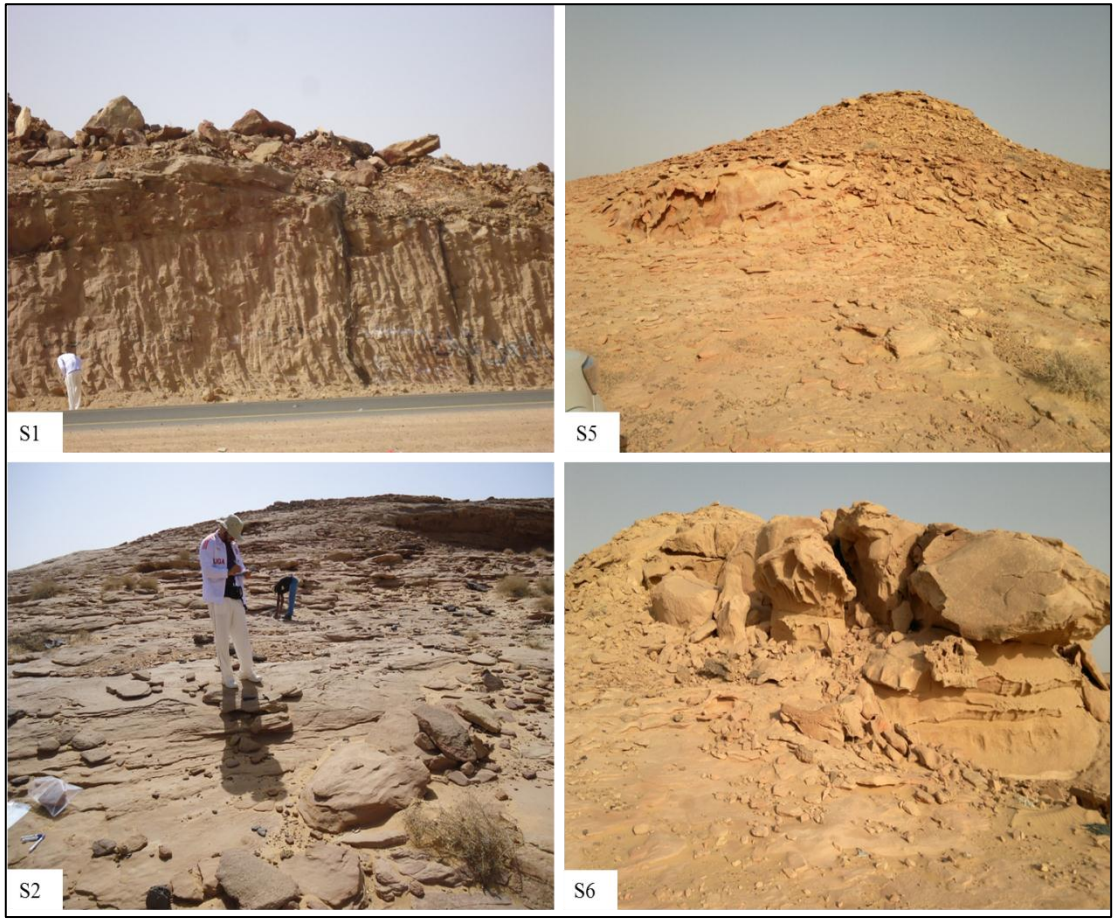


Figure 21: Photographs showing the lateral and vertical extension of Sarah Formation (S1, S2, S5 and S6) at Al-Ilb paleochannel.

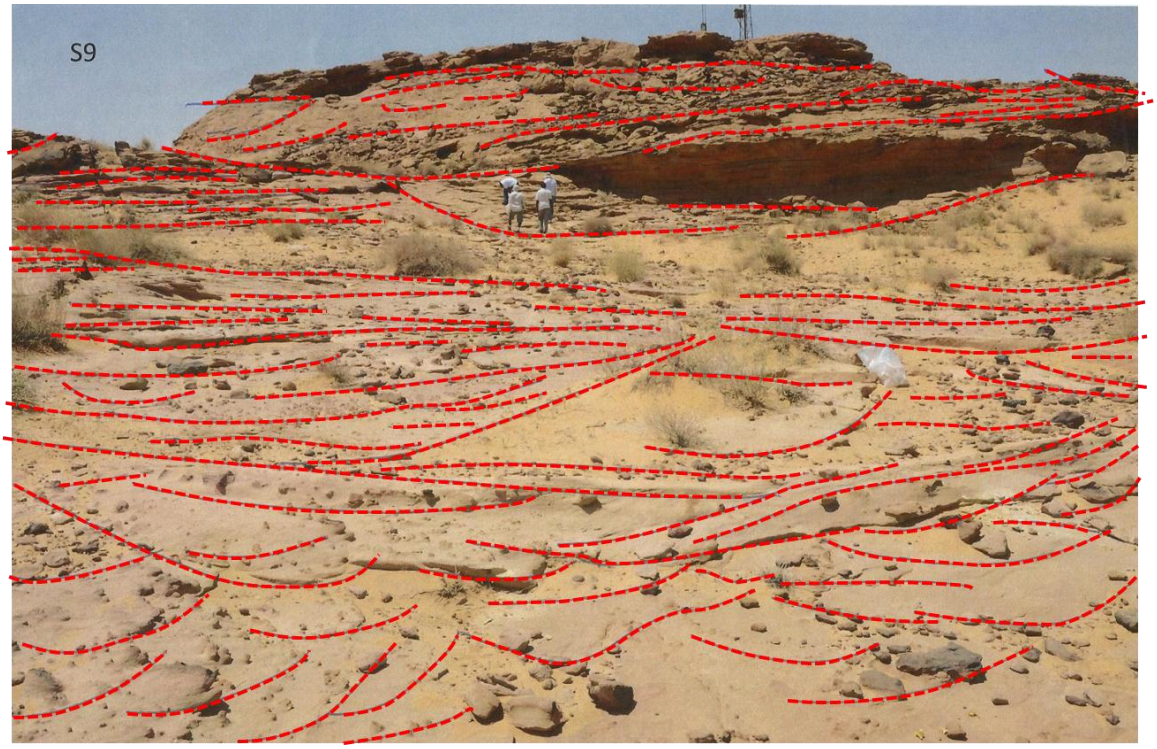


Figure 22: Photograph showing the outcrop S9 of Sarah Formation at Al-Ilb paleochannel, indicating lithofom architectural elements, vertical and lateral truncated channel bodies, sandy bedform and laminated sands are presents as architectural elements.


Figure 23: Photograph showing the outcrop S8 of Sarah Formation at Al-Ilb Paleochannel, indicating the lithofom and architectural elements (channels and lateral accretion are presents).

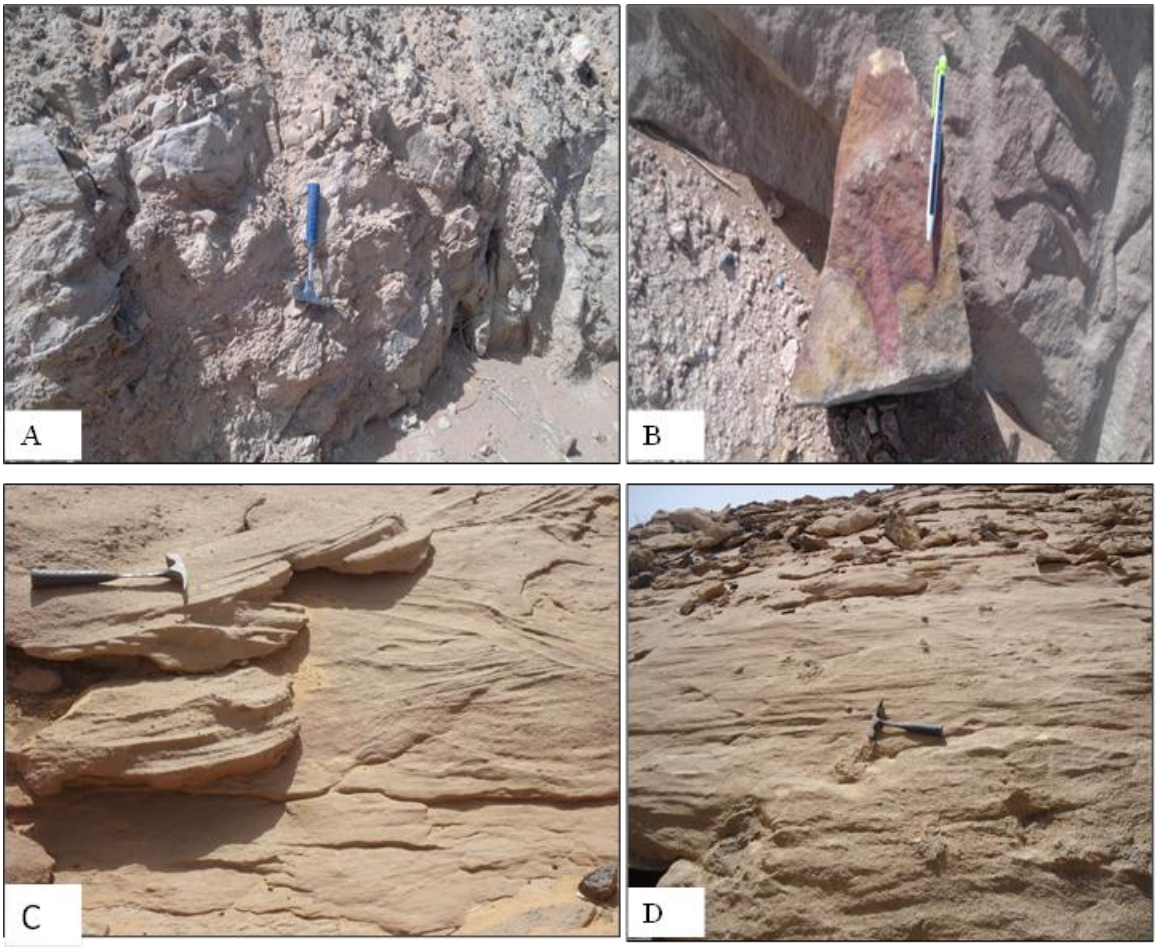


Figure 24: Photograph showing the sedimentary facies observed at S1, and S2. (A) Trough cross bedded sandstone facies at Section 1. (B) ferruginous sandstone facies at S1. (C) Trough cross bedded sandstone facies at S2. (D) Trough cross bedded sandstone facies l

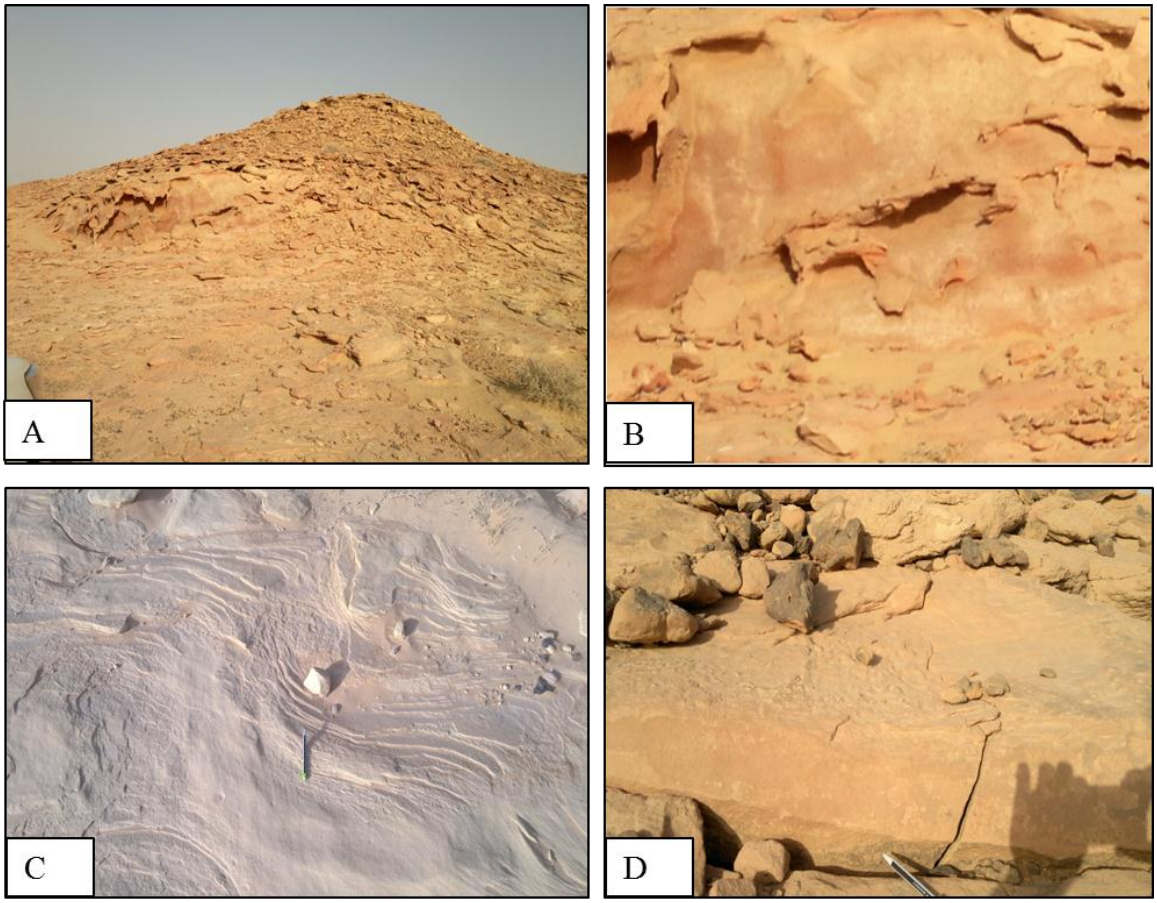


Figure 25: Photograph showing the sedimentary facies observed at the S5 and S6. (A) Vertical profile S5 (B) Horizontal stratification S5 (C) and (D) Trough cross bedded facies at S5 & S6.

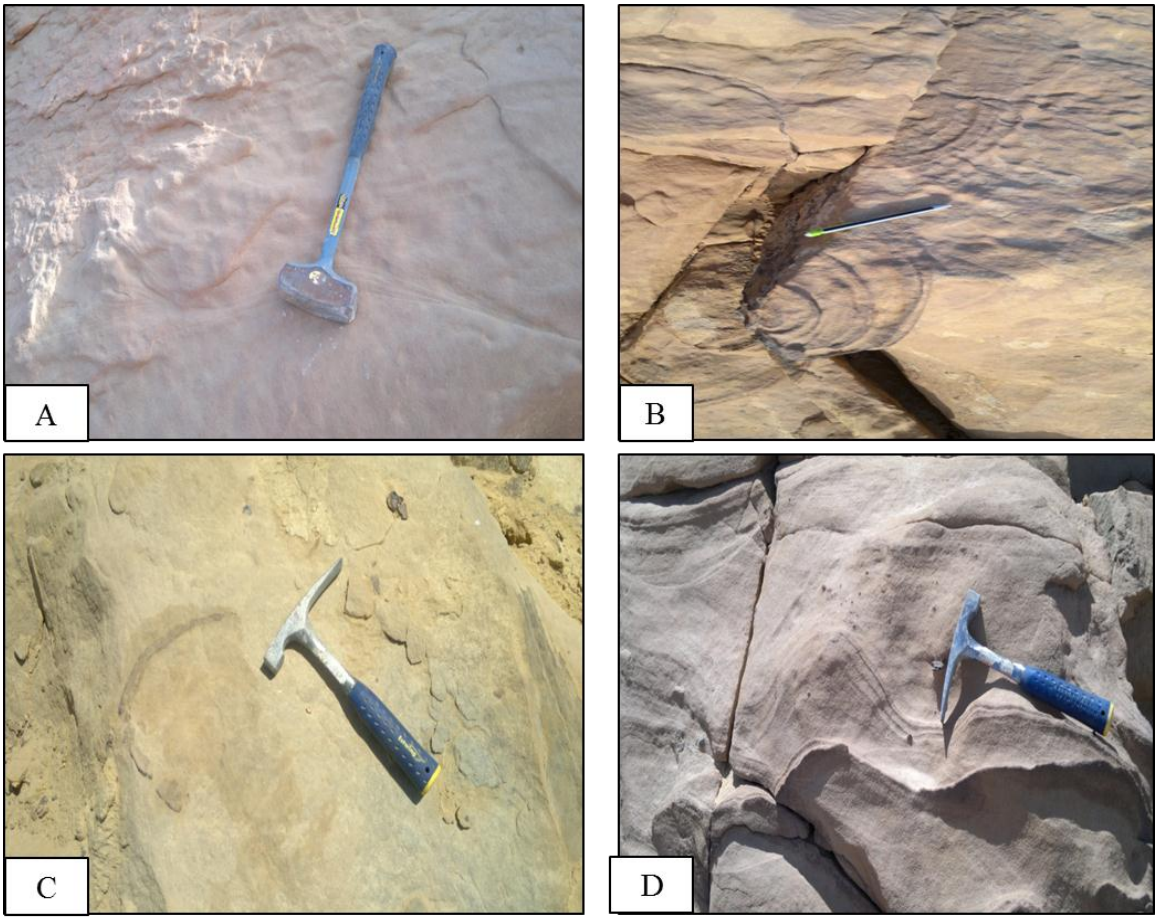


Figure 26: Photograph showing the sedimentary facies observed at S7 and S8. (A) Horizontally stratified sandstone facies at S7 (B) Trough cross bedded Ferruginous sandstone facies at S7 (C) Ferruginous sandstone facies S8 (D) Medium scale trough cross bedded facies at S8.

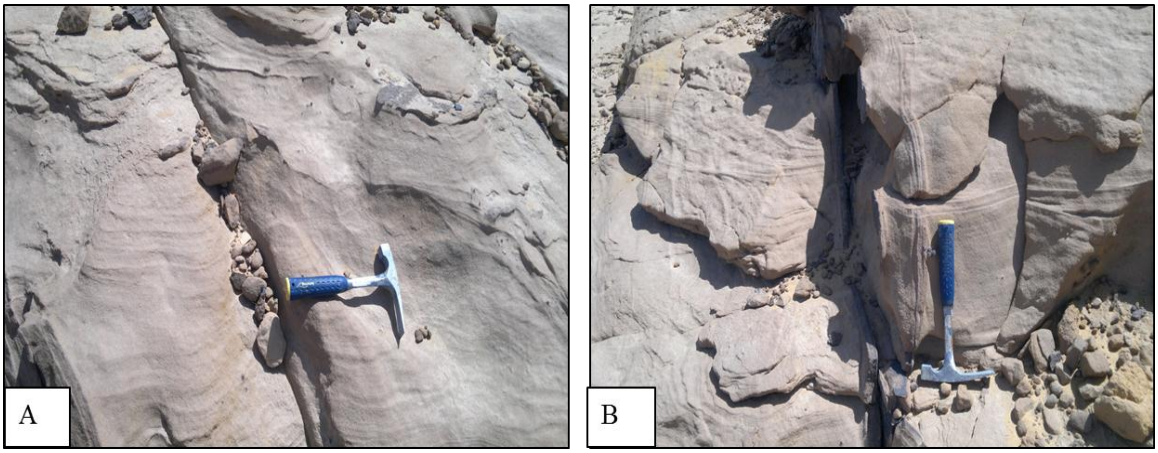


Figure 27: Photographs showing the medium to large scale trough cross bedded sandstone facies of Sarah Formation observed at the S8 (A, B), and horizontally bedded sandstone facies also observed at left side of (B)

## 4.6 Facies description and Analysis of Al-Ilb Paleochannel

Sarah Formation of Late Ordovician age is represented by glacio-fluvio facies at Al-Ilb paleochannel. This is recognized by the lithological criteria like coarse and medium grained sandstone, absence of shale or mud and carbonaceous material. The sedimentary structures observed in outcrops at Al-Ilb paleochannel give clear evidence of fluvial and glacio-fluvio environment. The sedimentary structures attributed for fluvial and glacio-fluvio environment is channel filled with trough cross bedding and planar cross bedding as well as horizontal stratification and channeling with scouring based (Miall 1985). Facies analysis of medial part was conducted using the facies codes, proposed by Miall (1985). The common facies occurring at proximal part of paleochannel are Sp, St-Sp, St and St-Sh (Figure 29). These lithofacies indicate that the proximal part is dominantly composed of medium to coarse and medium to fine grained sandstones. Dominantly

trough cross bedded, few planars cross beds and horizontal cross beds are observed at the base of section. The medial part of the Al-Ilb paleochannel represents fluvial braided stream facies with low to upper flow regime (Table 3). It is recognized by fine to medium grained sandstone. The sedimentary facies also support fluvial nature of medial part; channel filled with horizontally stratified sandstone, scouring or erosional surfaces filling the channel (Figure 17). The dominant facies that represent the medial part is horizontally stratified medium to coarse grained sandstone (Sh), representing low to upper flow regime.

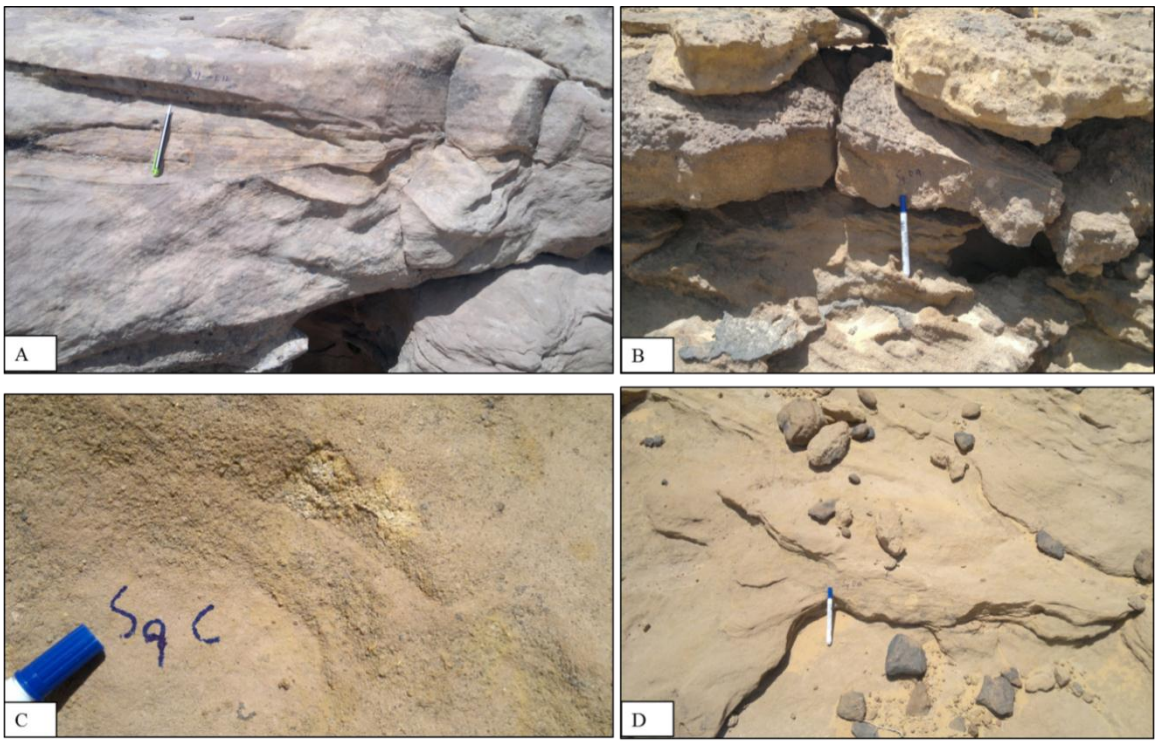


Figure 28: Photograph showing the sedimentary facies observed at the S9. (A) Small scale trough cross bedded sandstone facies. (B) Trough cross bedded very coarse grained sandstone facies. (C) Massive gravels (D) Medium scale trough cross bedded sandstone.

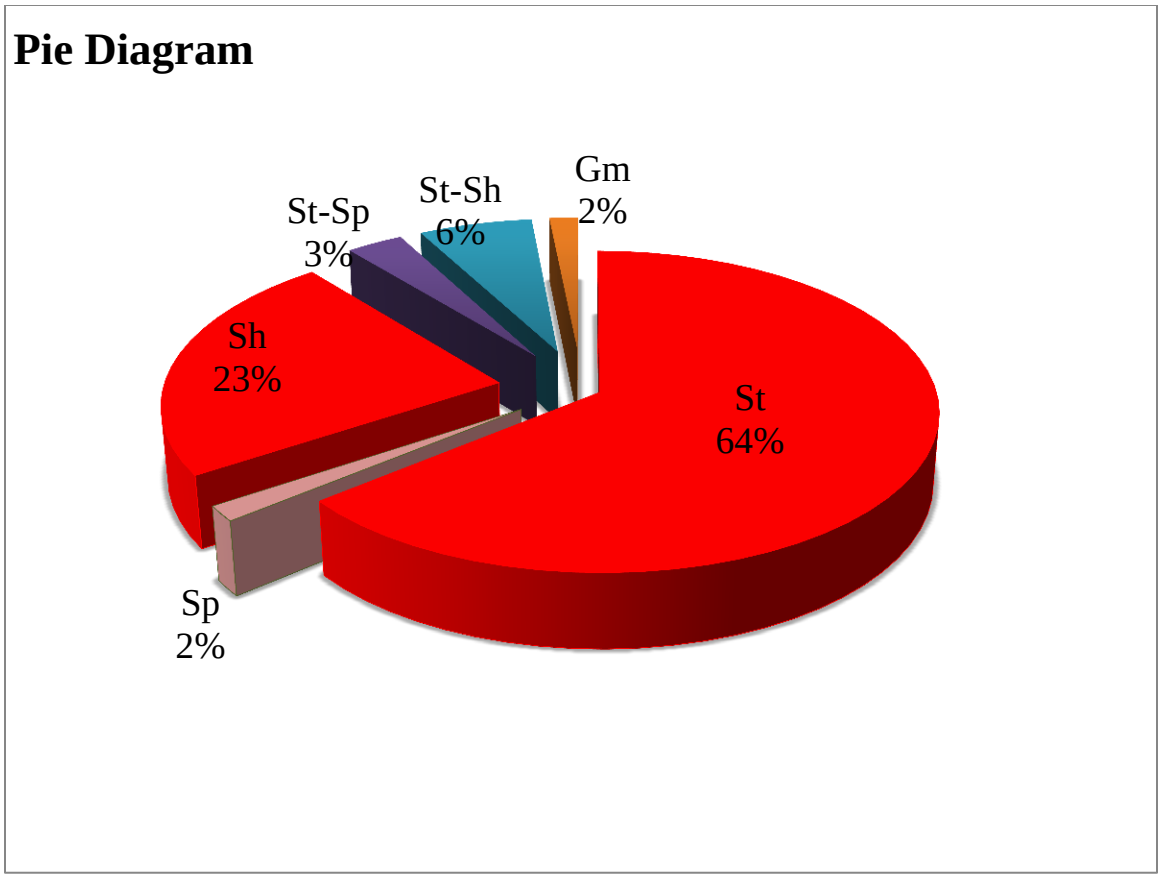


Figure 29: Pie Chart showing the distribution of Sarah Formation facies at proximal, medial and distal parts of Al-Ilb paleochannel.

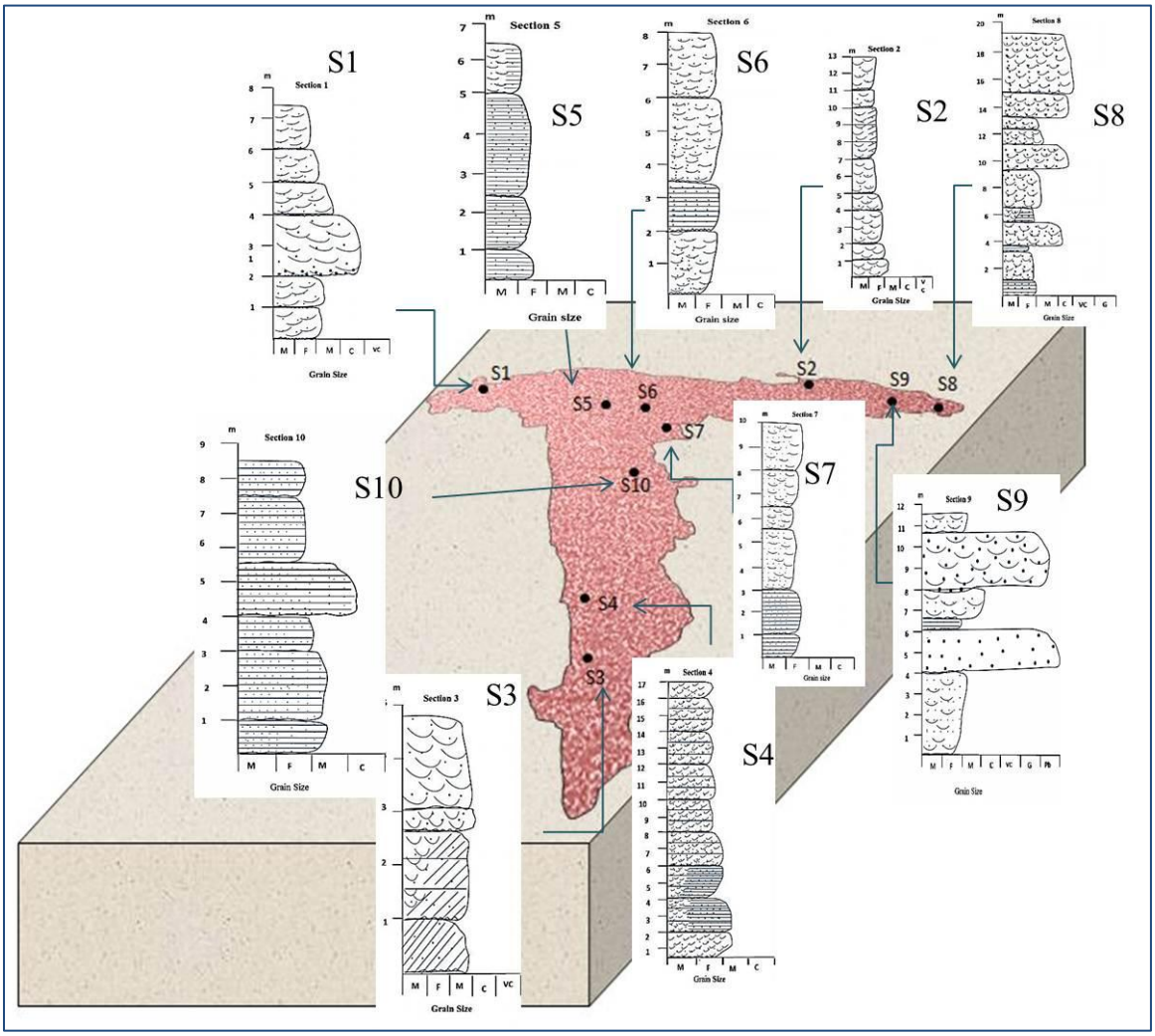


Figure 30: Distribution of the lithofacies of vertical profiles of Sarah Formation from the proximal, medial and distal part of Al-Ilb paleochannel.

Table 2:Lithofacies of Sarah Formation observed at Al-Ilb paleochannel.

| | Facies type | Facies code | Facies description | Observed sedimentary structure | Interpretation and environments |
|---|---|---|---|---|---|
| **Glacial Outwash** | **Sandstone facies** | St | Sand, fine to very coarse, pebbly | grouped trough cross beds | Sinuous-crested and linguoid (3D) dunes |
| | | Sh | Sand, fine to very caorse, pebbly | Horizontal lamination parting or streaming lineation | Plane-bed flow (critical flow) |
| | | Sp | Sand, fine to very caorse, pebbly | Grouped planar cross beds | Traverse and linguoid bedforms (2D) |
| | | St-Sp | Sand, fine to very coarse, pebbly | Trough cross beds changes to planar cross stratificatification with scouring surface | Low energy |
| | | St-Sh | Sand, fine to very coarse, pebbly | Trough cross beds changes to horizontal stratification with scouring surface | Low to higher energy |
| | **Glacial facies** | Gm | Pebbly to very coarse sandstone | includes mud clast, iron dropstone | Diamactite |

Distal part of the paleochannel is represented by glacio-fluvio facies. This is recognized from the lithological criteria including fine to medium and coarse to very coarse-grained sandstone for fluvial part, while poorly sorted diamictites (gravel) for the glacio-fluvio environment. The commonly occurring lithofacies (after Miall, 1985) are St, Sp, Hs, St-Hs, and Gm; indicating that the distal part is influenced by glacio-fluvio deposits (Table 4). Coarser grain size trough cross bedded sandstone lies in the S8 and S9; with erosive contact at the base. The gravel-size poorly-sorted, matrix supported diamictites overlying St bed with scouring at the base. The fine to medium grained horizontally stratified beds is also present (dominantly at S5). The glacial environment sediments occur as proglacial deposits developed on outwash plains known as sandure in front of continental glacier and ice sheets. The glacio-fluvial deposits contain significant column of sediments deposited by glacial melt-water river. Poorly sorted diamictites and dropstone are one of the criteria of recognition of glacial environments. The diamictites and dropstone are observed at S9 and S10 respectively. It is very difficult to say that the environment

Table 3: Summarized architectural elements of Sarah Formation observed at Al-Ilb paleochannel (after Miall, 1966)

| Element | Symbol | Principal lithofacies assemblage | Geometry and relationships |
|---|---|---|---|
| Channels | CH | any combination | finger, lens or sheet; concave-up erosional base; scale and shape highly variable; internal concave-up secondary erosion surfaces common |
| Gravel bars and bedforms | GB | Gm, Gp, Gt | lens, blanket; usually tabular bodies; commonly interbedded with SB |
| Sandy bedforms | SB | St, Sp, Sh, Sl, Sr, Se, Ss | lens, sheet, blanket, wedge; occurs as channel fills, crevasses splays, minor bars |
| Foreset macroforms | FM | St, Sp, Sh, Sl, Sr, Se, Ss | lens resting on flat or channelled base, with convex-up second-order internal erosion surfaces and upper bounding surface |
| Lateral accretion deposits | LA | St, Sp, Sh, Sl, Sr, Se, Ss; less commonly Gm, Gt, Gp | wedge, sheet, lobe; characterized by internal lateral accretion surfaces |
| Sediment gravity flows | SG | Gm, Gms | lobe, sheet; typically interbedded with GB |
| Laminated sand sheets | LS | Sh, Sl; minor St, Sp, Sr | sheet, blanket |
| Overbank fines | OF | Fm, Fl | thin to thick blankets; commonly interbedded with SB; |

is glacio-fluvio, but the occurrence of dropstone and diamictites give indication of glacial influx in the form of glacial melt-water also called glacial outwash.

## 4.7 Architectural Elements Analysis (AE)

Dominantly river gone pass through several turns' i.e. straight and curved channels also known as architectural elements. Miall (1985), define architectural elements as "The morphological subdivisions of particular depositional system characterized as distinctive assemblages of facies, facies geometries, and depositional processes. The eight architectural elements defined by Miall 1985 are channel (CH), gravel bars and bedform (GB), sand bedform (SB), downstream-accretion (DA), lateral-accretion (LA), laminated sand sheet (LS), and overbank fines (OF).

Based on architectural elements proposed by Miall (1985), three architectural elements have been identified and briefly described in Sarah Formation outcrops (Table 5. These elements focus on the principal facies assemblages and geometry relationships among each other (Table 5)

## 4.8 Interpretation

The previous sections were attributed for facies and architectural elemental analysis. This section includes interpretive depositional model for the recognized facies of Sarah Formation. Miall (1985) gave sixteen facies model of fluvial architectural elements i.e. is used as guidelines to build the depositional model for Sarah Formation. The vertical and lateral profiles show trough cross bedded sandstone (St), planar cross bedded sandstone

(Sp), horizontal stratification (Sh), trough cross bedding laterally changes to planar and horizontal stratification (St-Sp, St-Sh respectively), and pebbly to very coarse grained sandstone, these lithofacies are the characteristics feature of low sinuosity braided rivers (Miall 1985).

The ideal depositional model for Sarah Formation is nearly close to the "low sinuosity braided river" model. Keeping in mind the above mentioned architectural elements and facies found in the Sarah Formation; the proposed depositional model is "low sinuosity glacial outwash braided river deposits with linguoid bars".

Table 4: Showing architectural elements of fluvial deposits (after Miall, 1985)

| Element | Symbol | Principle lithofacies assemblage | Geometry and relationship |
|---|---|---|---|
| **Channels** | CH | Any combination possible | Lens or sheer; concave up erosional base; shape and scale highly variable. |
| **Sandy Bed forms** | SB | St, Sp, Sh, Se, Ss. | Lens, sheet, blanket, wedge; occur as channel fills, crevasses, splays, minor bars. |
| **Lateral accretion deposits** | LA | St, Sp,Sh,Se,Ss; less commonly Gm, Gt, Gp | Wedge, sheet, lobe; characterized by internal accretion surfaces |

Table 5: Basics architectural elements in fluvial elements (after Miall, 1985)

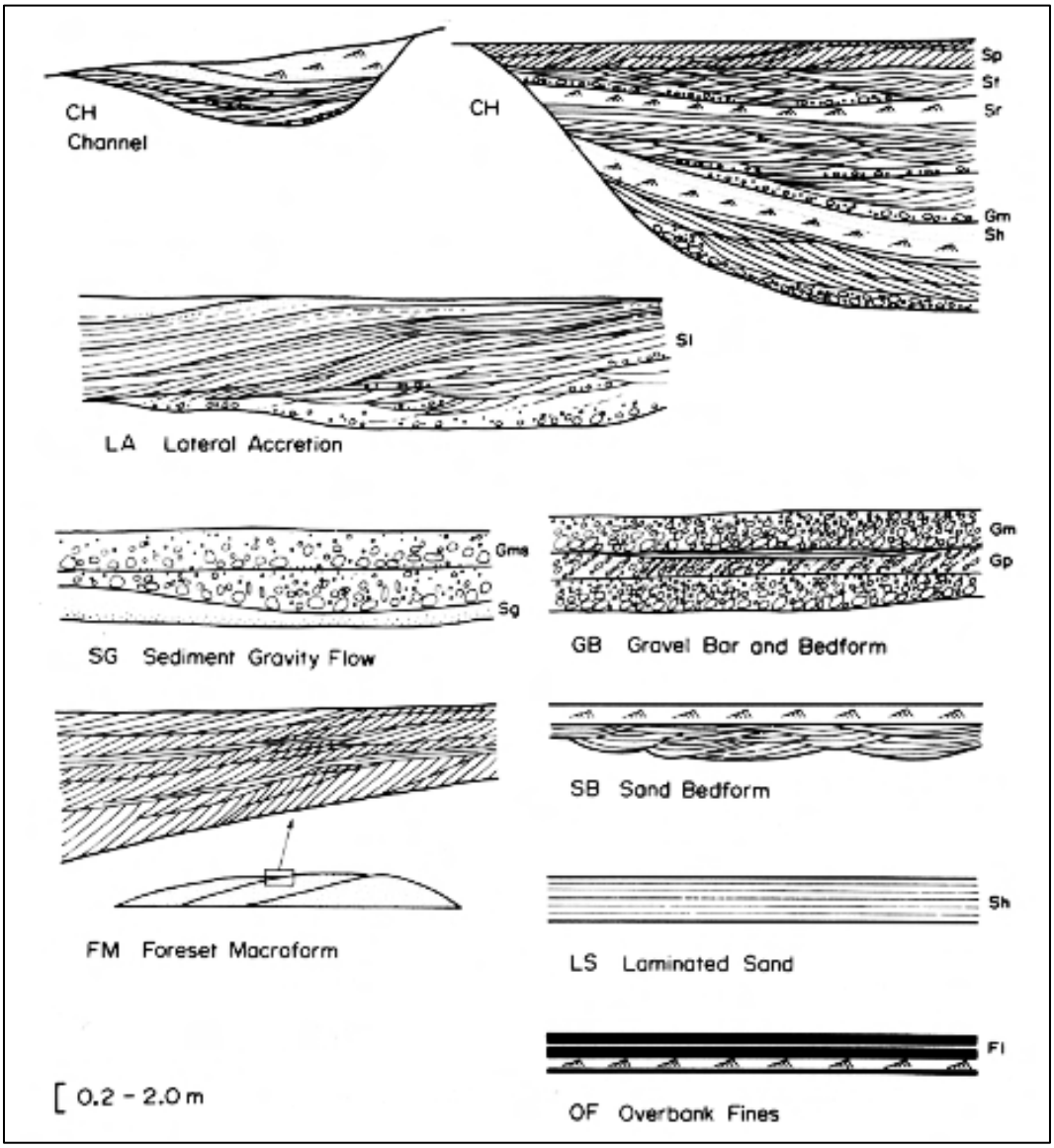

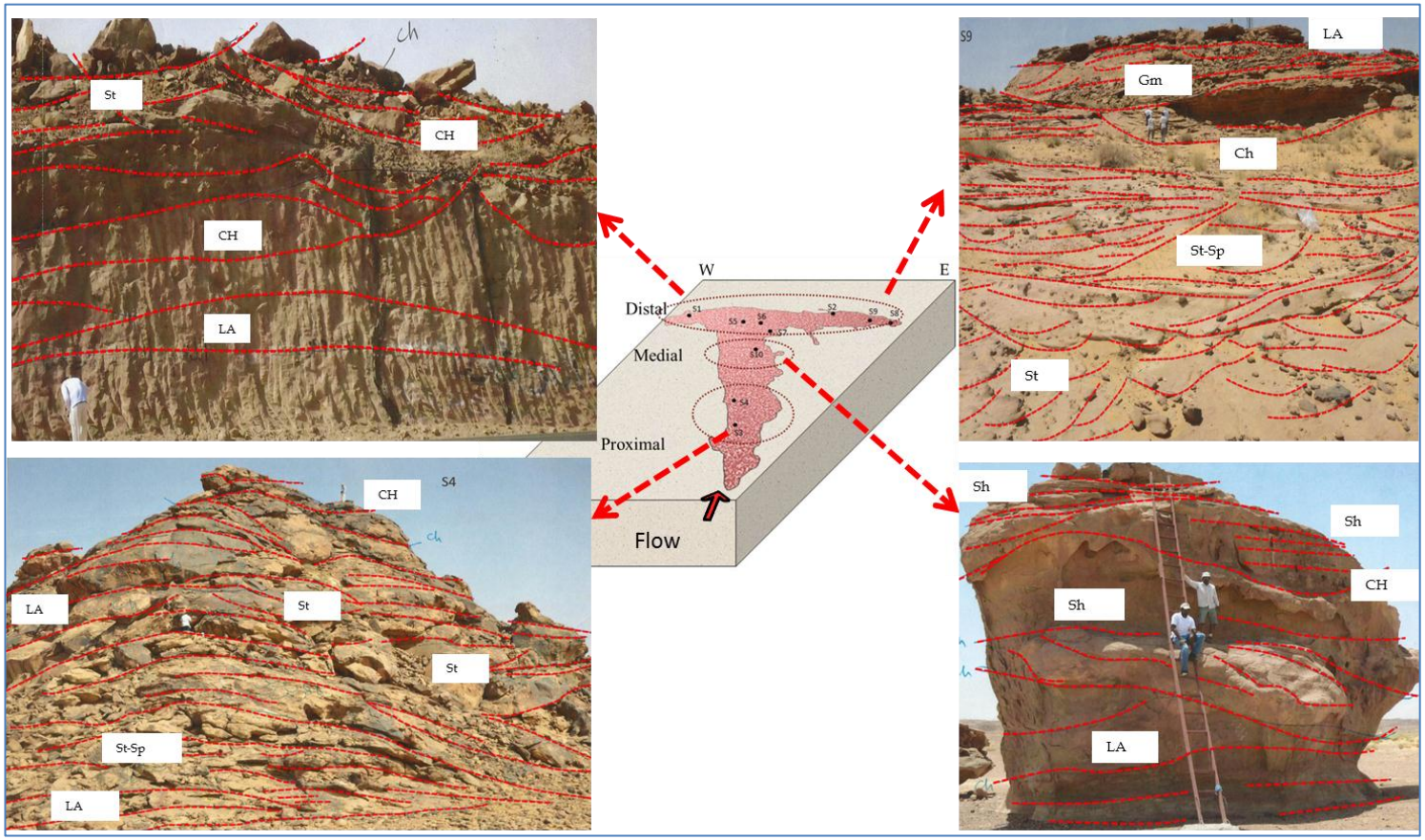


Figure 31: Conceptual block diagram with spatial distribution of architectural elements (dominantly sandy bedform, channel and lateral accretion) within the Al-Ilb paleovalley elements of Sarah Formation.

# Chapter 5

# Laboratory Analysis

## 5.1 Introduction

This chapter is devoted for laboratory analysis of outcrop samples collected from Al-Ilb paleochannel. This chapter covers two main parts of the study: sedimentological and petrophysical analysis. The sedimentological part covers the type and composition of samples, thin-section petrography, SEM-EDX, XRD and CT scan. The petrophysical part covers the porosity and permeability measurements, depositional and compositional controls on these variables. This chapter also includes determination of textural composition and classification of the sandstone types for the purpose of revealing information about environment, source area, paleoclimate and inferring the depositional history of the area. In addition, relationship of texture and composition with porosity and permeability is also examined. Finally, the heterogeneity is indicated by porosity and permeability has been explained.

## 5.2 Sandstone Petrography

As pointed out earlier, 27 samples (out of 105) were selected for thin-section petrography and these samples were collected from proximal, medial and distal parts of Al-Ilb paleochannel to understand the reasons of variability. To reveal the heterogeneous

behavior of petrophysical measurements, ten (10) samples were selected for micro studies. These samples were based on the high and low reading of porosity vs. permeability and vice versa.

### 5.2.1 Thin-section Petrography

The ternary diagram is commonly used for the classification of sandstone. Folks (1959); Dott (1964); Freidman and Sanderson (1978); Pettijhon et al. (1987): and Tucker (1991) adopted ternary classification using the percentage of quartz, feldspar and rock fragments. Triangular classification or count point is commonly used as primary means of classifying the sandstone. The sandstone of Sarah Formation is classified as quartz arenites (by using the Folks classification chart (1959). The summary of thin-section observations is listed in Table 6.

**Quartz Arenites**

Thin-section petrography of 27 representative samples shows that the sandstone of Sarah Formation is composed of quartz arenites; dominantly monocrystalline quartz (i.e. 97% on average). The polycrystalline is present as minor amount (i.e. 3% on average). The quartz arenites observed at proximal, medial, and distal part of Al-Ilb paleochannel is moderately to poorly sorted and in some cases well sorted (Figure 34). Therefore, the expectation for feldspar is low; as indicated by examined samples (1-2 %). The cement-matrix observed in 27 samples contains silica, calcite, iron and clay minerals (Table 6). This observation is also confirmed by the by SEM-EDX and the XRD results.

## Thin-section Petrography

The thin-section petrography shows that samples sands are dominantly fine to medium grained quartz rich sandstone. The observed grains are sub-rounded to rounded and, in some cases, it is angular to sub-angular (Table 6). The grains are moderately to poorly sorted and, in some cases, well sorted. The packing is tight to lose with floating grains texture, dominantly in highly cemented ferruginised sandstone.

## Quantitative Mineralogy

The comprehensive petrographical analysis of the selected samples revealed that it is dominantly composed of quartz in addition to small percentage of clay minerals, rock fragments and feldspar and rare amount of mica. The compositional analysis of Sarah Formation is described in (Table 6).

## Quartz

The detailed analysis indicates that the dominant mineral is quartz. The quartz is distinguished by its clear color, gray birefringence color, absence of cleavage. The percentage composition of quartz ranges from 97% to 99%, on QFL sandstone classification. The polycrystalline quartz belongs to metamorphic rocks of the Arabian Shield while the monocrystalline quartz exhibits straight extinction representing igneous origin. Some of the grains reflect fracturing along their internal boundaries; it is probably due to glacial outwash.

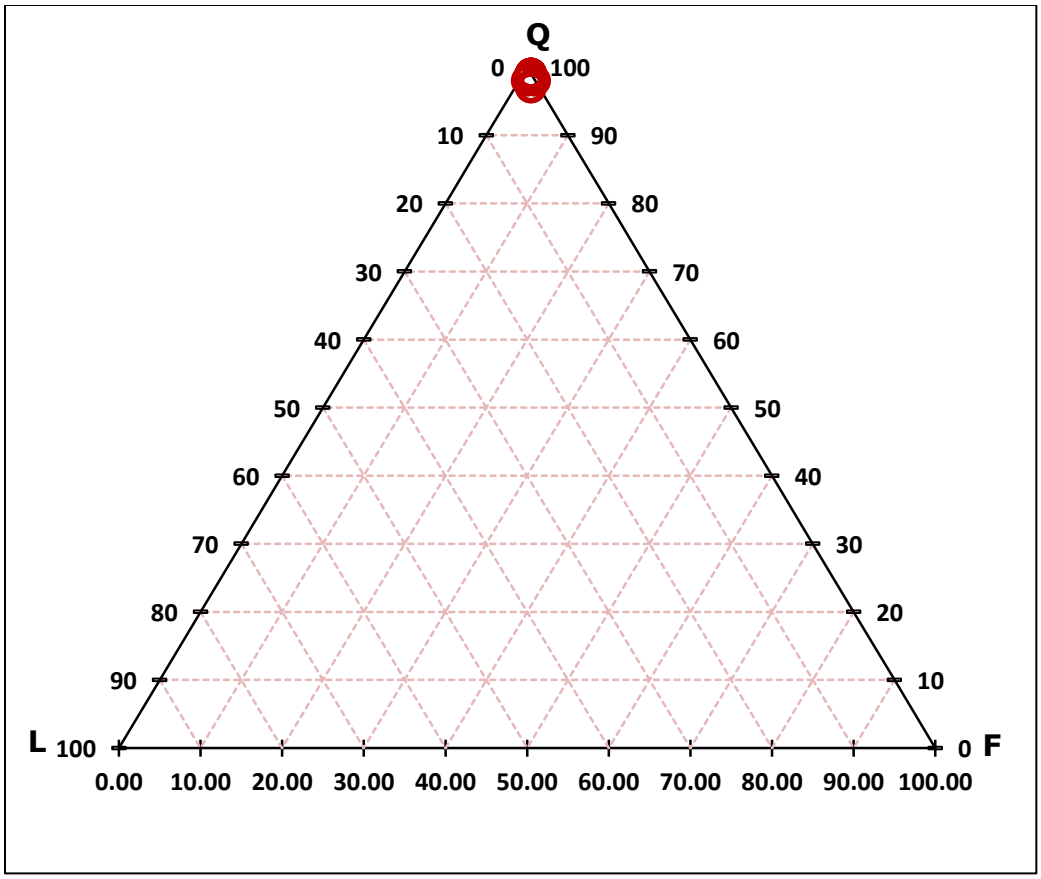


Figure 32: Classification of sandstone on the base of quartz, feldspar and lithic fragment (QFL) components (Folks, 1959)

Table 6: Summarized petrographical analysis of Sarah Formation thin sections at Al Ilb paleochannel, Baqa.

| Sect No. | Sample ID | MGS (μ m) | Sorting | | Shape | Quartz Grains | | | Feldspar (%) | Mica (%) | Lithic Fragment (%) | Heavy Mineral (%) | Cement (%)Iron Oxide | Matrix (%) | Vis.Porosity (%) | Q | F | L |
|---|---|---|---|---|---|---|---|---|---|---|---|---|---|---|---|---|---|---|
| | | | | | | Mono(%) | Poly (%) | Qz | | | | | | | | | | |
| S1 | S1-2A | 190.74 | MS | 1 | S. Rounded - Rounded | 96 | 4 | 95 | 2 | 0 | 1 | 0 | 4 | 1 | 22 | 97 | 2 | 1 |
| | S1-7 | 257.14 | PS | 1 | S. Rounded - Rounded | 98 | 2 | 87 | 2 | 0 | 1 | 0 | 4 | 1 | 20 | 97 | 2 | 1 |
| | S1-9 | 268.97 | PS | 1 | S. Rounded - Rounded | 96 | 4 | 92 | 1 | 0 | 0 | 0 | 3 | 1 | 22 | 99 | 1 | 0 |
| S2 | S2-2 | 121.43 | MS | 0.67 | Sub Angular | 98 | 2 | 94 | 1 | 0 | 0 | 0 | 3 | 2 | 24 | 99 | 1 | 0 |
| | S2-4 | 95.00 | MS | 0.67 | Angular | 98 | 2 | 92 | 1 | 0 | 0 | 0 | 4 | 6 | 22 | 99 | 1 | 0 |
| | S2-7 | 97.37 | WS | 0.36 | S. Rounded | 99 | 1 | 95 | 1 | 0 | 0 | 0.1 | 3 | 0 | 26 | 99 | 1 | 0 |
| S3 | S3-1A | 186.46 | MS | 1 | S. Rounded | 97 | 3 | 95 | 1 | 0 | 0 | 0 | 6 | 3 | 22 | 99 | 1 | 0 |
| | S3-3.5 | 373.40 | PS | 1 | S. Rounded | 95 | 5 | 94 | 2 | 0 | 0 | 0 | 5 | 1 | 20 | 98 | 2 | 0 |
| | S3-4 | 291.56 | MS | 1 | S. Rounded | 90 | 10 | 94 | 1 | 1 | 1 | 0 | 3 | 1 | 26 | 98 | 1 | 1 |
| S4 | S4-2 | 238.78 | MS | 1 | S. Rounded | 98 | 2 | 96 | 1 | 0 | 1 | 0 | 3 | 2 | 19 | 99 | 1 | 1 |
| | S4-3 | 260.00 | MS | 1 | S. Rounded | 95 | 5 | 92 | 1 | 0 | 0 | 0 | 1 | 3 | 23 | 99 | 1 | 0 |
| | S4-4 | 268.09 | MS | 1 | S. Rounded | 95 | 5 | 95 | 1 | 0 | 0 | 0 | 4 | 2 | 19 | 99 | 1 | 0 |
| | S4-9 | 176.47 | PS | 1 | Sub Angular | 98 | 2 | 92 | 1 | 0 | 0 | 0 | 8 | 6 | 25 | 99 | 1 | 0 |
| S5 | S5-2B | 72.62 | WS | 0 | Sub Angular | 99 | 1 | 86 | 1 | 0 | 0 | 2 | 7 | 6 | 24 | 99 | 1 | 0 |
| | S5-9 | 276.85 | MS | 1 | Sub Angular | 99 | 1 | 90 | 1 | 0 | 0 | 0 | 4 | 5 | 22 | 99 | 1 | 0 |
| | S5-13B | 213.41 | MS | 1 | Sub Angular | 98 | 2 | 92 | 1 | 0 | 0 | 1 | 4 | 8 | 25 | 99 | 1 | 0 |
| S6 | S6-1 | 109.59 | MS | 1 | Angular | 98 | 2 | 88 | 1 | 0 | 0 | 0 | 8 | 10 | 22 | 99 | 1 | 0 |
| | S6-6 | 87.50 | MS | 1 | Sub Angular | 98 | 2 | 88 | 1 | 0 | 0 | 0 | 6 | 3 | 22 | 99 | 1 | 0 |
| S7 | S7-2 | 162.50 | PS | 1 | S. Rounded | 97 | 3 | 93 | 1 | 0 | 0 | 0 | 3 | 8 | 20 | 99 | 1 | 0 |
| | S7-6 | 150.00 | MS | 1 | S. Rounded | 98 | 2 | 93 | 1 | 0 | 0 | 0 | 5 | 8 | 21 | 99 | 1 | 0 |
| S8 | S8-10 | 258.59 | MS | 1 | S. Rounded | 96 | 4 | 95 | 1 | 0 | 0 | | 3 | 3 | 25 | 99 | 1 | 0 |
| | S8-12 | 92.86 | WS | 0 | S. Rounded | 98 | 2 | 90 | 1 | 0 | 0 | 0 | 4 | 2 | 28 | 99 | 1 | 0 |
| | S8-16 | 217.39 | MS | 1 | Rounded | 98 | 2 | 94 | 1 | 0 | 0 | 0 | 2 | 4 | 27 | 99 | 1 | 0 |
| S9 | S9-9 | 373.61 | PS | 1 | Rounded-W. Rounded | 98 | 2 | 95 | 1 | 0 | 0 | 0 | 4 | 2 | 25 | 99 | 1 | 0 |
| | S9-12 | 316.67 | PS | 1 | Rounded-W. Rounded | 95 | 5 | 95 | 1 | 0 | 0 | 0 | 2 | 3 | 27 | 99 | 1 | 0 |
| S10 | S10-1 | 152.94 | PS | 1.15 | S. Rounded | 85 | 15 | 95 | 1 | 0 | 0 | 0 | 5 | 5 | 21 | 99 | 1 | 0 |
| | S10-5 | 328.13 | MS | 0.74 | Sub Angular | 98 | 2 | 92 | 1 | 0 | 0 | 0 | 4 | 2 | 18 | 99 | 1 | 0 |

Quartz overgrowth is observed in some of the samples. This overgrowth is responsible for decreasing the porosity and permeability values to some extent. The quartz grains are moderately to poorly sorted (in general) and in some cases the sorting is very well (Figure 39). But the shapes of the grains are sub-rounded to rounded and in some cases it is angular. No heavy minerals are observed in all the examined samples except some traces in sample S2 (Figure 34).

**Feldspar**

Low percentage of feldspar is observed in samples i.e. 1-2 %. Very rare percentage of microcline and plagioclase are examined. Most of the observed grains are altered and rugged, and alteration is clearly noticed. The reason of feldspar alteration and ruggedness is low mechanical stability as compared to quartz. Chemical alteration of feldspar typically involves replacement by clay such as kaolinite and smectite consequently feldspar shows some dusty and rusty dirty appearance. Such alteration may be responsible for the development of secondary porosity as indicated by Tucker, 2005.

**Lithic Fragments**

Lithic fragments are observed in few samples (less than 1%) on average. These fragments are believed to have been derived from the Arabian Shield rocks.

**Iron Oxide**

Iron oxide cement is dominantly present almost in all samples, as revealed by the SEM_EDX results (Figure 53). Small spots of iron oxide are observed in most sections.

In SEM images, iron oxide appears like cluster of grapes (Figure 53). It is believed to be autogenic mineral since it has been formed as grains coating (North, 1985). The presence of iron oxides reduces the porosity and permeability as it fills the pores.

**Clays Minerals**

The clays, observed in the studied samples, contain authigenic type. The authigenic clays develop subsequent to burial and include both new and regenerated forms. The SEM-EDX studies reveal that the dominant clays found in the Sarah Formation samples are kaolinite, chlorite and palygorskite (Figure 54, Figure 55, Figure 56, Figure 57, Figure 58, Figure 59, and Figure 62). The booklet granular-vermicular texture of kaolinite occurs dominantly in most of samples (Figure 55, Figure 56, Figure 59, Figure 60). The amount and type of clays predominantly affect the petrophysical properties. The individual pseudo-hexagonal stacked plates (books) generally range from 3.20micron meter. The pore lining kaolinite predicates early in diagenesis where the loosely packed pore-filling forms later after grain coating or pore-lining clays. Clays coating minerals form after grains-coating or pore lining clays, clays coating minerals form at earlier stage of diagenetic origin. It is commonly distributed in patched, pore-filling as the best authigenic mineral (Figure 38, Figure 39, Figure 36). The chemical elements for kaolinite

formation are thought to be derived from leaching of some pre-existing minerals, such as potash feldspar and mica (Chamley, 1989). It reflect tropical and subtropical environments under hot and wet condition climate, where leaching is very intensive due to high rainfall and active drainage system. Walker et al. (1978) showed that clay coating can result from mechanical infiltration of detrital clay. An authigenic origin has been assumed for the clay rim or coats that form rims around detrital sand grains (Wilson and Pittman, 1977). The clay coats and rims are mainly homogeneous. Therefore clay minerals growth perpendicular to the grains surface supports an authigenic origin (Pittman et al., 1992).

**Mica**

No appreciable amount of mica was observed in sandstone samples. Only, in one sample some mica flags were noticed. Mica is more prone to weathering and it is easily washed away from coarse grained sediments and accumulated in fine sand or silt.

**Matrix**

Thin-section petrography of Sarah Formation sandstone samples collected from Al-Ilb paleochannel exhibits consistent results in terms of presence of matrix. The amount of matrix present in each sample is less the 10 %, (4% on average) (Figure 38). The presence of low matrix and high percentage of quartz provide the evidence of maturity in the studied samples. The presence of matrix results in the hindrance pore connectivity leading to decrease the porosity (Table 6).

**Cement**

The amount of cement varies in the Sarah Formation samples. It ranges from 2% to 8 %, with an average of 4% (Table 6). The dominant cementing material is iron oxide as hematite and kaolinite. Along with the kaolinite, chlorite and silica (as quartz overgrowth) are also present. The other observed clays are chlorite and palygorskite acting as cementing agent.

**Visual Porosity**

The visual porosity of the studied samples (proximal) shows minimum values of 18% and maximum values of 28%. The average value of visual porosity is 23% (Table 8). On the other hand, the average porosity measurement (from equipment) of proximal part is 20%, highest and lowest readings are 25% and 20%, respectively (Table 9). The average porosity reading (from equipment) of medial of Al-Ilb paleochannel is 19%, and highest and lowest readings are 22% and 17%, respectively. The visual and calculated porosity (from equipment) of distal part of Al-Ilb paleochannel shows very similar readings; with average 23%, minimum % 18 and maximum 33% (Table 10).

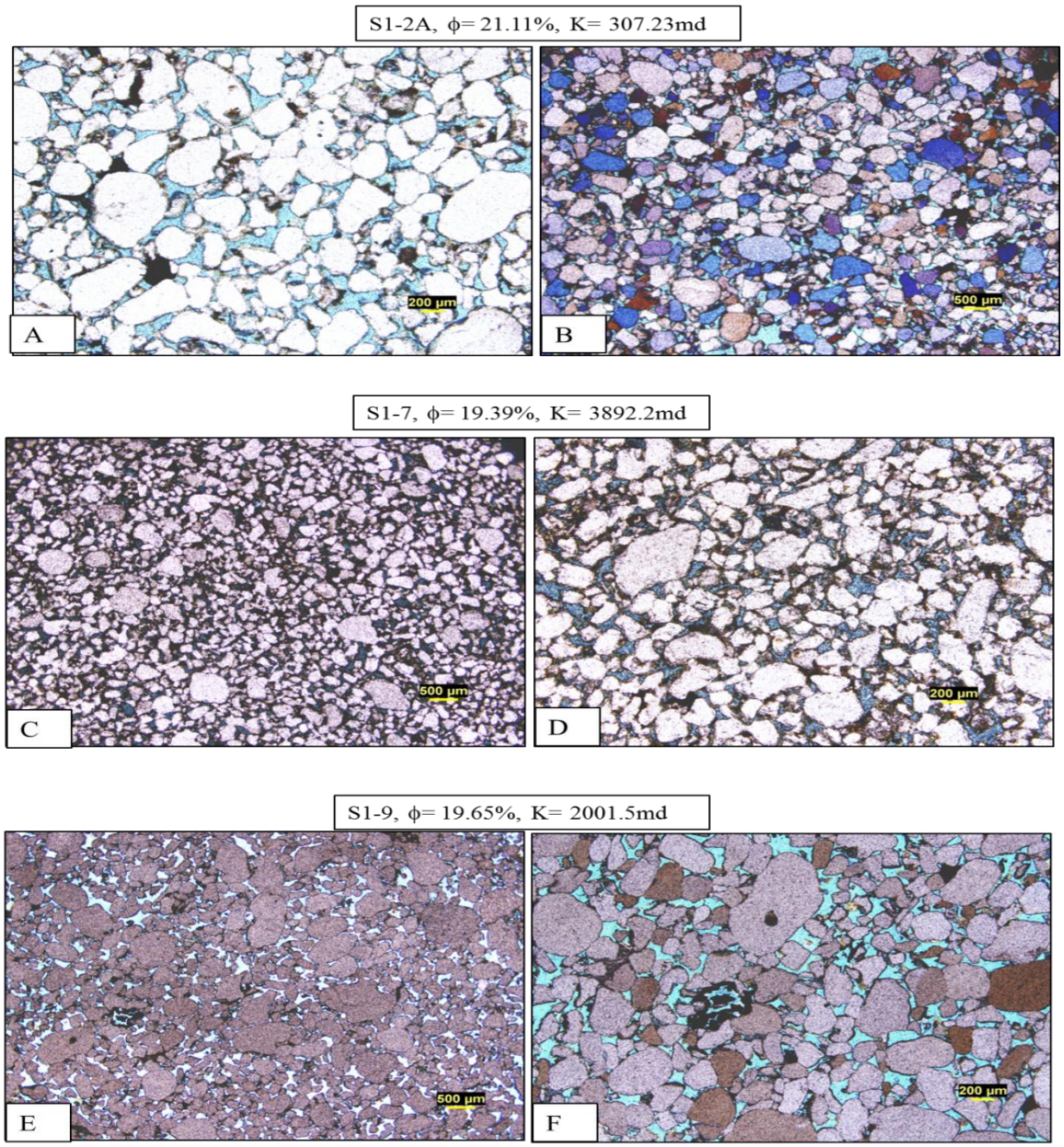


Figure 33: Photomicrographs of Sarah Formation; showing thin-section images of S1, representing the distal part of Al-Ilb paleochannel. (A) and (B) Poorly sorted quartz (monocrystalline ) grains is common (C) and (D) Rounded to sub rounded quartz , Poorly sorted quartz grains, and iron cement is dominant. (E) and (F) Poorly sorted quartz grains Ferruginous iron cement coating the sand grains. In all the samples the cement to grains ratio is very low and grains are floating.

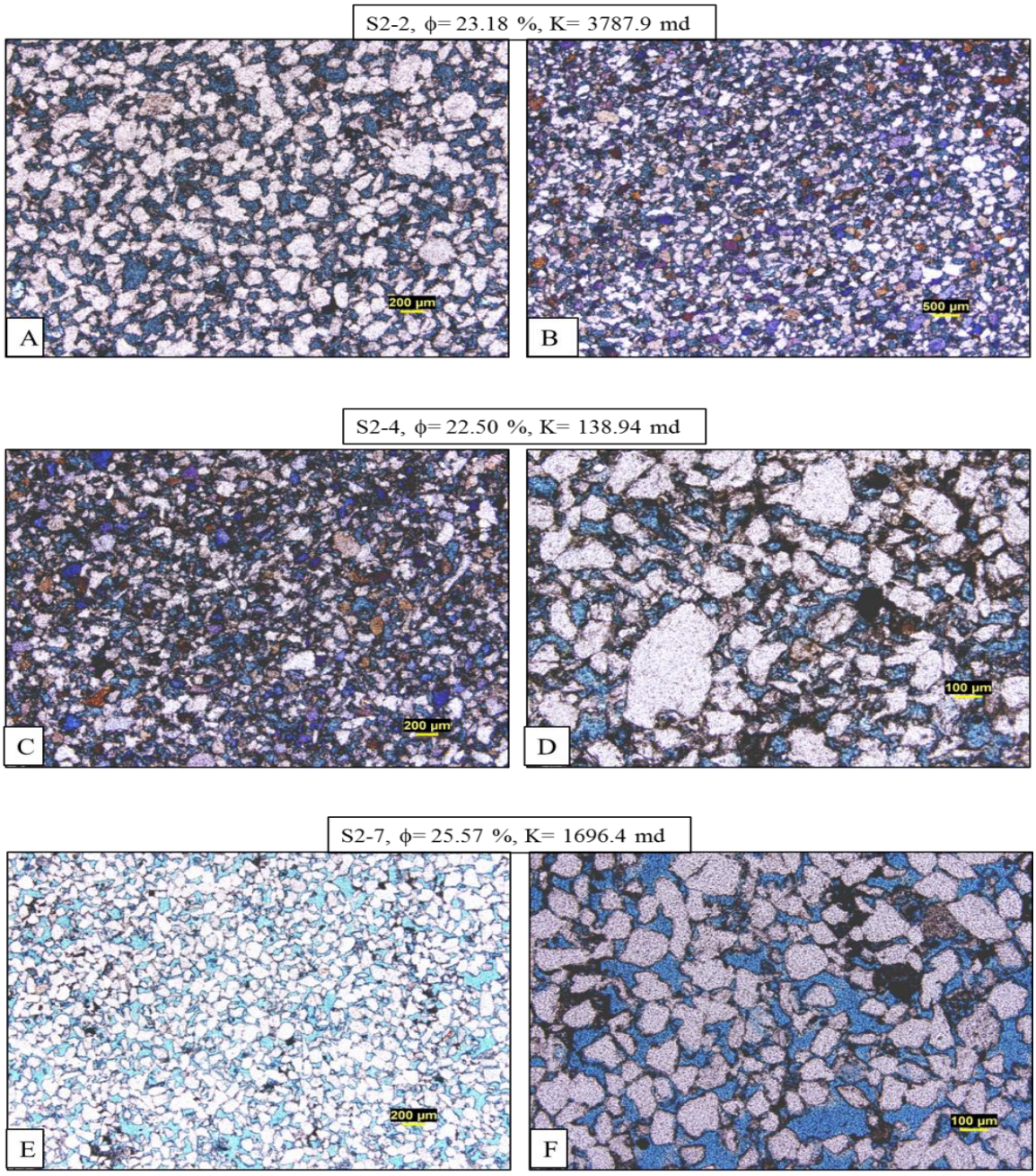


Figure 34: Photomicrographs of Sarah Formation; showing thin-section images of S2, representing the distal part of Al-Ilb paleochannel; (A) and (B) Moderately sorted iron cemented quartz grains (C) and (D) Angular to sub angular, moderately sorted quartz (E) and (F) Sub rounded, rugged, well sorted ferruginous sand grains

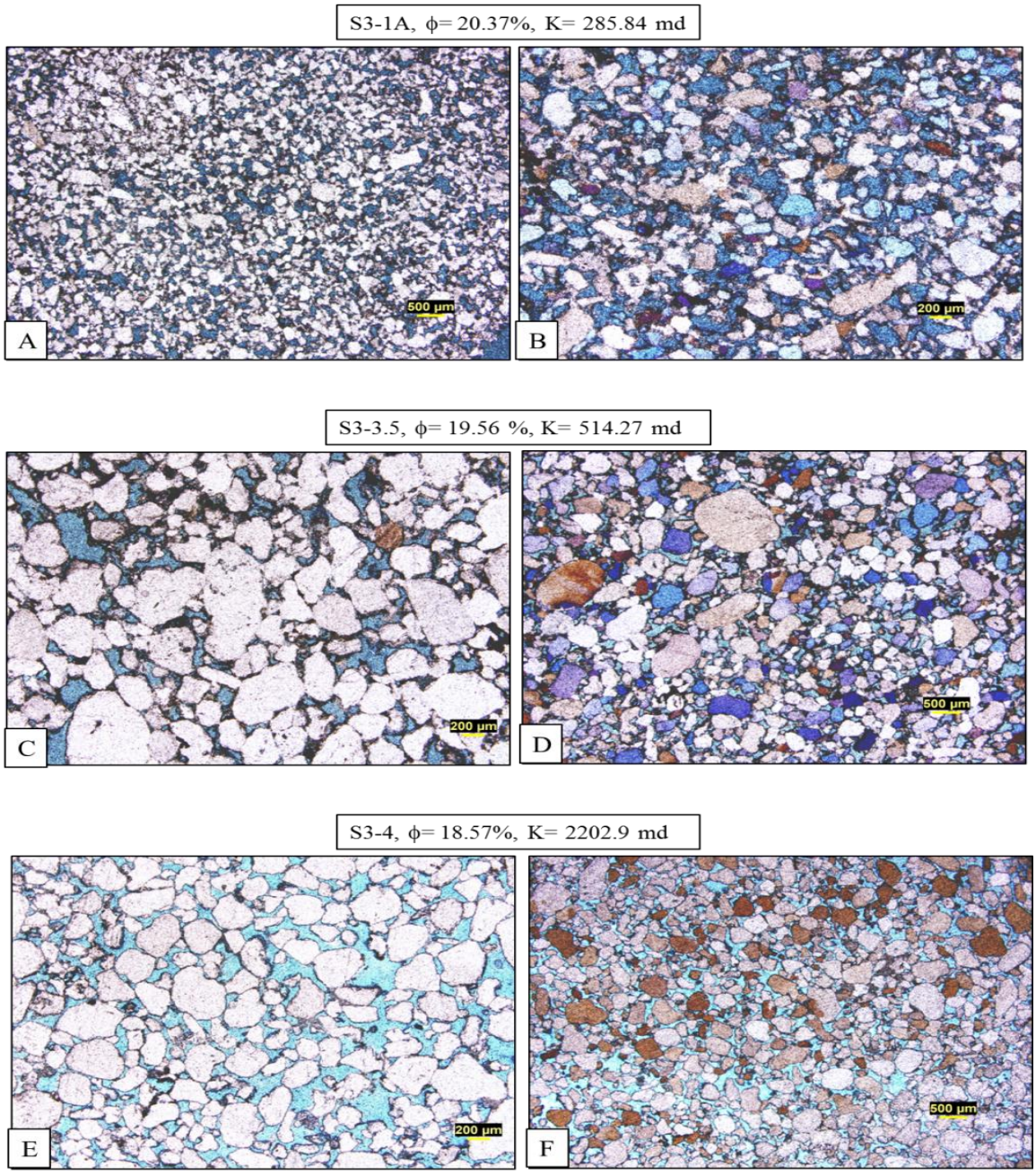


Figure 35: Photomicrographs of Sarah Formation; showing thin-section images of S3, representing the proximal part of Al-Ilb paleochannel; (A) and (B) fine grained, moderately sorted sandstone, dominantly monocrystalline quartz. (C) and (D) Poorly sorted, sub-rounded sandstone, dominantly monocrystalline and few grains of polycrystalline quartz (E) and (F) moderately sorted, sub rounded sandstone, dominantly monocrystalline

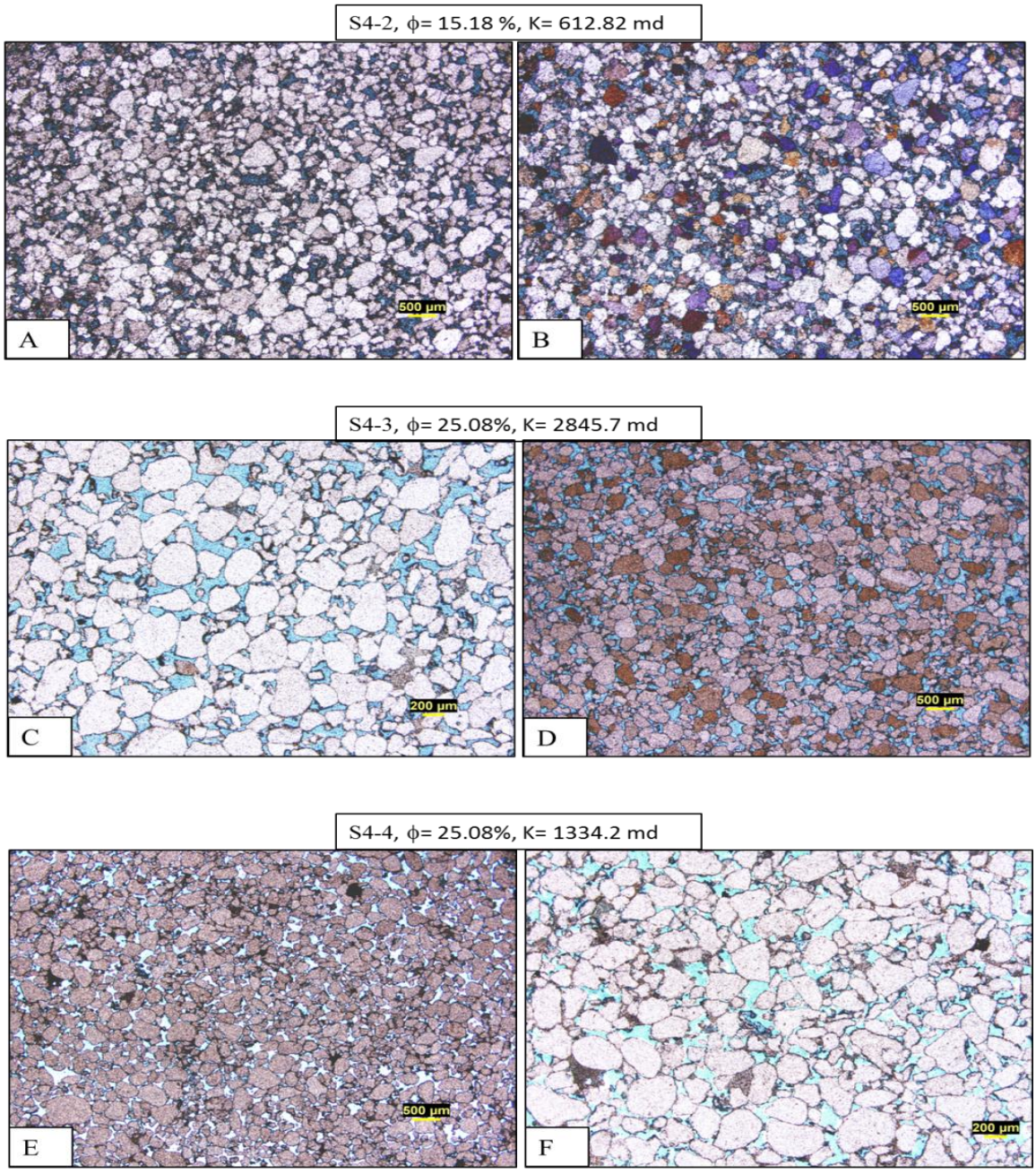


Figure 36: Photomicrographs of Sarah Formation; showing thin-section images of S4, representing the proximal part of Al-Ilb paleochannel; (A) and (B) moderately sorted, sub rounded sandstone, dominantly monocrystalline quartz (C) and (D) Moderately sorted sub-rounded sandstone, dominantly monocrystalline quartz and few grains of polycrystalline quartz (E) and (F) Moderately sorted sub-rounded sandstone, well defined pores

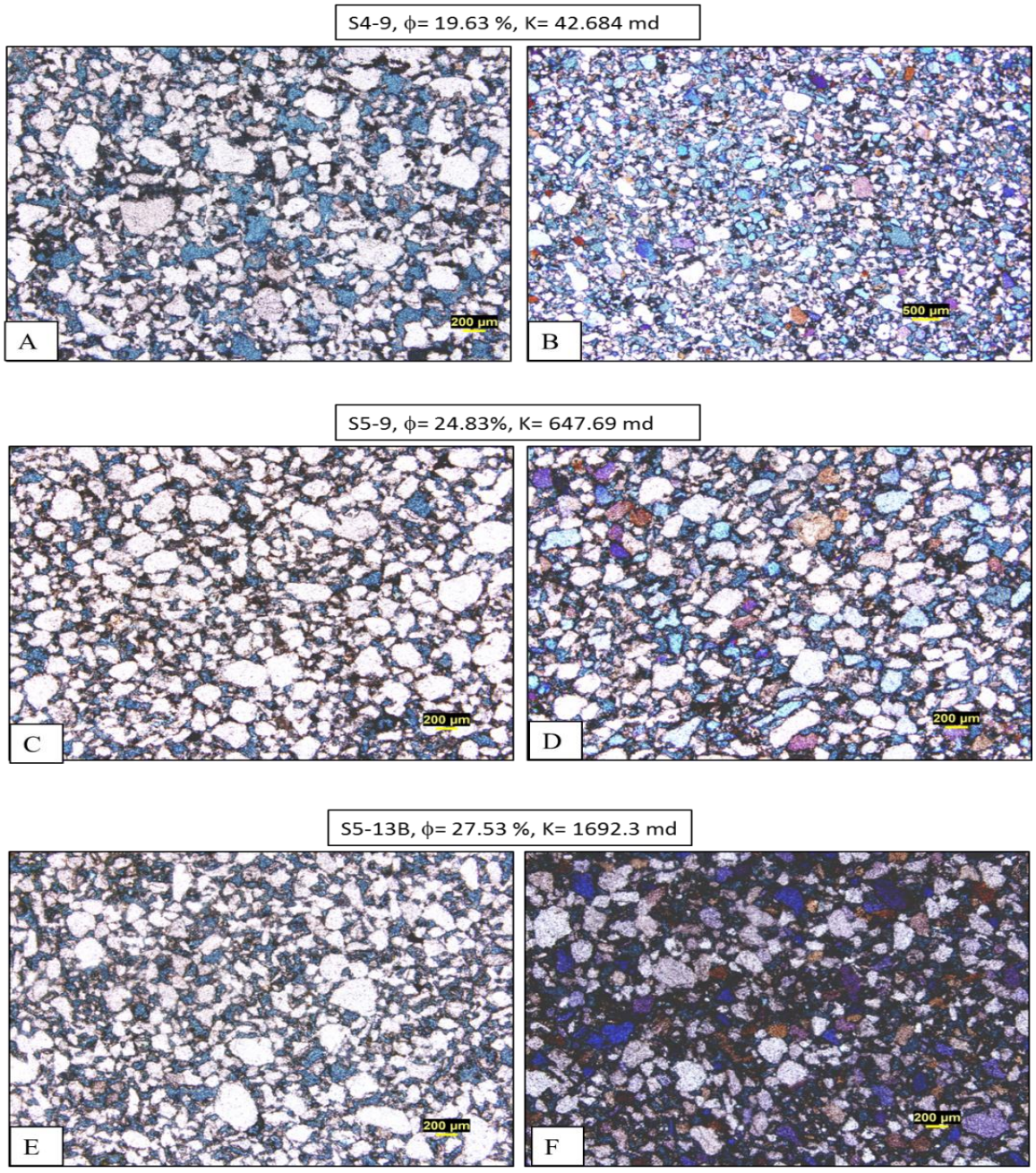


Figure 37: Photomicrographs of Sarah Formation; showing thin-section images of S4-proximal and S5 distal part of Al-Ilb paleochannel; (A) and (B) poorly sorted, sub angular grained sandstone, dominantly monocrystalline quartz. (C) and (D) Moderately well sorted, sub angular, ferruginous sandstone (E) and (F) Ferruginous, monocrystalline, moderately sorted sandstone.

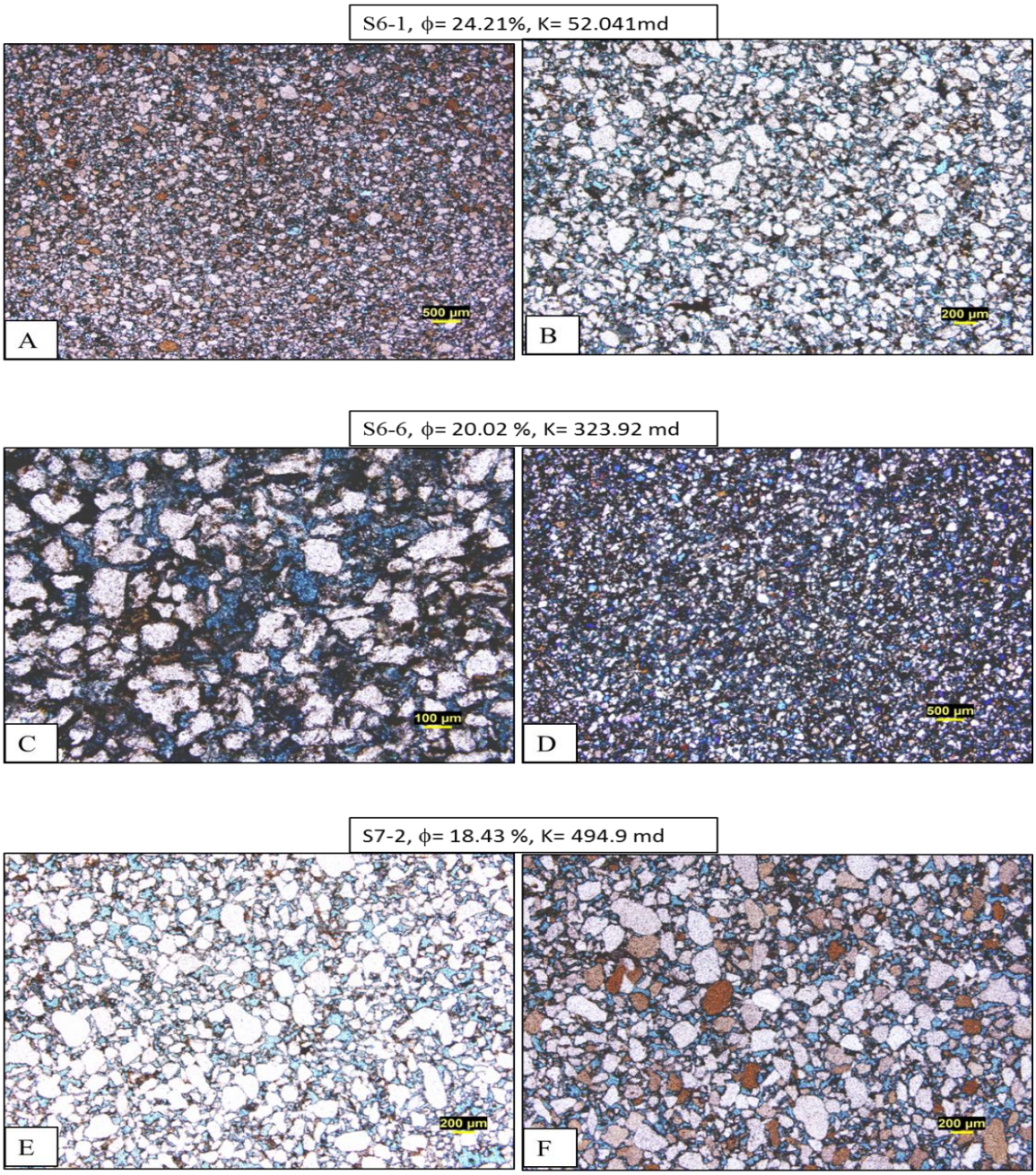


Figure 38: Photomicrographs of Sarah Formation; showing thin-section images of S6 and S7 representing distal part of Al-Ilb paleochannel; (A) and (B) fine grained, ferruginised moderately sandstone. (C) And (D) Highly Ferruginous moderately sorted sandstone, dominantly monocrystalline quartz. (E) and (F) ferruginous sandstone grains, cemented together, poorly sorted, dominantly monocrystalline quartz.

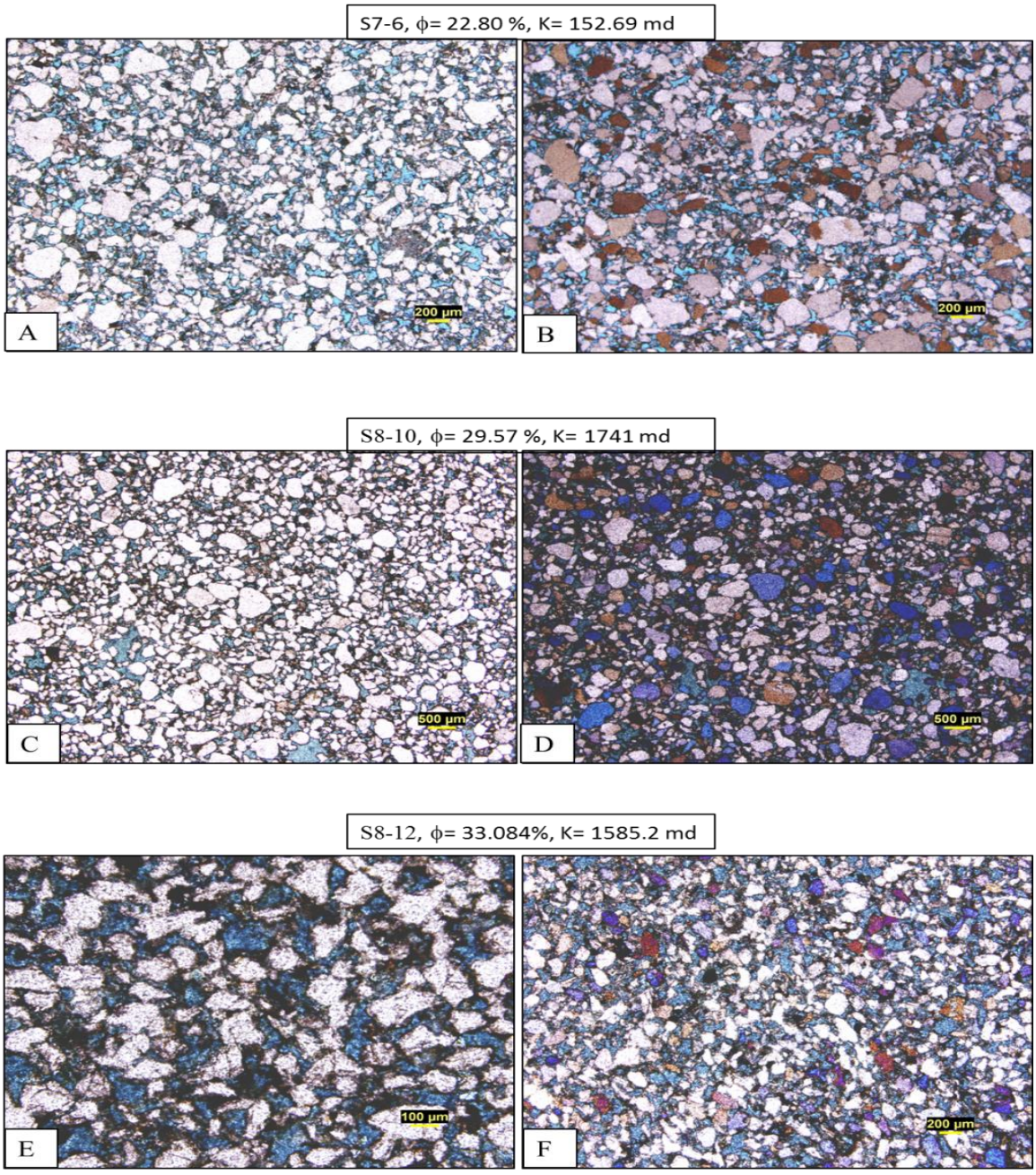


Figure 39: Photomicrographs of Sarah Formation; showing thin-section images of S7 and S8 representing distal part of Al-Ilb paleochannel; (A) and (B) moderately sorted sandstone, ferruginous, dominantly monocrystalline but few polycrystalline. (C) and (D) Moderately sorted, sub rounded grains, ferruginous, dominantly monocrystalline and few polycrystalline (E) and (F) Fine grained, ferruginous sandstone, well sorted, dominantly monocrystalline quartz.

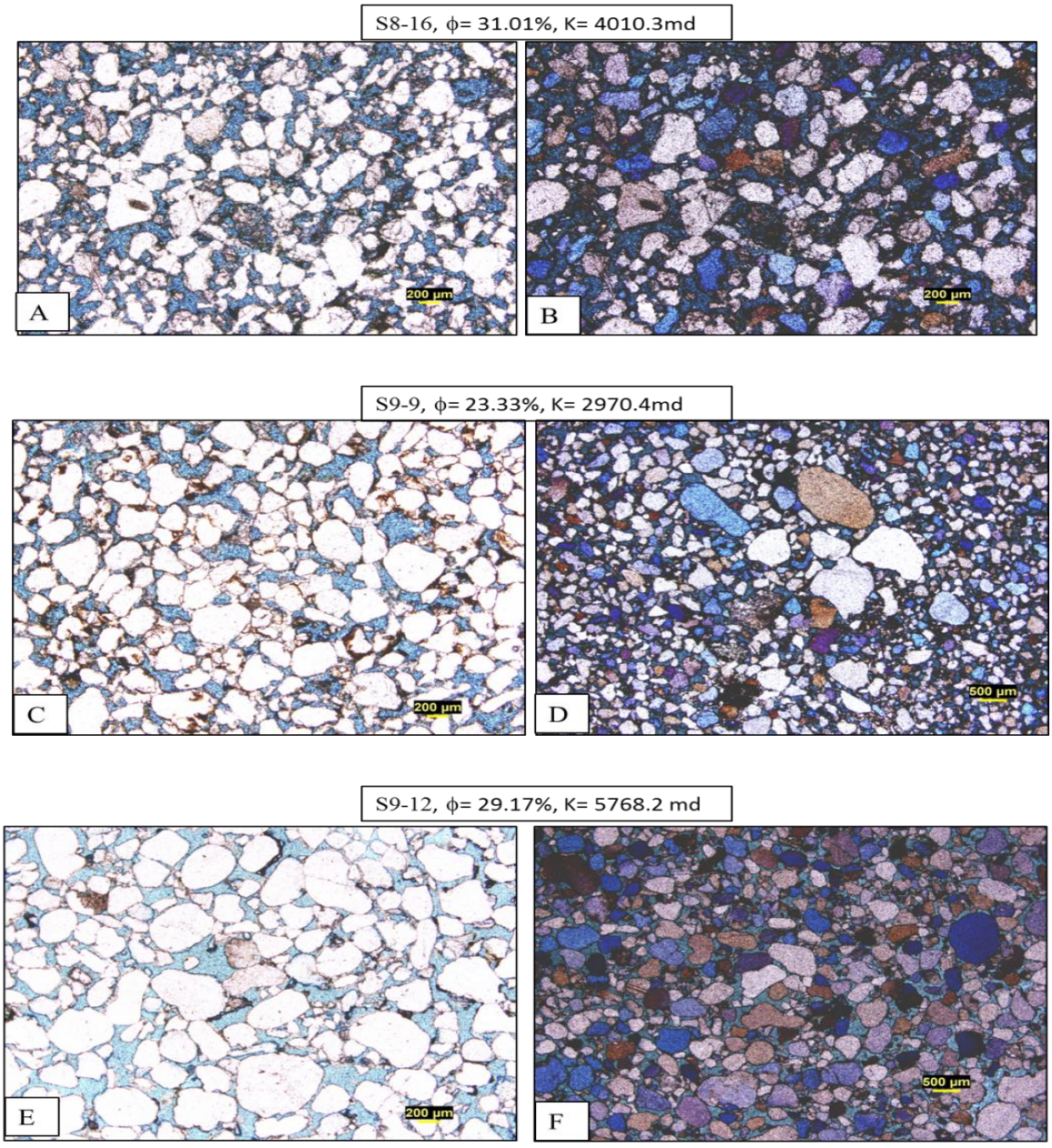


Figure 40: Photomicrographs of Sarah Formation; showing thin-section images of S8 and S9, representing the distal part of Al-Ilb paleochannel; (A) moderately sorted, rounded grains with few iron cement, dominsntly monocrystalline quartz with very good porosity resulting in higher permeability. (C) and (D) Poorly sorted sandstone with rounded grains, dominantly monocrystalline quartz. (E) and (F) Poorly sorted sandstone rounded grains, but very well connected pores increasing permeability.

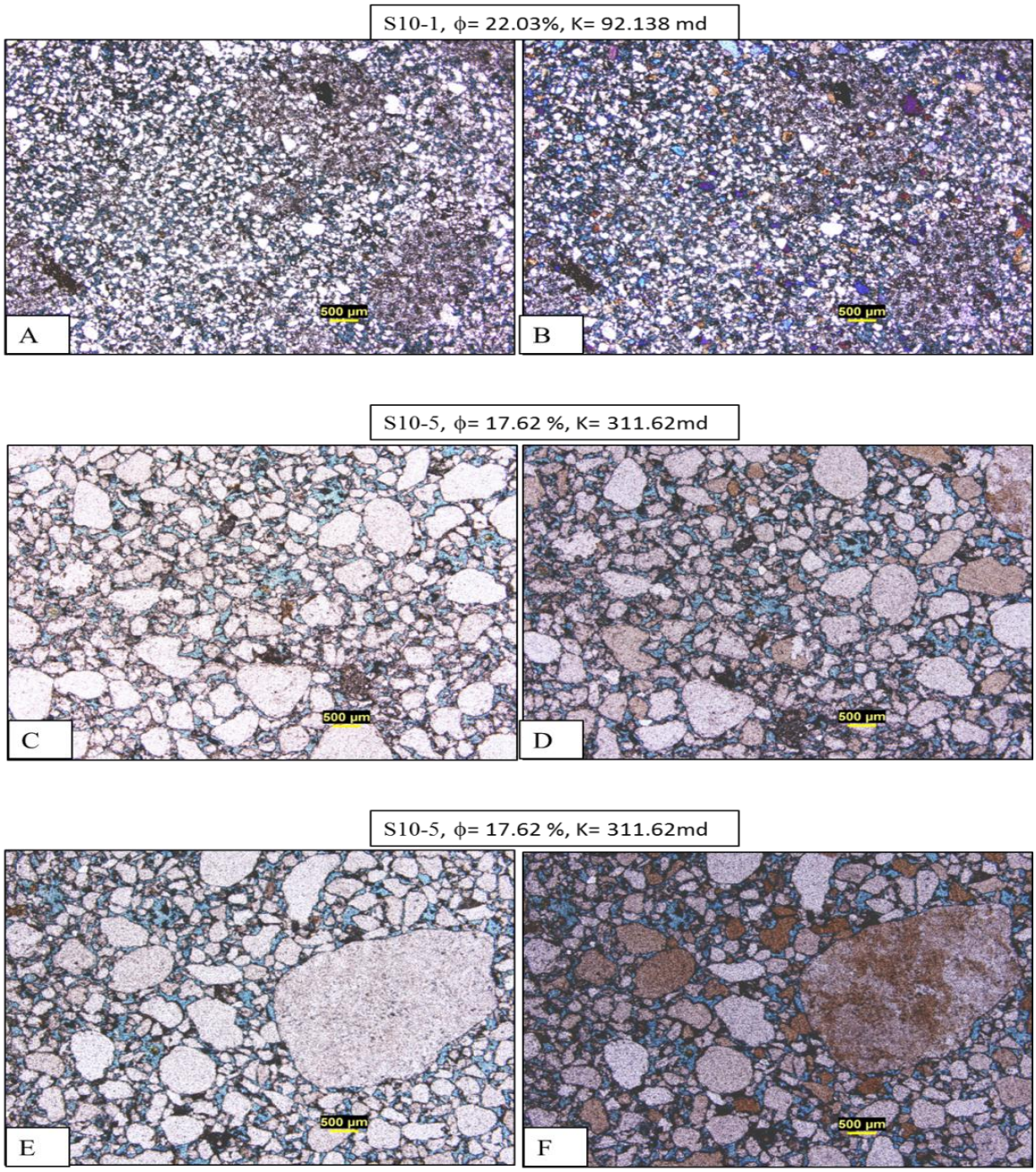


Figure 41: Photomicrographs of Sarah Formation; showing thin-section images of S10, representing the medial part of Al-Ilb paleochannel; (A) and (B) Poorly sorted sandstone with sub rounded grains. Dominantly monocrystalline and appreciable amount of polycrystalline are observed. (C), (D), (E) and (F) Representing the poorly sorted sandstone with iron cementing. Dominantly monocrystalline and little polycrystalline quartz are observed.

### 5.2.2 Sandstone Diagenesis

The Sarah Formation sandstone is classified as “Quartz Arenites” according to Folks scheme of classification. The triangular classification of Sarah Formation shows that 99% of quartz falls within the range of Quartz Arenites. This indicates that the Sarah Formation sandstone is dominantly mature. The diagenesis is mainly depends on composition, depositional environment and burial temperature of sandstone. Both the sandstone facies and glacial facies show the dominance of quartz i.e. more stable mineral over less stable mineral like feldspar, mica and rock fragment. The samples show no clear evidence of feldspar or any other less stable minerals (Figure 62). Monocrystalline is dominant over polycrystalline quartz in general in all the studied samples of (Table 6). The dominance of monocrystalline quartz may indicate reworking process, leading to the removal of undulatery in polycrystalline. Most of the depositional environment shows common digenetic features on quartz. It occurs in mineralogically matured sandstone. The mature quartz arenite samples suggest a shallower burial condition.

The absence of iron cement, grain coating, pore filling clay minerals and initial dissolution of detrital grains in sandstone indicates early diagenesis. No such clear evidence is observed that leads to the indication of early diagenesis. Only authigenic clays are present dominantly in most of the samples. Preferably, authigenic quartz overgrowth, pore filling clay, authigenic feldspar, illite and chlorite are the key indications of burial diagenesis.

In general, the burial diagenesis reduces the porosity, but primary porosity may be preserved because of clay coating and pore lining. Cementation process is being ceased by further clay coating (Wilson and Pittman, 1977). The observed digenetic features are discussed in the following paragraph.

**Cement**

Different stages of cementation are observed in samples. Calcite represents the earliest cementation episode and it occurs in patchy or thin rims around the detrital grains it has been formed by replacement. If replacement doesn't happen then calcite occurs as poiklitic calcite, occupying most of the available pores. Some calcite (SEM) has been observed in few samples. This was also proved by the XRD results. The XRD analyses indicate minor calcite cement in some samples. It is due to the precipitation of calcium from detrital minerals and other carbonates components of the sediments.

The next episode of cementation is identified by the presence of the ferruginous cement i.e. hematite (Figure 33, Figure 34, Figure 35, Figure 37, Figure 38, Figure 39, Figure 40, Figure 41). Almost all the samples are ferruginised and it is clearly identified by the thin-section and as well as the SEM-EDX and the XRD results. The origin of iron leaching is caused by the decomposition of hornblende and mica or from lateritic soils (Burly, 1984).

Silica cement is also observed in some of the samples. And the possible source of silica cement is weathering or digenetic dissolution of detrital silicates especially feldspar (by meteoric water). Another possible source of silica cement is unstable volcanic glass, rock

fragment and etc. The cause of silica cement in Sarah Formation is probably feldspar dissolution or kaolinization. Another cause of silica cement may be pressure solution as noticed in some of the samples. Clay cement is very common in most of the samples that coat the quartz grains from all the sides. It is due to the mechanical infiltration of detrital clays or the authigenic origin.

To summarize the authigenic minerals in the thin-sections of Sarah Formation include clay minerals i.e. (kaolinite, illite, chlorite and palygorskite) (Figure 56, Figure 57, Figure 62), and pore filling poikilotopic chlorite, authigenic quartz, potash-feldspar and iron oxide along with the grain coating. The quartz overgrowth is observed in some samples. It starts around the rim of the grains and usually grows inward filling of pores.

### 5.2.3 Scanning Election Microscopy (SEM)

The samples were examined with the SEM, and elemental composition of each element was identified to reveal the textural relationship and mineralogy. Ten representative samples were selected for SEM micro studies. The microphotographs show textural relationship at low magnification i.e. 200 micro meters. High magnification up to 2 micro meters is needed for further surficial details and crystal morphological studies

The SEM studies of the samples show the grain surface morphology, the contact and relationship of grains with cementing material, (Figure 54, Figure 55Figure 56, Figure 57, Figure 58, Figure 59, Figure 60, Figure 61 and Figure 62). The images show that the hematite occur as the pore filling cement with honey comb, ball shaped bodies occupying

the pores and coating the grains in fan shaped i.e. cover from all sides (Figure 57, Figure 58, Figure 54). Booklet structure of kaolinite is clearly observed in most of the samples (Figure 55, Figure 56, Figure 59, Figure 60 and Figure 62). The most important palygorskite clay occurs in sample S10-1 (Figure 62), imparting the distinguishing characteristics. The EDX results revealed that the samples are dominantly rich in silica cement and iron is recoded in all the samples. Significant amount of Al, Fe, Mg, and Ca are also recorded; because of the presence of kaolinite, illite, chlorite, palygorskite.

### 5.2.4 X-Ray Diffraction (XRD)

The XRD is a semi-quantitative technique primarily used for crystalline materials to determine the weigh percentage of major crystalline phase to few weight percent (phase identification). Phase identification technique basically calculates the most likely matched peaks for the given phase based on the peak intensity and 2theta. Then it is compared with the standard phase to identify the exact mineral phase. Ten powered samples were analyzed to identify the mineral phase. The XRD results confirm the thin-section petrographic findings and the SEM-EDX results. The results indicate that quartz is the dominant mineral. Besides the presence of quartz, the dominant phases identified in almost all the samples are kaolinite and iron oxide.

Table 7: Thin section petrographic results of selected samples of Sarah Formation for XRD and SEM-EDX

| Thin Section ID | Poro(%) | K(md) | MGS (µm) | Porosity (%) Vis | Sorting | | Shape | Quartz Grains | | | Feldspar (%) | Mica (%) | Lithic Fragment (%) | Heavy Mineral (%) | Cement (%)Iron Oxide | Matrix (%) |
|---|---|---|---|---|---|---|---|---|---|---|---|---|---|---|---|---|
| | | | | | | | | Mono(%) | Poly (%) | Qtz | | | | | | |
| S1-9 | 18.32 | 1742.10 | 254.72 | 22 | PS | 1.15 | S. Rounded - Rounded | 96 | 4 | 92 | 1 | 0 | 0 | 0.1 | 3 | 1 |
| S2-4 | 22.50 | 138.94 | 100.00 | 22 | MS | 0.67 | | 98 | 2 | 94 | 1 | 0 | 0 | 0 | 7 | 2 |
| S3-1A | 20.37 | 285.84 | 186.17 | 22 | MS | 0.67 | S. Rounded | 97 | 3 | 95 | 1 | 0 | 0 | 0 | 6 | 3 |
| S4-12 | 19.63 | 53.00 | 256.25 | 25 | PS | 1.15 | | 98 | 2 | 92 | 1 | 0 | 0 | 0 | 8 | 6 |
| S5-2B | 28.28 | 177.04 | 78.13 | 24 | WS | 0.36 | Sub Angular | 99 | 1 | 86 | 1 | 0 | 0 | 2 | 7 | 6 |
| S6-1 | 24.22 | 50.40 | 151.89 | 22 | MS | 0.74 | | 98 | 2 | 88 | 1 | 0 | 0 | 0.1 | 8 | 10 |
| S7-6 | 22.81 | 152.69 | 181.03 | 21 | MS | 0.74 | S. Rounded | 98 | 2 | 93 | 1 | 0.1 | 0 | 0.1 | 5 | 8 |
| S8-16 | 31.02 | 3881.60 | 229.17 | 27 | MS | 0.74 | | 98 | 2 | 94 | 1 | 0 | 0 | 0 | 2 | 4 |
| S9-9 | 23.33 | 2970.40 | 483.87 | 25 | PS | 1.15 | Rounded-W. Rounded | 98 | 2 | 95 | 1 | 0 | 0 | 0 | 4 | 2 |
| S10-1 | 22.04 | 92.14 | 227.94 | 21 | MS | 0.74 | | 98 | 2 | 92 | 1 | 0 | 0 | 0 | 4 | 2 |

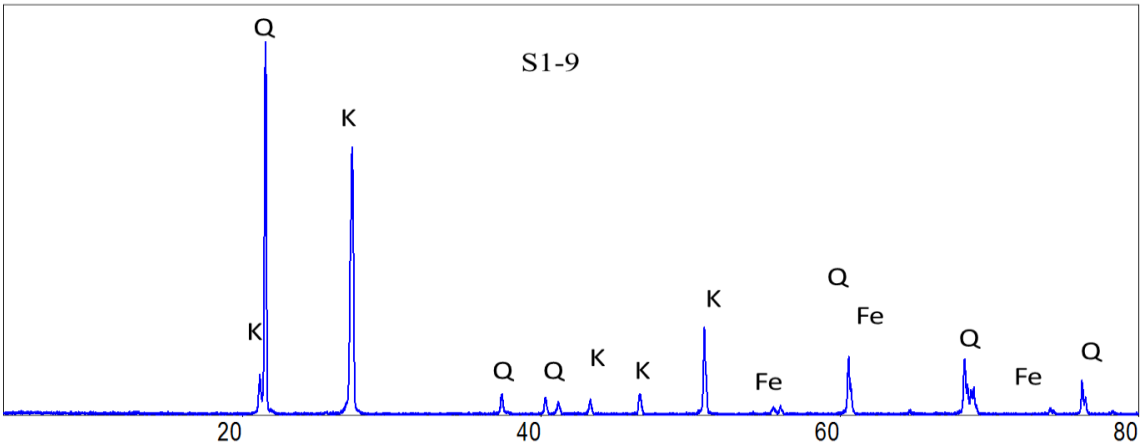


Figure 42: XRD results of Sarah Formation samples; Q= Quartz, K= Kaolinite and Fe= Iron oxide.

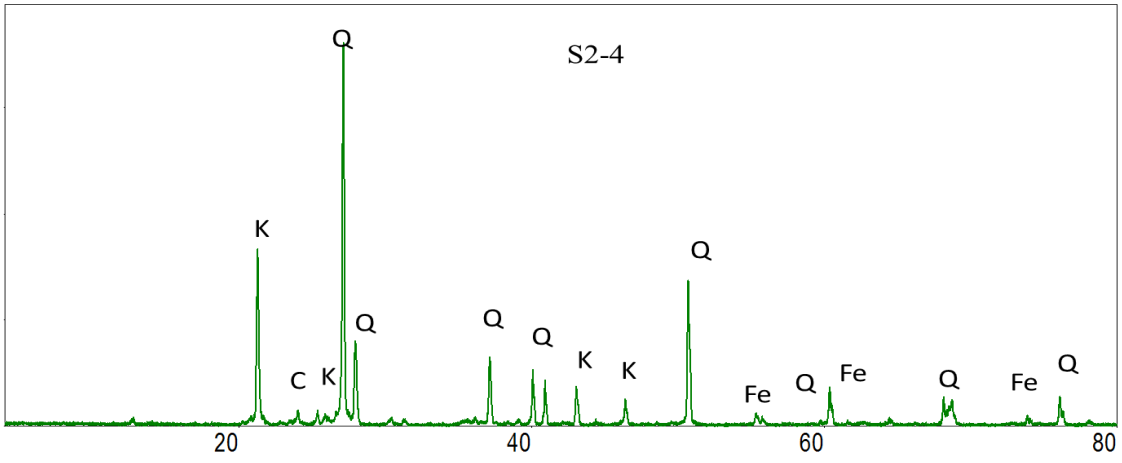


Figure 43: XRD results of Sarah Formation samples; Q= Quartz, K= Kaolinite Fe= Iron oxide and C= Chlorite.

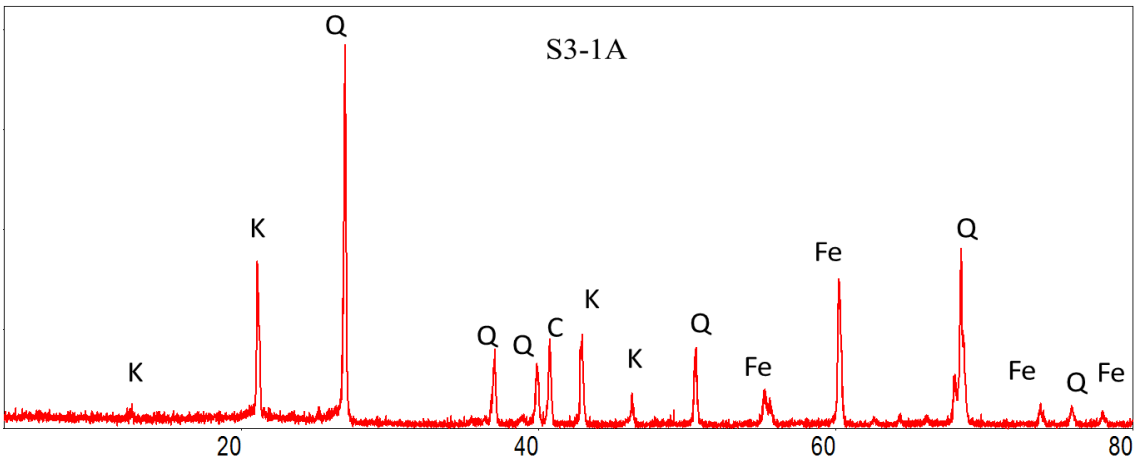


Figure 44: XRD results of Sarah Formation samples, Q= Quartz, K= Kaolinite Fe= Iron oxide and C= Chlorite.

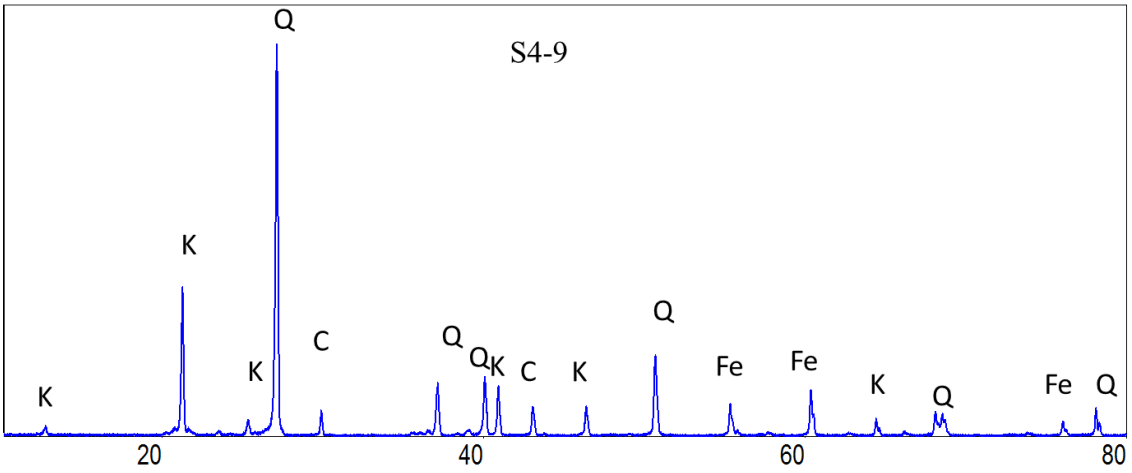


Figure 45: XRD results of Sarah Formation samples, Q= Quartz, K= Kaolinite Fe= Iron oxide and C= Chlorite.

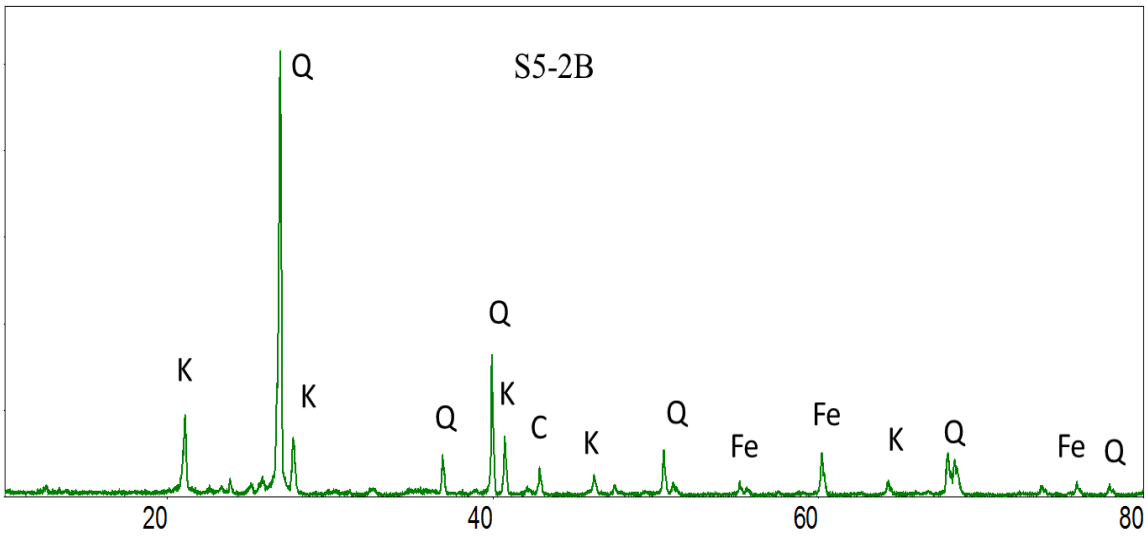


Figure 46: XRD results of Sarah Formation samples, Q= Quartz, K= Kaolinite Fe= Iron oxide and C= Chlorite.

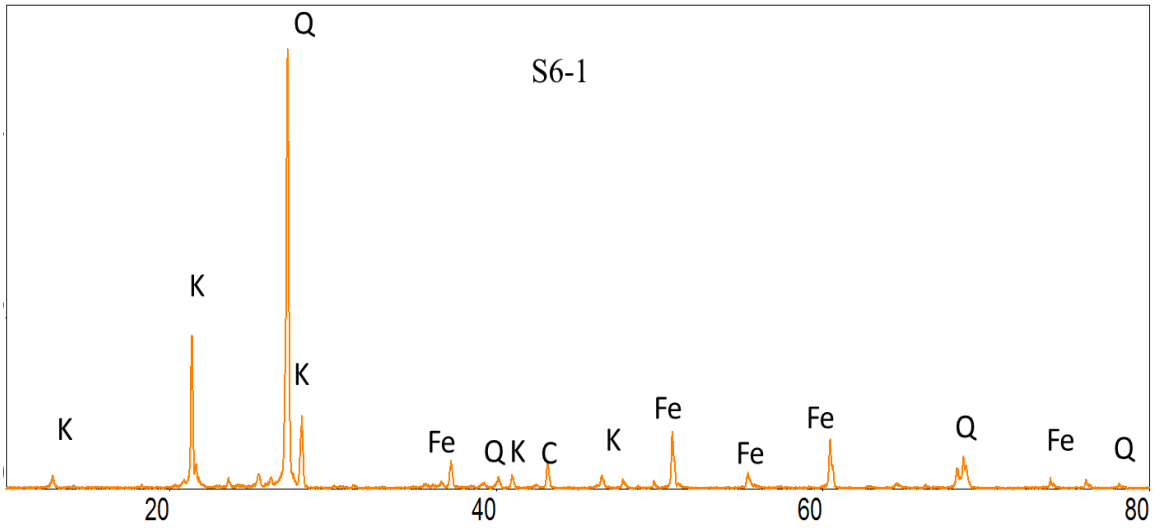


Figure 47: XRD results of Sarah Formation samples, Q= Quartz, K= Kaolinite Fe= Iron oxide and C= Chlorite.

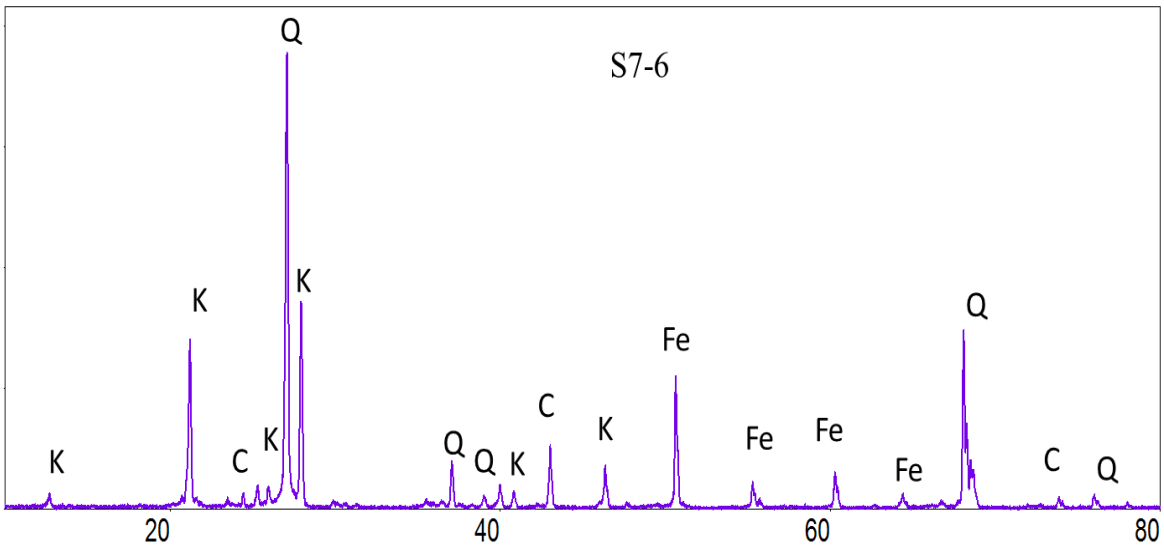


Figure 48: XRD results of Sarah Formation samples, Q= Quartz, K= Kaolinite Fe= Iron oxide and C= Chlorite

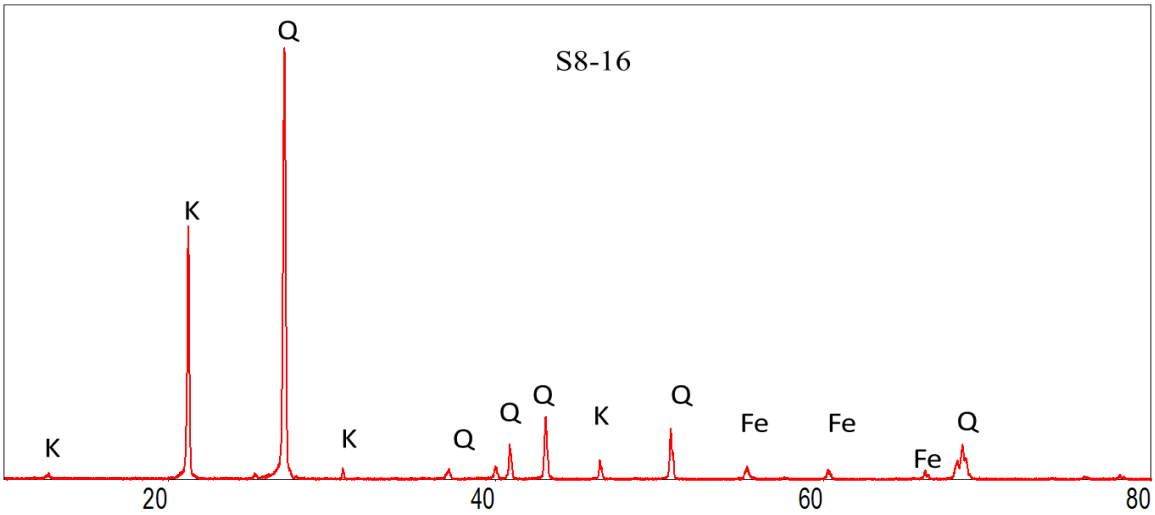


Figure 49: XRD results of Sarah Formation samples, Q= Quartz, K= Kaolinite and Fe= Iron oxide.

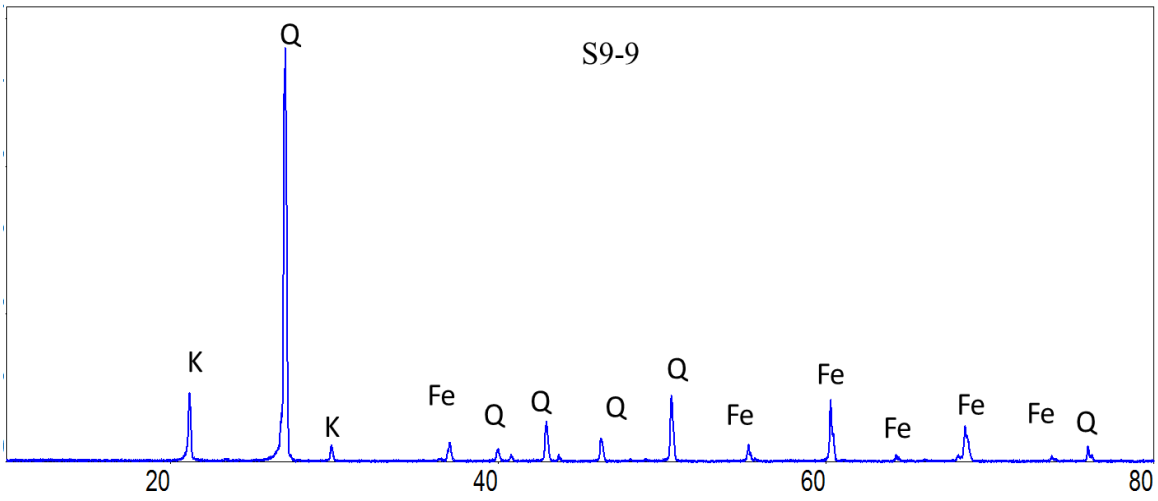


Figure 50: XRD results of Sarah Formation samples, Q= Quartz, K= Kaolinite Fe= Iron oxide and C= Chlorite

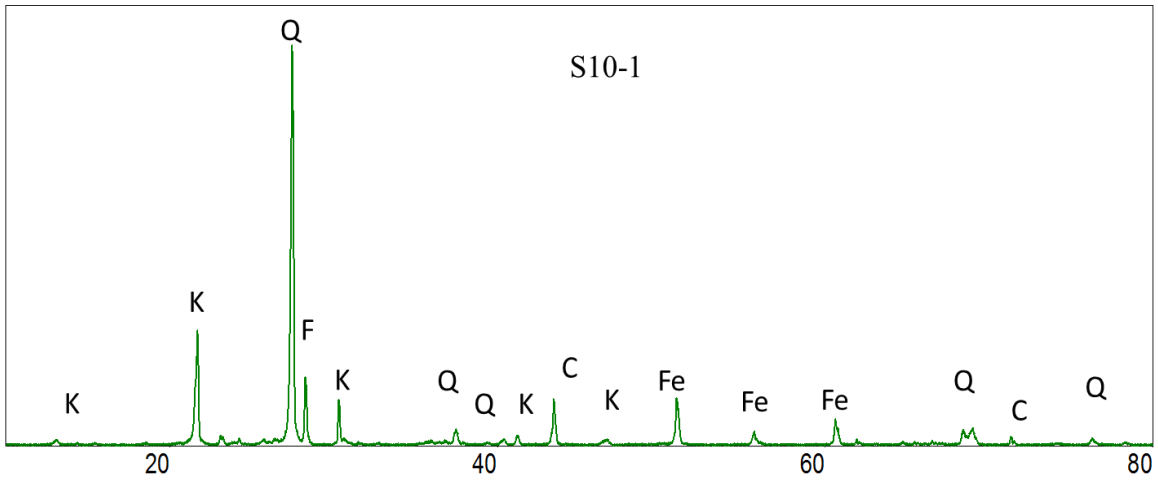


Figure 51: XRD results of Sarah Formation samples, Q= Quartz, K= Kaolinite Fe= Iron oxide and C= Chlorit e

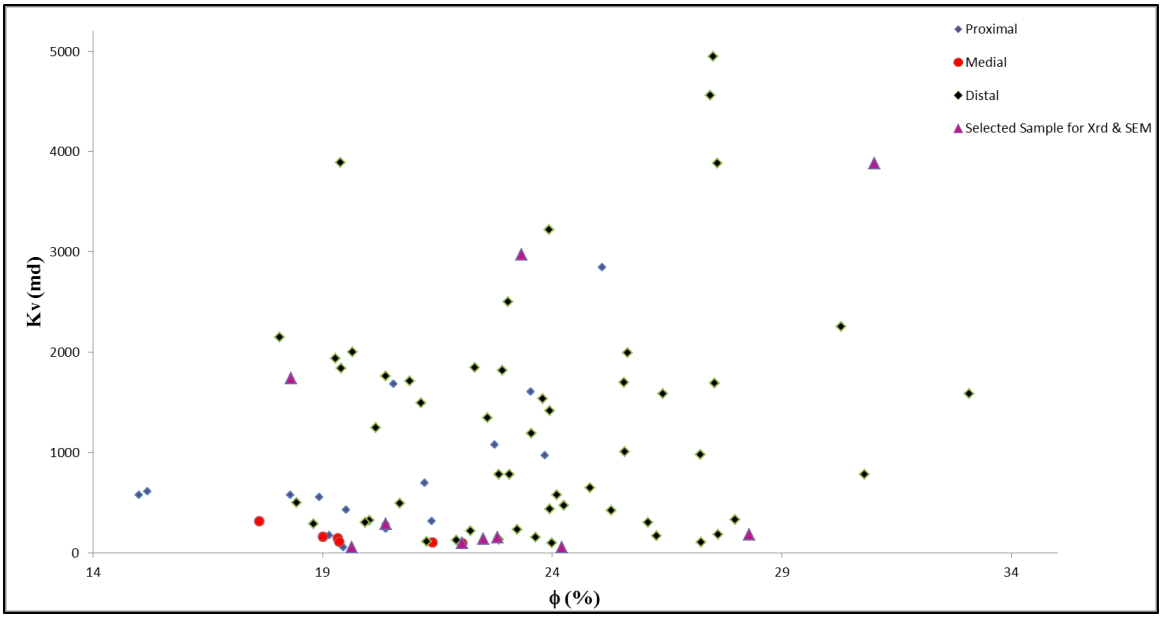


Figure 52: Selected samples for SEM-EDX, CT-scan and XRD from the whole data set covering different categories of porosity vs. permeability cross plot.

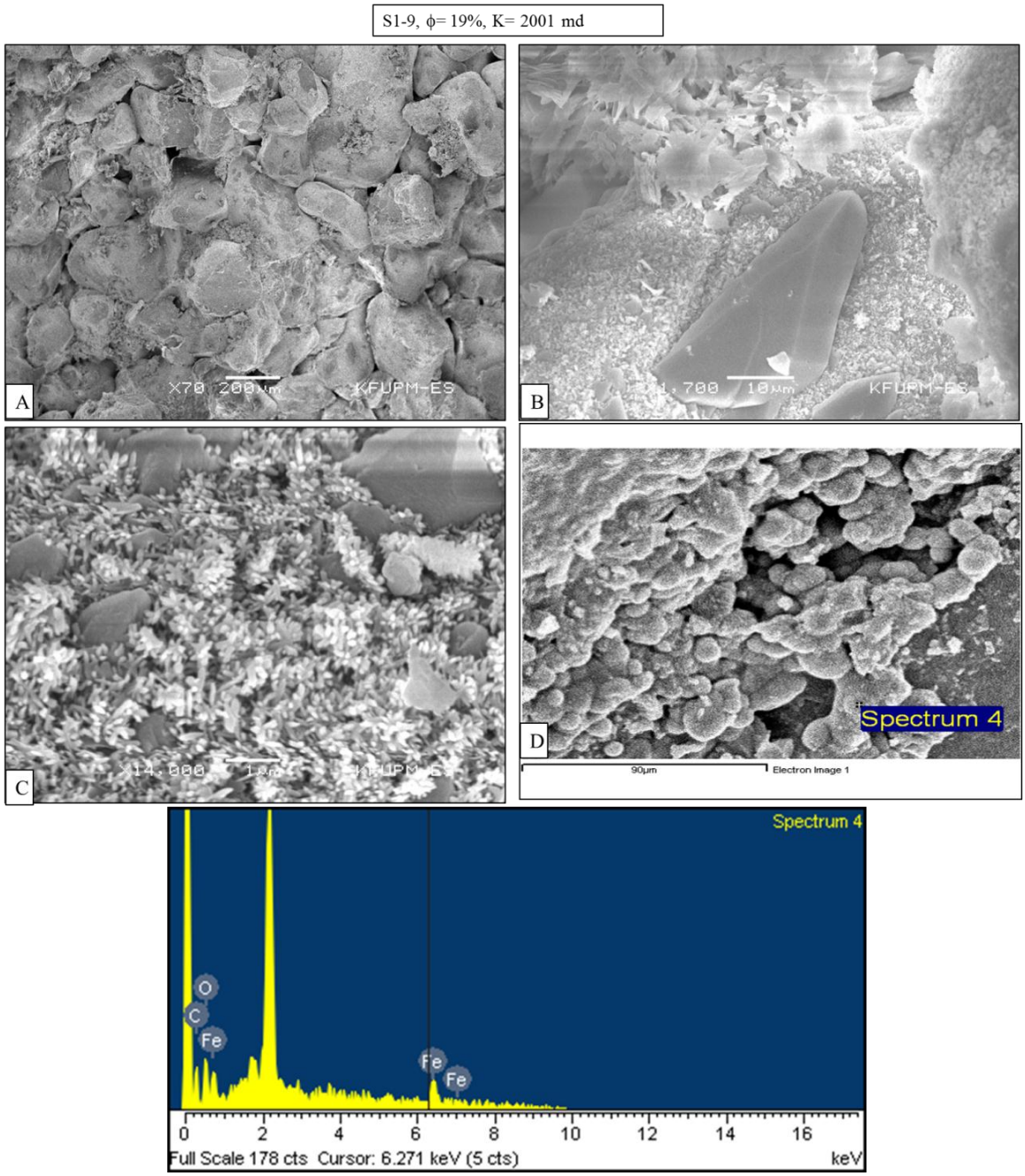


Figure 53: SEM photomicrograph of Sarah Formation (A) moderately to poorly sorting, highly leached sandstone. (B) And (C) Sub-angular quartz grains along with iron oxide. (D) Grape structure of iron oxide.

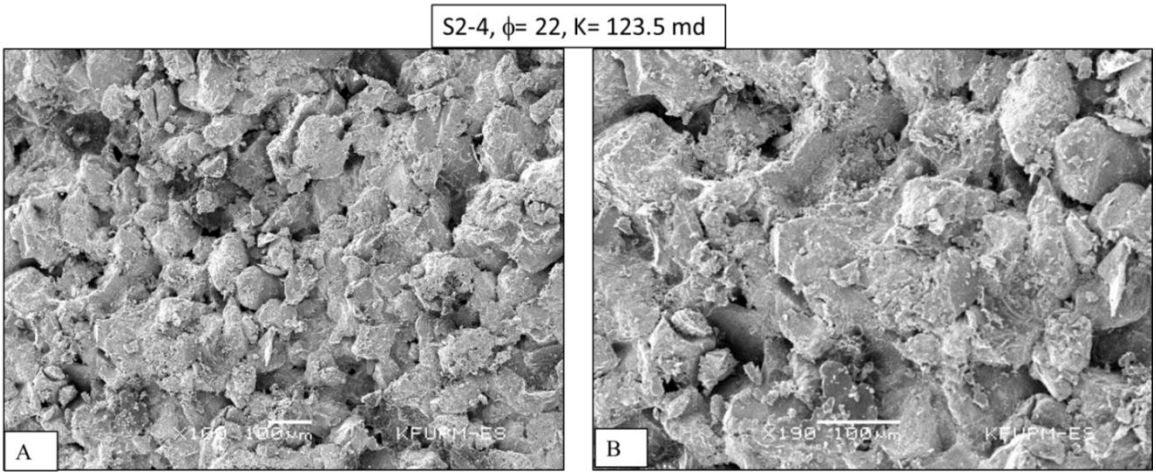


Figure 54: Photomicrograph of Sarah Formation showing (A) Moderately sorted, highly leached sandstone. (B) Dominance of iron coating and filling the pores, responsible for low porosity.

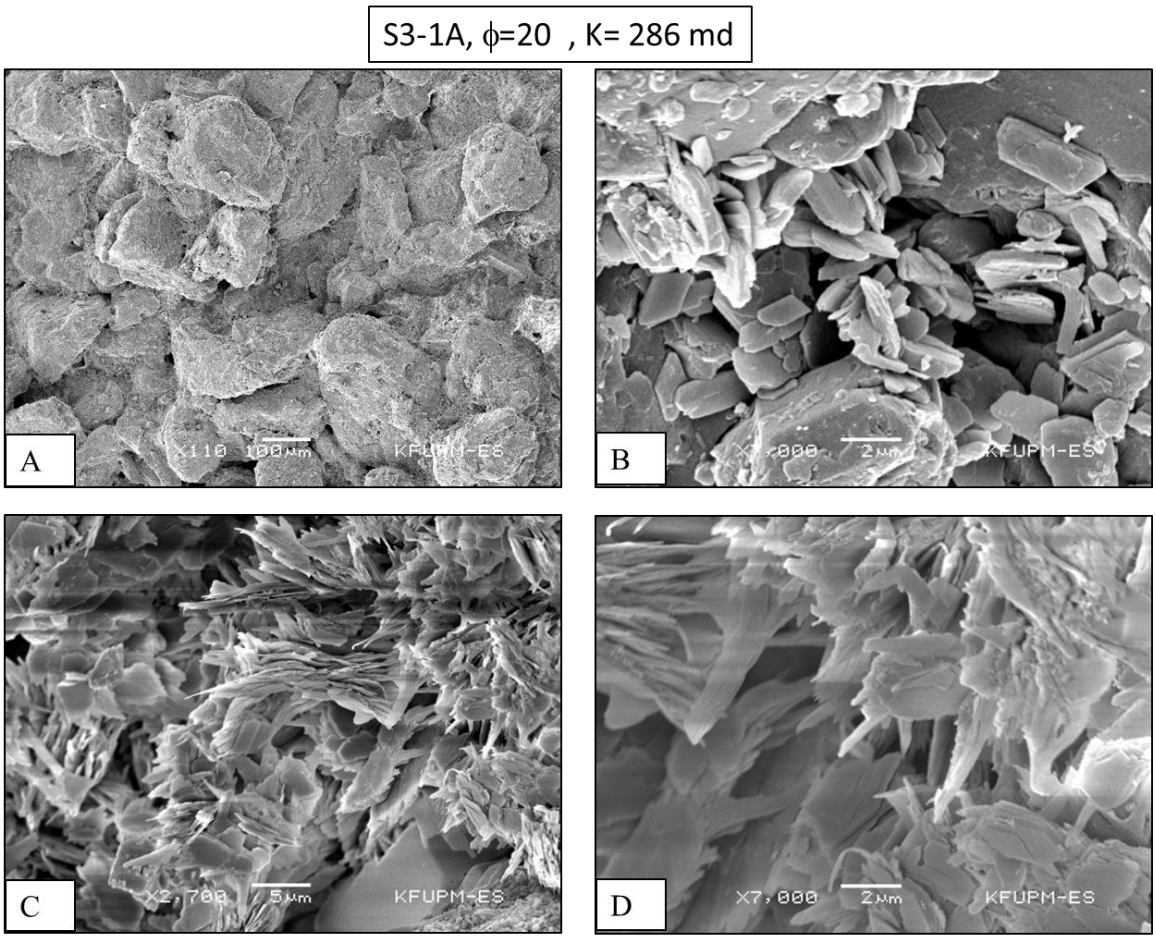


Figure 55: Photomicrograph of Sarah Formation sandstone representing the proximal part of Al-Ilb paleochannel. (A) Moderately sorted sandstone. (B) Booklet structure of kaolinite filling the pores (C) Mixture of quartz and kaolinite (D) Kaolinite and iron oxide filling the pores, (responsible for the low permeability)

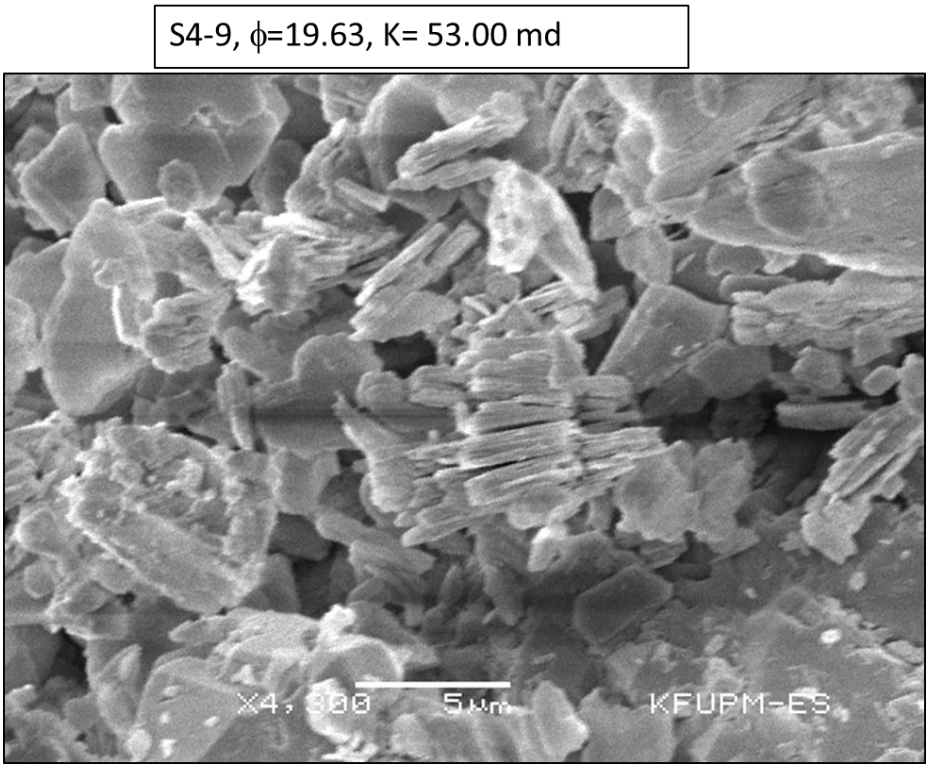


Figure 56: Photomicrograph of Sarah Formation sandstone representing the proximal part of Al-Ilb paleochannel. (A) Booklet structure of kaolinite filling the pores responsible for low permeability.

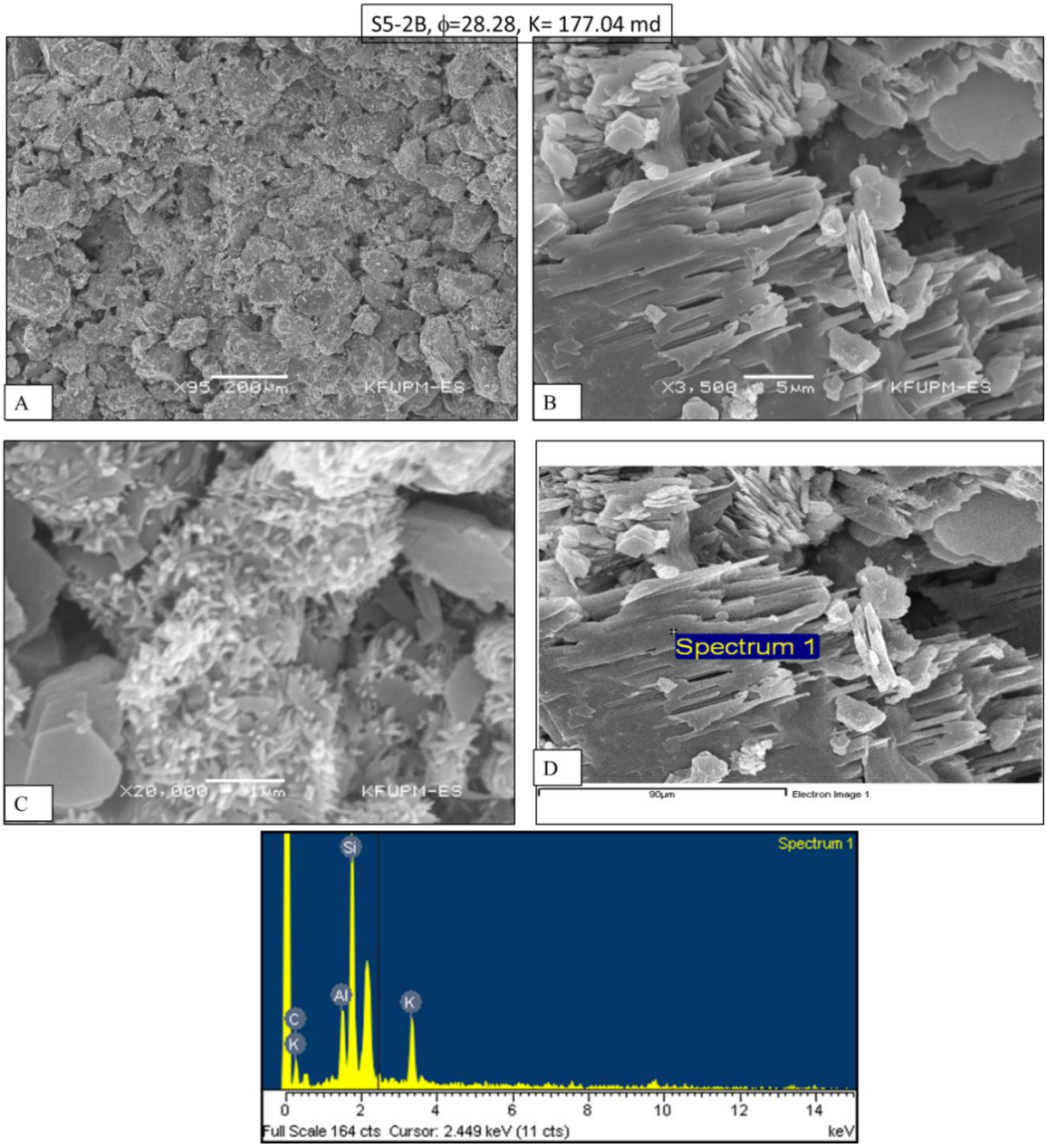


Figure 57: Photomicrograph of Sarah Formation sandstone representing the distal part of Al-Ilb paleochannel. (A) Well sorted highly leached grained sandstone. (B) Kaolinite filling the pores (C) Iron oxide and kaolinite filling the pores; (responsible for low porosity). (D) EDX results, confirming the presence of kaolinite.

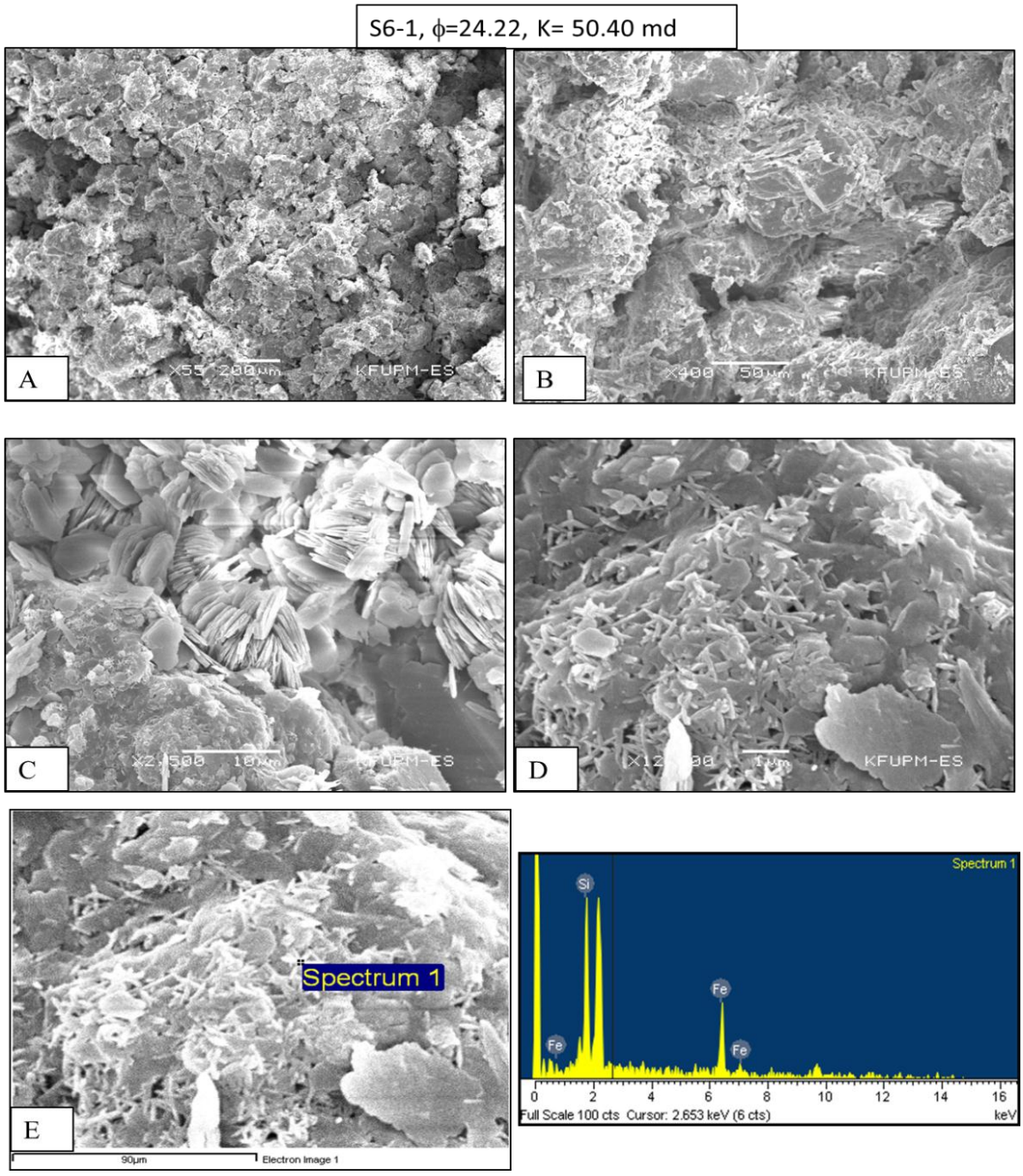


Figure 58: Photomicrograph of Sarah Formation sandstone representing the distal part of Al-Ilb paleochannel. (A) And (B) Moderately sorted, highly leached grained sandstone. (C) Booklet structure of kaolinite filling the pores (D) and (E) highly oxidized (iron) cement on kaolinite filling the pores, (highly responsible for the reduction of effective porosity)

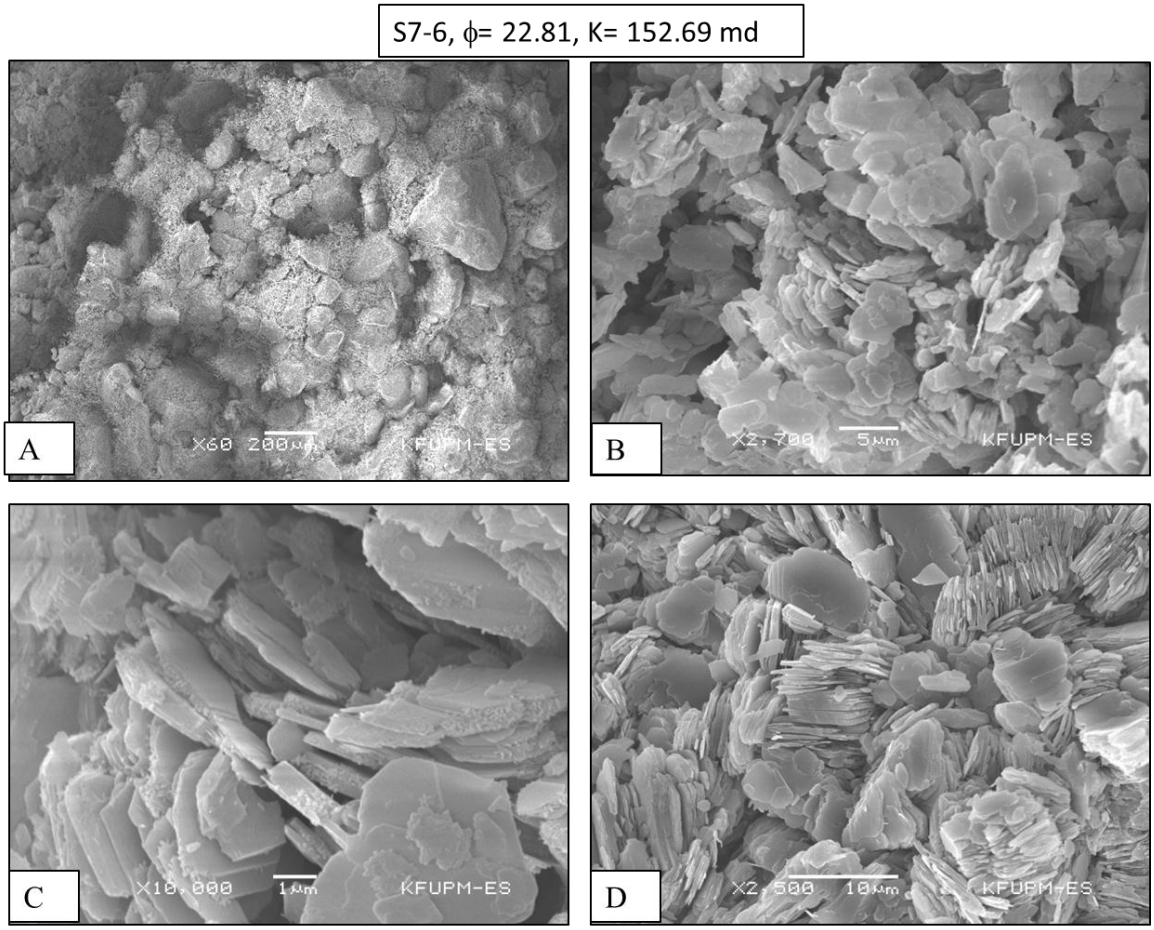


Figure 59: Photomicrograph of Sarah Formation sandstone representing the distal part of Al-Ilb paleochannel. (A) Moderately sorted highly leached sandstone. (B), (C) and (D) Platy structure of kaolinite is responsible for low permeability; (C) showing some fractures on kaolinites.

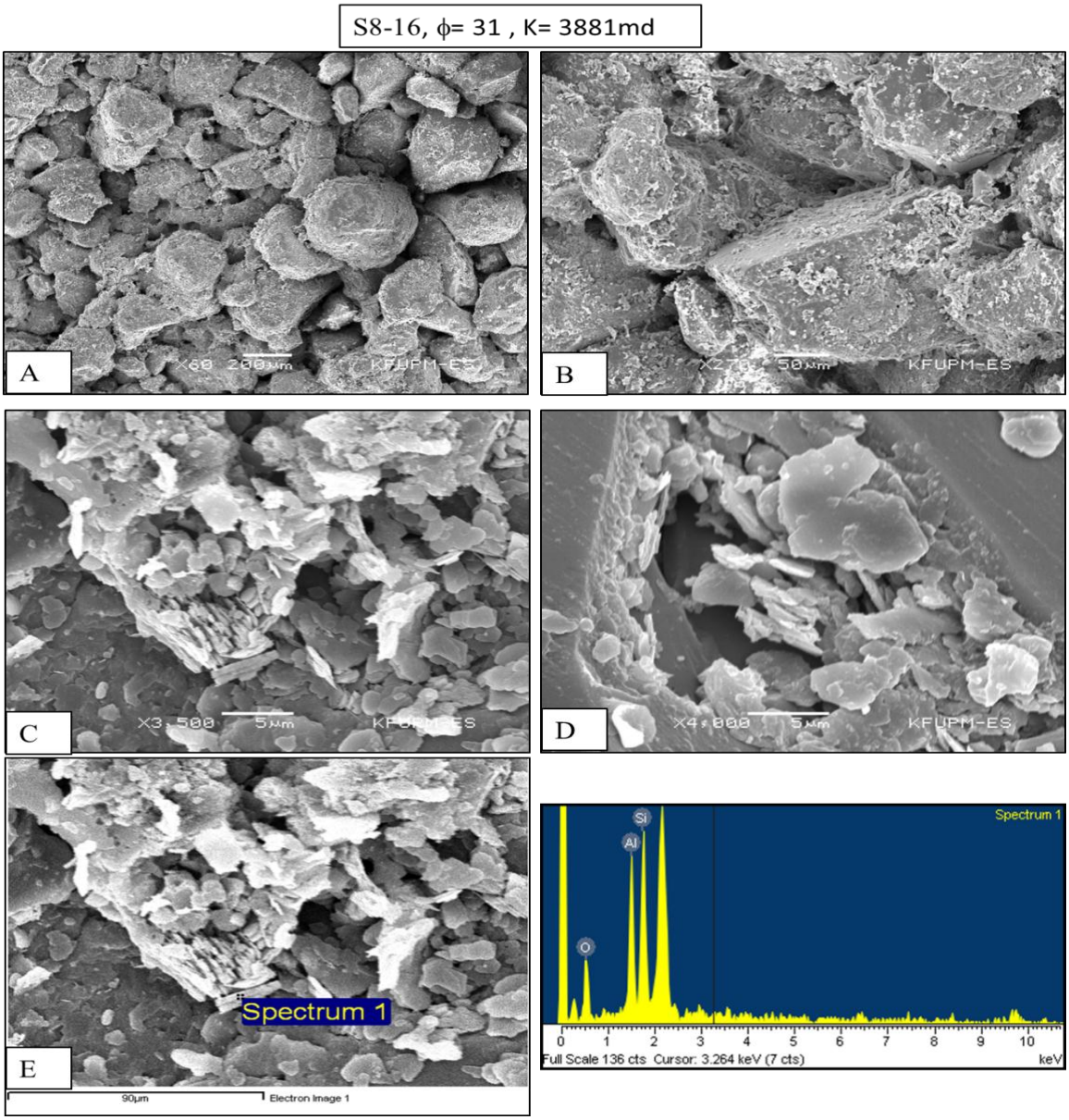


Figure 60: Photomicrograph of Sarah Formation sandstone representing the distal part of Al-Ilb paleochannel. (A) Moderately to well sorted sandstone. (B) Leached quartz, representing high degree of weathering (C), (D) and (E) platy structure of kaolinite filling the quartz, The permeability of the sample is high because of low quantity of kaolinite filling the pores.

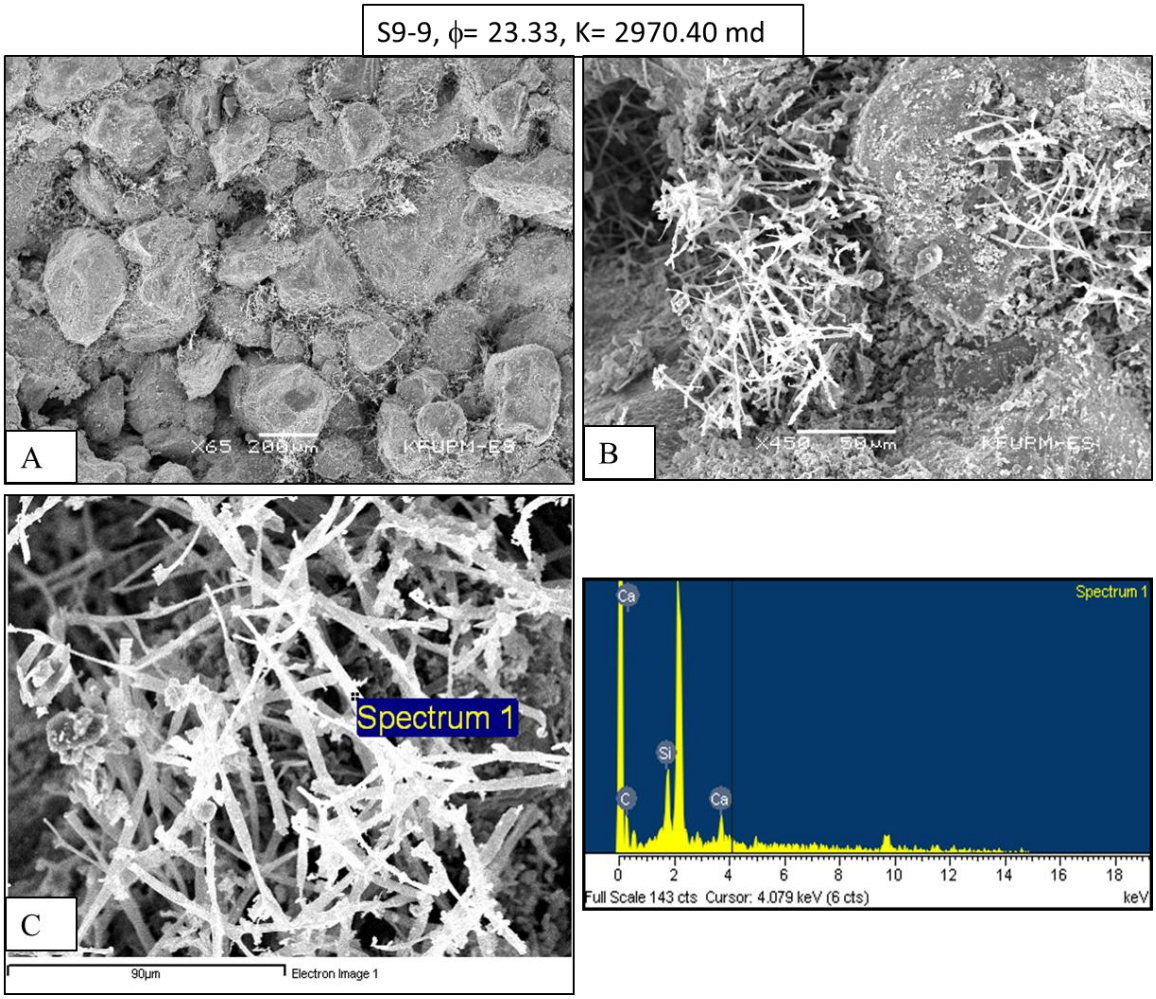


Figure 61: Photomicrograph of Sarah Formation sandstone representing the distal part of Al-Ilb paleochannel. (A) Poorly sorted, highly leached sandstone. (B) Palygorskite clay found within the pores. (C) Palygorskite clay acting as bridge between the pores.

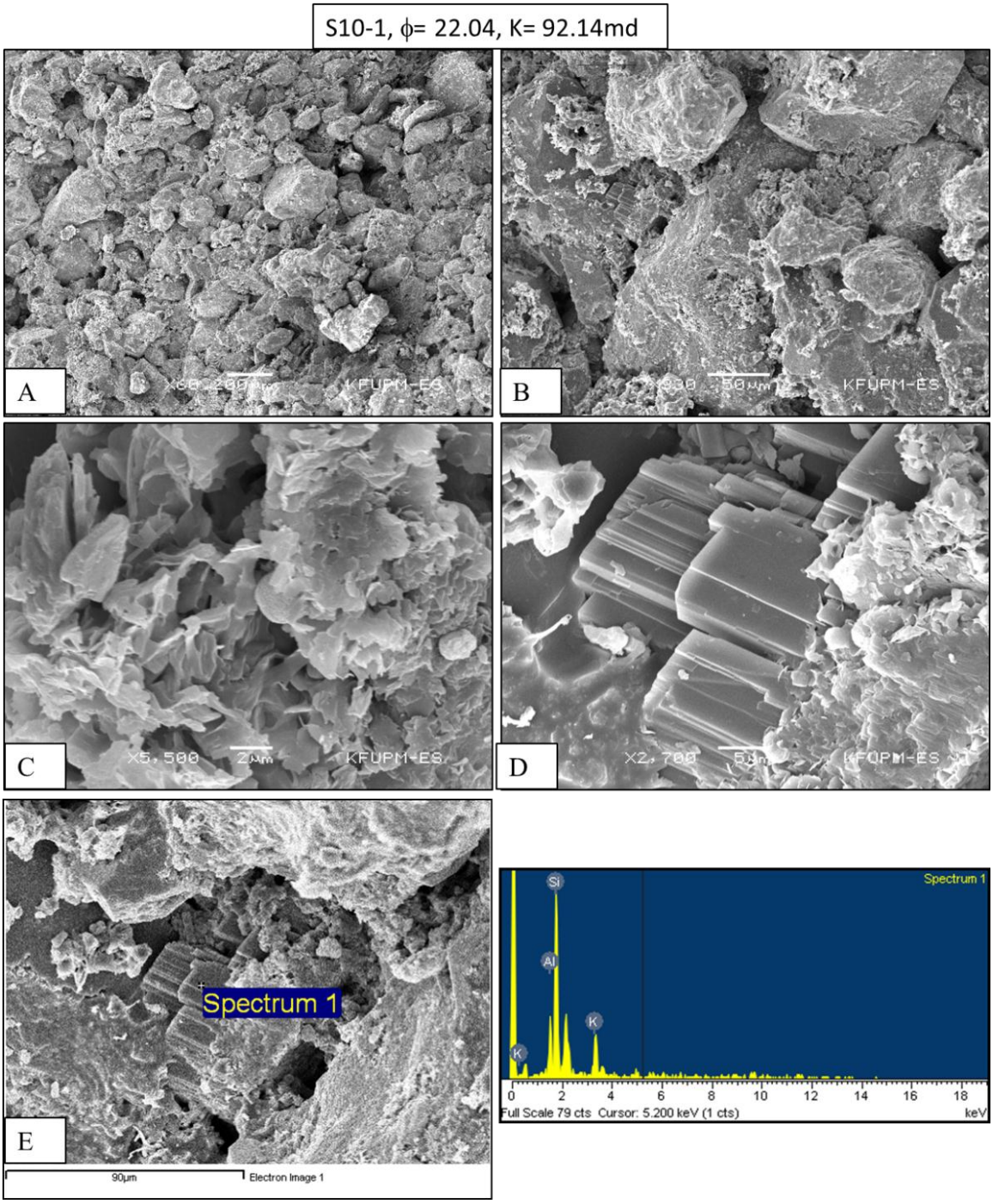


Figure 62: Photomicrograph of Sarah Formation sandstone representing the distal part of Al-Ilb paleochannel. (A) & (B) Moderately to poorly sorted, highly leached sandstone. (C) Smectite clay showing leaf like structure. (D) and (E) feldspar partially altered to clay; smectite clay block the pores and responsible for low permeability.

### 5.2.5 Computed Tomography Scanning (CT-Scan)

The CT-scan is based on digitally cutting sample in to several hundreds of thousands of slices and then reconstructs it into one unified image. This technique is non-destructive and one can easily see the internal feature of the object form different dimensions. The CT-scan gives in both quantitative and qualitative information for the samples. Qualitative analysis in term of visual identification of different material on the base density contrast. And quantitative analysis in term of no. of open pores, close pore and porosity. The CT-scan images reveal the dominantly the sample is composed of one material i.e. Quartz and some bright spots represents iron oxide (because of highest density) Figure 63.

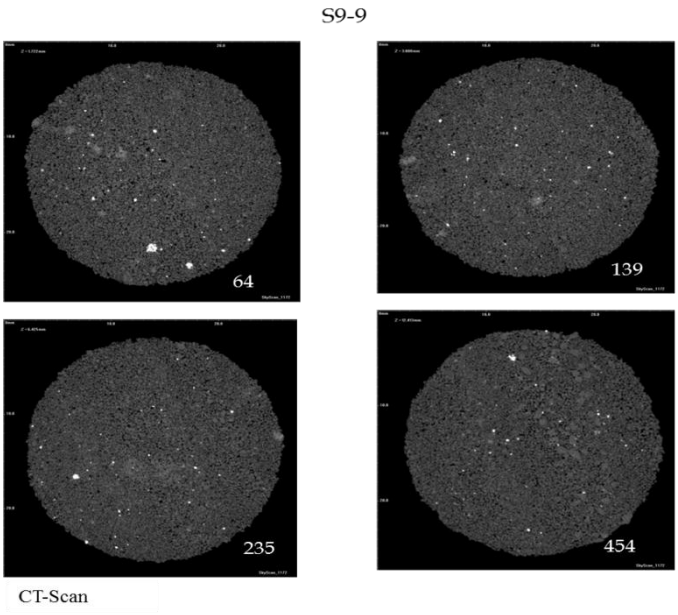


Figure 63: CT-Scan images showing different slices of sample S9-9, indication the distribution iron oxide (bright spots) and grayish (quartz) and black pores.

## 5.3 Discussion and Interpretation of Petrographic Studies

The sandstones of Sarah Formation are classified as mature quartz arenites with 99% quartz. Feldspar and rock fragment are less than 1% (Figure 29). The dominant clay is kaolinite. Small percent of chlorite and palygorskite is also observed. The stacked booklet texture of kaolinite is present in almost all the samples (Figure 55, Figure 56, Figure 57, Figure 58, and Figure 59, Figure 60, Figure 62). The iron oxide is interpreted as authigenic grains coating the quartz. The iron oxide present as cluster of grapes chocking the pores and ultimately reducing the effectively porosity. The presence of kaolinite sometimes reduces and sometimes increases the porosity as it is proportional to the amount of clay present in the samples. On the other hand, the presence of palygorskite clay increases the permeability, because its needle like structure acts as a bridge between the pores.

## 5.4 Petrophysical Studies

Porosity and permeability characterize the quality and they are of primary importance. The quality of reservoir is determined by the magnitude, pattern and variability of porosity and permeability. They ultimately influence the migration, accumulation, and distribution of hydrocarbon in the reservoir. Much effort is needed in exploration and production phase to predict the degree and patterns of heterogeneities in petrophysical

parameters. This section is attributed to generate the relationship between petrographic and petrophysical findings in the Sarah Formation.

The petrophysical properties (i.e. porosity and permeability) were measured in the laboratory to carry out this research. As mentioned earlier, 105 samples were collected from the Sarah Formation outcrops at Al-Ilb paleochannel, and 226 core plugs were cut from these samples. A total of 150 core plugs having both horizontal and vertical measurement were selected for the analysis. The vertical and horizontal plugs were used for the statistical analysis of petrophysical properties of proximal, medial and distal part of Al-Ilb paleochannel. Thin-section study of 27 samples were performed to identify the petrographic parameters and 10 samples were used for further micro studies (i.e. SEM, and XRD).

For each sample, porosity and permeability measurement were conducted. The samples were analyzed by using gas expansion and saturation method for porosity calculation. Gas permeability method is used for calculating permeability of the samples.

### 5.4.1 Porosity

Al-Ilb paleochannel was divided into proximal, medial and distal parts (Figure 11). The porosity measurements of proximal part lie between 15% and to 25%. It shows consistent results with an average of 20% (Table 8). The porosity measurements of distal part of Al-Ilb paleochannel show 17% and 22 (Table 10). While the distal part shows 15% and 33% porosity values (Table 10). Dominantly primary (inter-granular) porosity has been

noticed in samples. Some secondary porosity is also observed; based on the thin-section study and SEM results. They indicate leaching and grain dissolution, which resulted in the formation of secondary inter-granular and intra-granular micro-porosity (Figure 54).

### 5.4.2 Permeability

The permeability measurements display wide range, from few milliDarcy (mD) to thousands of milliDarcy (mD). The proximal part shows the horizontal permeability values with a minimum of 53 mD and maximum of 2845 mD. The minimum values of vertical permeability are 71 mD, and maximum of 1868 mD (584.24 mD average values (Table 8). The medial part shows very low values as compare to proximal part. The minimum value of permeability of medial part of Al-Ilb paleochannel is 92 mD, and maximum value of 311mD (Table 9). The distal part shows higher value as compared to proximal and distal part of Al-Ilb paleochannel. The minimum horizontal permeability of distal part is 53mD, maximum of 4948 mD (average of 1169 mD). While the vertical permeability of distal part shows appreciably lower readings; minimum 50mD, maximum 4316 mD and average of 972 mD (Table 10). Since permeability is the property of medium of allowing fluids to pass through it without damaging its structure of medium (North, 1985). So permeability greatly depends on grain size, shape, sorting, grain packing, the degree of consolidation and cementation. (Taib and Donaldson, 2004).

Table 8: Porosity and Permeability measurements of proximal part of Al-Ilb paleochannel.

| Sample No. | ϕ (%) | $K_H$(md) | $K_V$(md) |
|---|---|---|---|
| **S3-1A** | 20.37 | 285.84 | 172.3 |
| **S3-1B** | 19.15 | 175.94 | 202.94 |
| **S3-2** | 20.37 | 236.61 | 128.82 |
| **S3-4** | 19.51 | 426.46 | 436.12 |
| **S3-5** | 18.93 | 554.43 | 392.28 |
| **S3-3** | 18.3 | 576.29 | 355.71 |
| **S4-1** | 20.55 | 1683.3 | 1336.7 |
| **S4-2** | 15.18 | 612.82 | 487.27 |
| **S4-3** | 25.09 | 2845.7 | 1868.2 |
| **S4-4** | 23.53 | 1604.6 | 1334.2 |
| **S4-6** | 22.74 | 1075.5 | 985.69 |
| **S4-7** | 21.22 | 697.05 | 393.28 |
| **S4-8** | 23.84 | 973.03 | 498.47 |
| **S4-10** | 21.37 | 313.79 | 189.46 |
| **S4-12** | 19.45 | 53 | 71.55 |
| **S4-2** | 15 | 573.59 | 494.78 |

Table 9: Porosity & Permeability measurements of medial part of Al-Ilb paleochannel.

| **Sample No.** | **ϕ (%)** | **K(md)** |
|---|---|---|
| **S10-7** | 19.34 | 143 |
| **S10-7** | 19.37 | 110.6 |
| **S10-5** | 17.62 | 311.6 |
| **S10-6** | 19.01 | 158.1 |
| **S10-1** | 21.39 | 100.7 |
| **S10-1** | 22.04 | 92.14 |

Table 10: Porosity & Permeability measurements of Distal part of Al-Ilb paleochannel.

| Sample No. | ϕ (%) | $K_H$(md) | $K_V$(md) | Sample No. | ϕ (%) | $K_H$(md) | $K_V$(md) |
|---|---|---|---|---|---|---|---|
| **S1-2B** | 21.1443 | 1490.5 | 1495 | S5-13A | 26.42 | 1584.7 | 1230.3 |
| **S1-3** | 22.32 | 1846 | 1520.9 | S5-11 | 24.1 | 578.15 | 422.46 |
| **S1-5** | 19.4 | 3892.2 | 1148.5 | S5-9 | 24.83 | 647.69 | 447.45 |
| **S1-8** | 20.9 | 1708.8 | 1627.6 | S5-3 | 25.29 | 418.9 | 522.79 |
| **S1-9** | 19.65 | 2001.5 | 1742.1 | S5-13B | 27.53 | 1692.3 | 1602.3 |
| **S1-10** | 18.07 | 2145.9 | 1498 | S6-1 | 24 | 96.26 | 50.4 |
| **S2-1B** | 23.05 | 2499.5 | 1137.5 | S6-2 | 26.27 | 164.18 | 87.69 |
| **S2-3A** | 23.94 | 430.98 | 292.86 | S6-3 | 27.25 | 100.11 | 79.51 |
| **S2-4** | 21.92 | 123.05 | 138.94 | S6-5 | 23.65 | 152.85 | 86.65 |
| **S2-5** | 20.38 | 1760.4 | 1373.3 | S6-6 | 20.03 | 323.92 | 214.31 |
| **S2-7** | 25.57 | 1696.4 | 955.28 | S7-2 | 18.44 | 494.9 | 450.81 |
| **S2-8** | 23.79 | 1535.8 | 1199.3 | S7-3 | 18.81 | 288.5 | 144.39 |
| **S2-9** | 22.91 | 1815.3 | 2323.6 | S7-4 | 21.27 | 112.79 | 105.15 |
| **S2-10** | 19.28 | 1936.3 | 1881.9 | S7-5 | 19.93 | 299.55 | 270.99 |
| **S2-11** | 22.59 | 1347.3 | 1143.7 | S7-6 | 22.22 | 213.75 | 152.69 |
| **S2-3A** | 23.07 | 777.93 | 621.15 | S7-6 | 23.23 | 228.76 | 170.09 |
| **S2-4** | 22.84 | 132.51 | 103.9 | S8-10 | 30.29 | 2253.3 | 1668.8 |
| **S2-5** | 20.16 | 1244.8 | 896.44 | S8-12 | 33.08 | 1585.2 | 1256.8 |
| **S2-7** | 25.58 | 1002.8 | 965.44 | S8-15 | 27.6 | 3881.6 | 3686.5 |
| **S2-8** | 23.55 | 1188.1 | 1268.7 | S9-1 | 22.83 | 780.15 | 1585.1 |
| **S2-10** | 19.41 | 1838.5 | 1851.3 | S9-2 | 25.65 | 1990.2 | 1993.7 |
| **S5-2B** | 27.61 | 177.04 | 173.3 | S9-4 | 30.8 | 783.32 | 852.67 |
| **S5-2B** | 27.98 | 327.94 | 177.04 | S9-5 | 27.22 | 980.55 | 811.99 |
| **S5-3** | 20.69 | 490.72 | 412.02 | S9-8 | 27.44 | 4558.6 | 4267.1 |
| **S5-10** | 26.08 | 300.4 | 730.81 | S9-8 | 27.51 | 4948.2 | 4316.5 |
| **S5-8** | 24.25 | 469.38 | 426.36 | S9-9 | 23.93 | 3217.7 | 2970.4 |
| **S5-12** | 23.95 | 1417.4 | 1196.8 | | | | |

So the factors that are responsible for such unexpected results will be discussed in the following paragraph.

### 5.4.3 Porosity and Permeability Patterns in Sarah Formation Outcrops

The petrophysical (porosity and permeability) patterns of Sarah Formation at proximal, medial and distal part of Al-Ilb paleochannel are illustrated in the Figure 64, Figure 66, and Figure 65, respectively. The porosity values for proximal, medial, and distal part of Al-Ilb paleochannel does not show any significant variation. However permeability values show wide range of variability. The maximum, minimum and average porosity measurements of proximal part are 15%, 25% and 20%, respectively. The maximum, minimum and average horizontal permeability values are 2845 mD, 53 mD and 793mD. The maximum, minimum and average vertical permeability values are 1868 mD, 71 mD and 584 mD. The maximum, minimum and average porosity readings of medial part are 17%, 22% and 20%, respectively. Permeability values of medial part is about 152 mD on average, maximum is 311 mD and minimum 92 mD. The maximum, minimum and average porosity measurements of distal part are 18%, 33% and 23%, respectively. Average horizontal permeability value of distal part is 1282 mD, average vertical permeability value is 1089 mD. On the other hand, maximum and minimum values of horizontal permeability are 4949 mD and 96 mD, and the vertical permeability the maximum and minimum values are 4316 mD and 50mD.

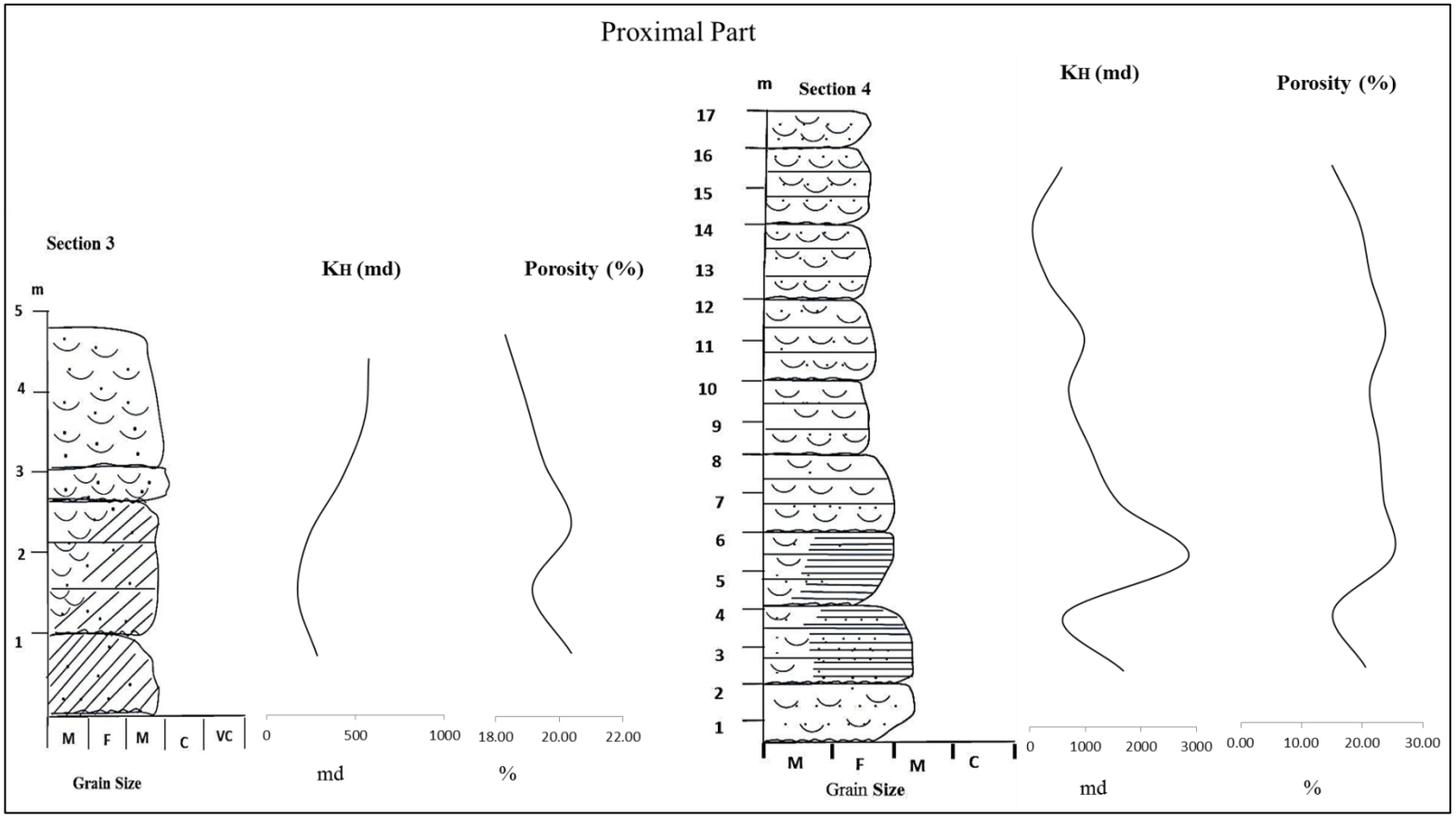


Figure 64: Porosity and permeability patterns in the proximal part of Al Ilb paleochannel, showing porosity and permeability increases with the increases in grain size.

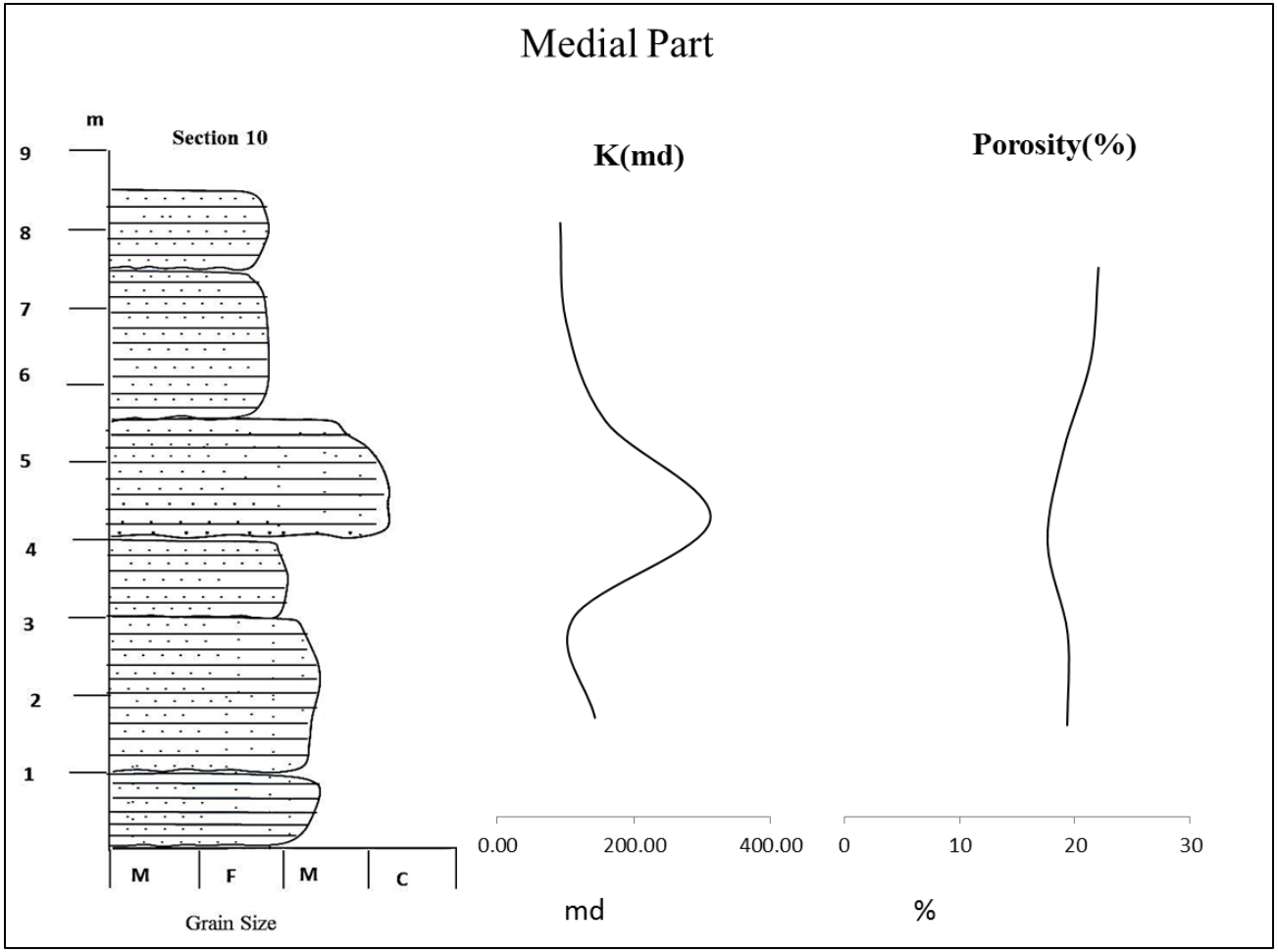


Figure 65: Porosity and permeability patterns of the medial part of Al Ilb paleochannel, porosity and permeability increases with the increases of grain size.

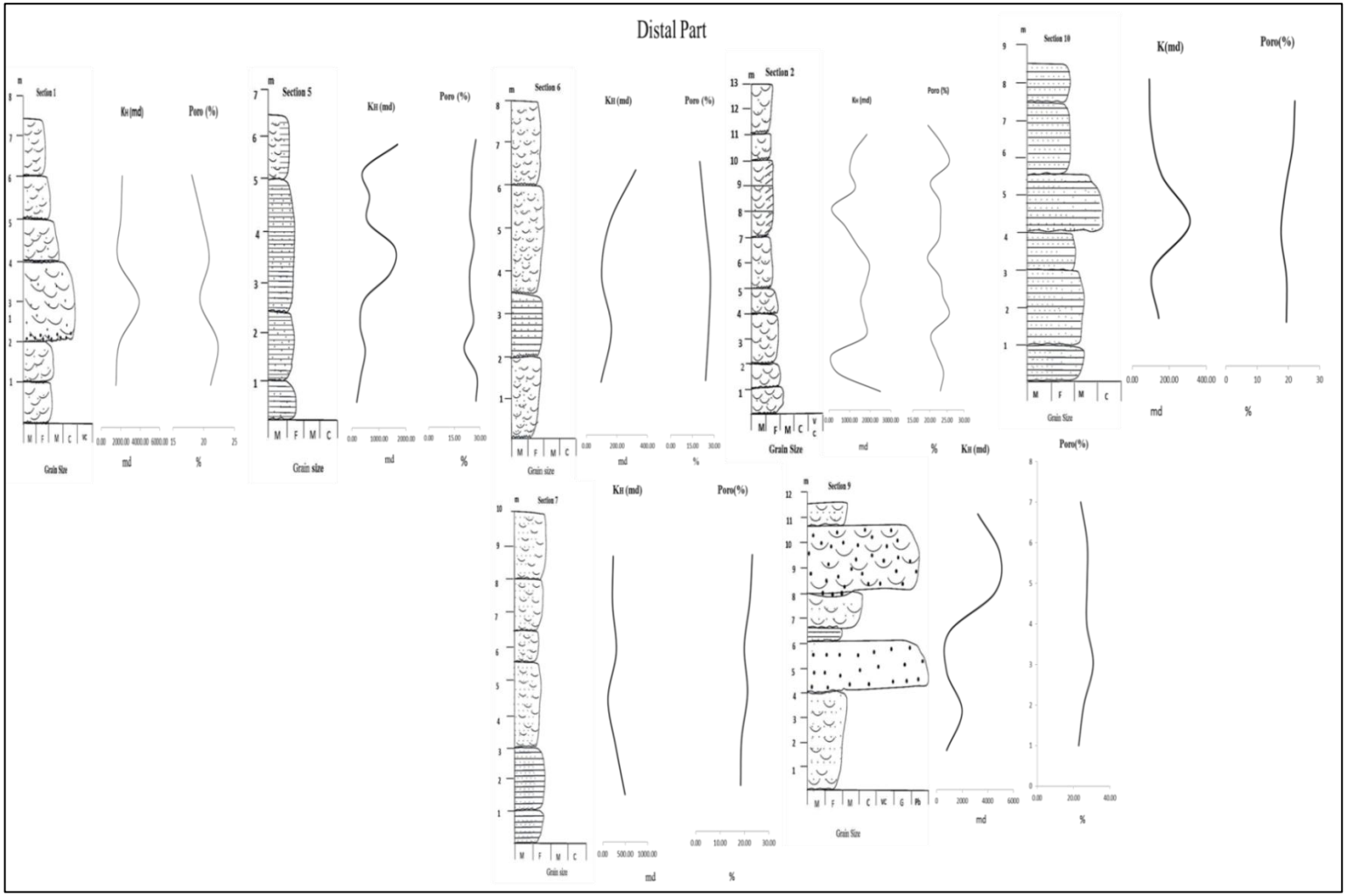


Figure 66: Porosity and permeability patterns in the distal part of Al Ilb paleochannel, showing porosity and permeability increases with the increases of grain size with some exceptions. Dominantly controlled by depositional and post depositional processes.

### 5.4.4 Controlling Factors of Petrophysical Parameters

The Sarah Formation shows highly heterogeneous behavior in term of petrophysical analysis, especially permeability shows heterogeneous behavior, but porosity shows homogeneous trend. The main controlling factors effecting the porosity and permeability is clay cementation especially kaolinite and iron oxide. These factors are revealed by thin-section studies, SEM, and XRD analysis and discussed in the following sections.

**Authigenic Clays**

Kaolinite, chlorite and palygorskite clays are the main clays that are observed in the studied samples. Kaolinite appears as pore filling and pore lining material. The amount of kaolinite dominantly influences the permeability. The representative samples of high permeability shows the presence of needle-like structure of palygorskite that act as pore bridging material (Table 7 ) The bridging shape of palygorskite has greatest influence on sandstone properties.

**Quartz Overgrowth**

Quartz overgrowth reduces the permeability and porosity because it is nonporous. Quartz overgrowth is a syntaxial overgrowth of silica around the quartz grains. The overgrowth persist the same crystallographic continuity of quartz framework. On the other hand, some grains are free of quartz coating because the chlorite generally prevents quartz overgrowth (North 1985). Therefore, the presence of early diagenetic chlorite may

preserve the porosity and permeability. Several of the thin-sections of display show quartz overgrowth, but most of them are free form quartz coating.

**Iron Oxide**

Another factor controlling the porosity and permeability is iron cementation. The radial growths of iron cement completely block the pore and reduce the pore throat. This ultimately results in the reduction of petrophysical measurements. Thin-section, SEM and XRD results confirm the effect of iron cement almost in all samples, but the amount of iron cement varies from sample to sample (Table 7).

**Compaction and Packing**

The higher values of porosity are mainly dependent on the degree of sorting. It is commonly observed that poorly-sorted sandstone is less porous and well sorted sandstone is highly porous. On other hand, the packing helps in sorting the grains so compaction and packing are the main process that refers as depositional process. The primary depositional packing is followed by post depositional packing and it is then gone through compaction process under high load. The thin-section images of Sarah Formation show wide range of sorting, Out of 27 selected samples, seven samples show poorly-sorting and while three samples shows well-sorting. The porosity measurements of these samples confirm that higher porosity values observed in the case of well-sorting, and vice-versa.

### 5.4.5 Composition, Texture and Diagenesis Affecting Petrophysical Parameters

The cross plot is prepared against depositional texture, composition, diagenesis versus porosity and permeability. Using point count method, compositional and textural data are obtained for analysis. The cross plot between porosity versus matrix, cement and sorting shows no clear relationship and the same are happened with the cross plot of permeability versus matrix, cement and sorting (Figure 67 and Figure 68). In both cases the increase of matrix, cement and sorting (percentage) leads towards the reduction of porosity but the examined samples show the converse relationship. This relationship is due to the effect of presence of clays and in some cases it is affected by the presence of pore-throat and pore size distribution.

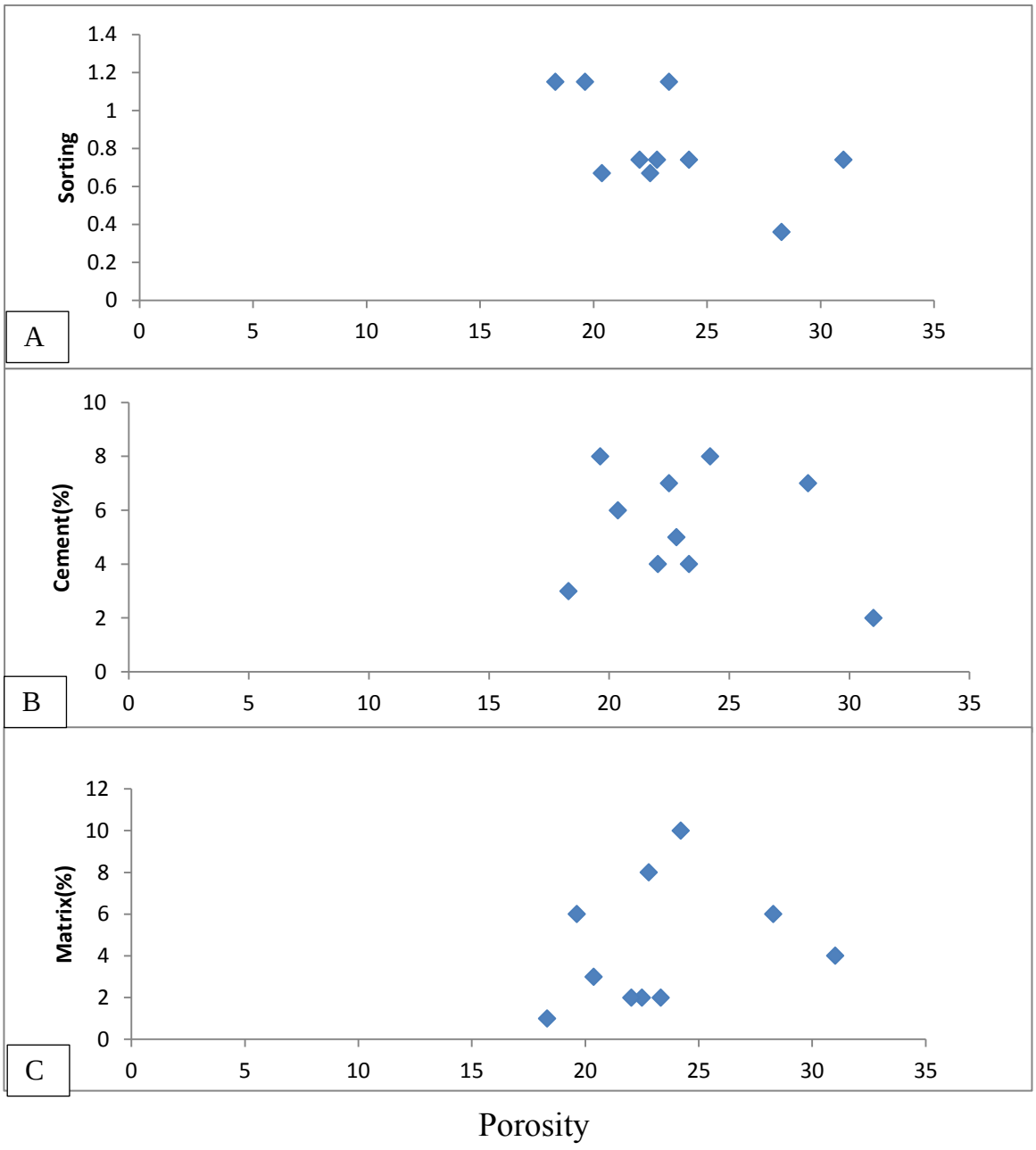


Figure 67: (A) Relationship of porosity Vs sorting (phi), (B) Relationship of porosity Vs cement (%) (C) Relationship of porosity vs. matrix (%)

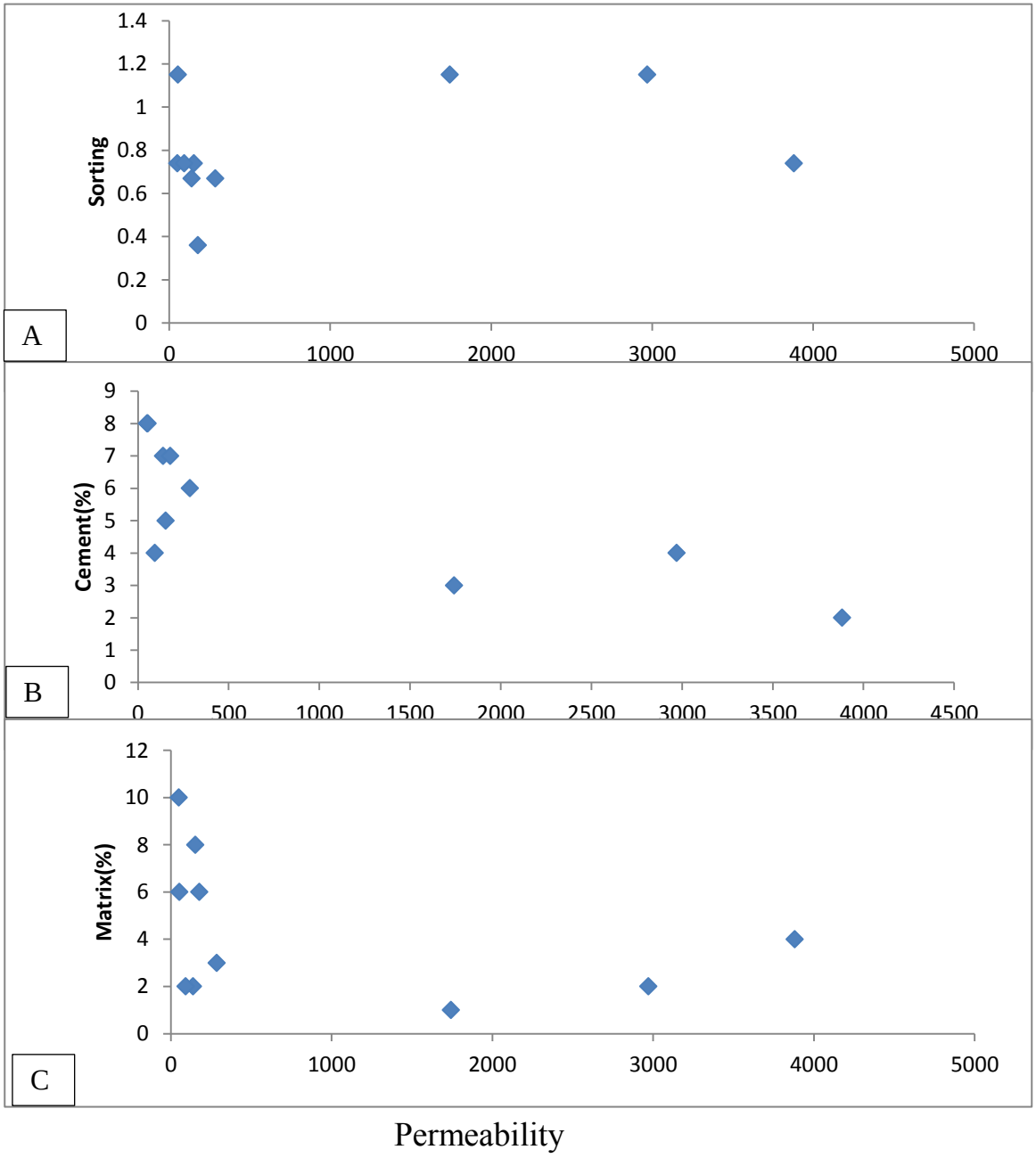


Figure 68: (A) Relationship of permeability vs sorting (phi) (B) Relationship of permeability vs. cement (%) (C) Relationship of permeability vs. matrix (%).

# Chapter 6

# Statistical Analysis

## 6.1 Introduction

The standard parameters that indicate the reservoir quality are porosity and permeability and their statistical distributions give significant insight into reservoir rocks (Sahin and Saner, 2001). The petrophysical parameters are greatly affected by grains size and grain relationship among each other, shape of grains, packing, sorting, amount and type of matrix, cement and clays, environment of deposition and post depositional processes. The wide ranges of geologic control lead to complex relationship between porosity and permeability (Surdam et al., 1989; Sahin and Saner, 1999; Gier, 2000; Ketzr et al., 2002; sun et al., 2007).

This chapter deals with the univariate statistical analysis of porosity and permeability in the Sarah Formation at Al-Ilb paleochannel channel. The calculated statistical parameters include skewness, kurtosis, mean, median, range, standard deviation, coefficient of variation, and sample variance. The cross plots were constructed between porosity and permeability to understand the relationships between these variables.

## 6.2 Sampling and Data Set

Ten outcrops of Sarah Formation at Al-Ilb paleochannel were selected. The best cores are selected for detailed analysis; the criteria of selection were based on non-friable, non-fractured and those samples that have vertical and the corresponding horizontal core plugs. After removing outliers, 140 core plugs were left for the detailed analysis; these plugs represent the proximal, medial, and distal part of Al-Ilb paleochannel. The dimension of the core plug is 2.5 cm diameter and 4 cm length on average. The samples were analyzed using gas expansion and saturation method for porosity calculation. Gas permeability method is used for calculating permeability of the samples. Both the equipment require well defined core plug in term of length and diameter.

As discussed in the previous chapters, Al-Ilb paleochannel was divided into proximal medial and distal parts. The statistical analysis of petrophysical parameters were derived accordingly for each part and presented in the following sections.

## 6.3 Statistical Analysis of Proximal part of Al-Ilb paleochannel

### 6.3.1 Porosity

As pointed out earlier, the proximal part of the Al-Ilb paleochannel is represented by S3 and S4. Statistical parameters of porosity for these sections are listed in Table 8. This analysis deals with the histogram and statistical parameters of porosity. The histogram of porosity measurements for the proximal part is illustrated in Figure 69. The histogram shows that the porosity measurements are normally distributed. The porosity data is

ranging from 16 to 28 with highest no. of observations with 8 at 22% porosity. The descriptive statistics of proximal part of Al-Ilb paleochannel is listed is Table 12. The median and mean indicate that porosity is normally distributed. The coefficient of variation for porosity values are less the 0.5 i.e. 0.14 (Table 12), representing homogeneity of porosity distribution. The skewness (i.e.-0.031) of the data also confirming the symmetrical distribution as it is approaches to zero. The kurtosis of porosity values is less than 3, indicating leptokurtic nature of distribution.

Table 11: Porosity and permeability measurements of Sarah Formation samples, representing the proximal part of Al-Ilb paleochannel.

| Sample No. | $K_H$ (md) | $K_V$ (md) | Porosity (%) |
|---|---|---|---|
| **S3-1A** | 285.84 | 172.3 | 20.37 |
| **S3-1B** | 175.94 | 202.94 | 19.15 |
| **S3-2** | 236.61 | 128.82 | 20.37 |
| **S3-4** | 426.46 | 436.12 | 19.51 |
| **S3-5** | 554.43 | 392.28 | 18.93 |
| **S3-3** | 576.29 | 355.71 | 18.3 |
| **S4-1** | 1683.3 | 1336.7 | 20.55 |
| **S4-2** | 612.82 | 487.27 | 15.18 |
| **S4-3** | 2845.7 | 1868.2 | 25.09 |
| **S4-4** | 1604.6 | 1334.2 | 23.53 |
| **S4-6** | 1075.5 | 985.69 | 22.74 |
| **S4-7** | 697.05 | 393.28 | 21.22 |
| **S4-8** | 973.03 | 498.47 | 23.84 |
| **S4-10** | 313.79 | 189.46 | 21.37 |
| **S4-12** | 53.00 | 71.55 | 19.45 |
| **S4-2** | 573.59 | 494.78 | 15 |

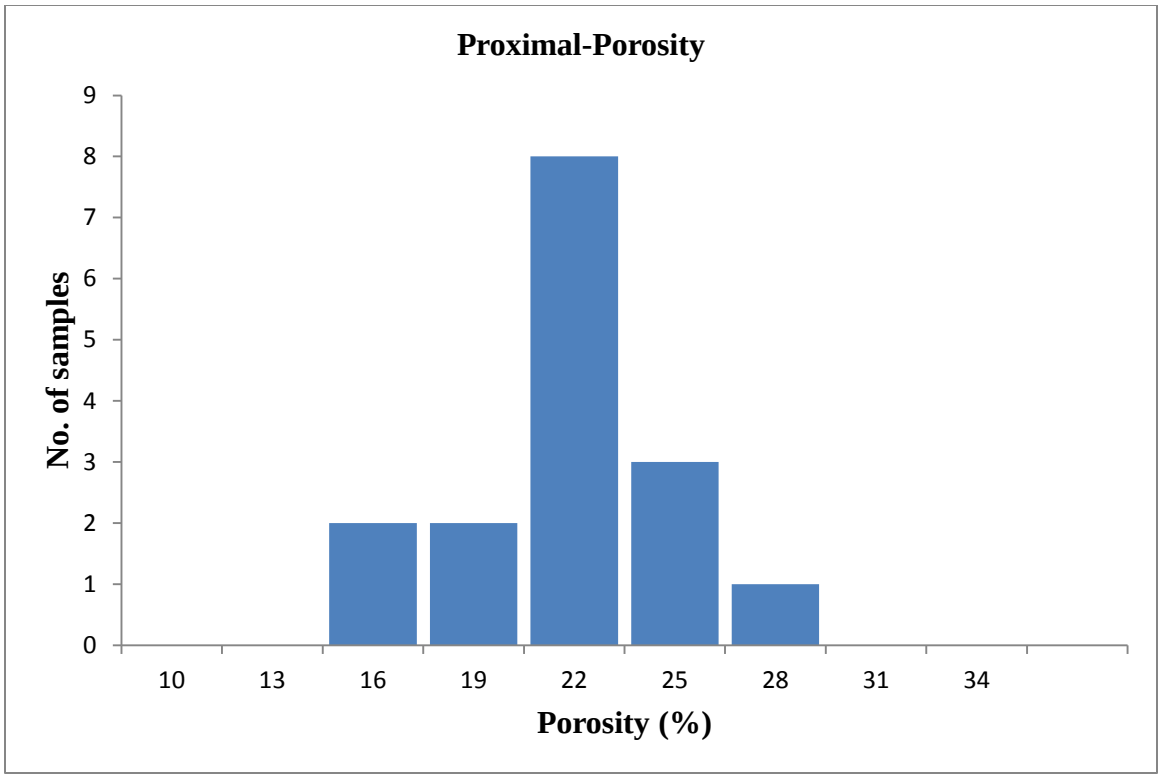


Figure 69: Histogram of porosity representing proximal part of Al-Ilb paleochannel

Table 12: Statistics of porosity and permeability measurements of Sarah Formation samples, representing the proximal part of Al-Ilb paleochannel.

| **Proximal-Descriptive Statistics** | | | |
|---|---|---|---|
| **Statistical Parameters** | **$K_H$ (md)** | **$K_V$ (md)** | **$\phi$(%)** |
| **Mean** | 793 | 584.24 | 20.29 |
| **Median** | 574.94 | 414.7 | 20.37 |
| **Standard Deviation** | 722.49 | 519.73 | 2.79 |
| **Kurtosis** | 3.43 | 1.17 | 0.11 |
| **Skewness** | 1.77 | 1.4 | -0.31 |
| **Range** | 2792.7 | 1796.66 | 10.08 |
| **Minimum** | 53 | 71.55 | 15 |
| **Maximum** | 2845.7 | 1868.2 | 25.09 |
| **Sum** | 12687.95 | 9347.77 | 324.61 |
| **Count** | 16 | 16 | 16 |
| **CV** | 0.91 | 0.89 | 0.14 |

### 6.3.2 Permeability

The descriptive statistics of permeability are listed in the Table 11 and Table 12. Comparison of permeability values shows that the mean and median of horizontal permeability are higher than those of the vertical permeability. The maximum horizontal permeability are 2845 mD and minimum 53 mD. While the maximum vertical

permeability is 1868 mD, and minimum 71 mD. The coefficient of variation values horizontal and vertical permeability lie between 0.5 and 1, indicating the heterogeneity of the distribution.

The histograms for permeability measurements at proximal part are illustrated in (Figure 70 and Figure 71). The horizontal and vertical permeability are positively skewed, indicating that large number of values have lower permeability. Most data lies below 1250 mD for horizontal permeability and for vertical permeability most of the measurements are less than 500 mD. The kurtosis of horizontal permeability is greater than 3; interpreted as platy kurtic. While the vertical permeability values are distributed with higher peak i.e. leptokurtic.

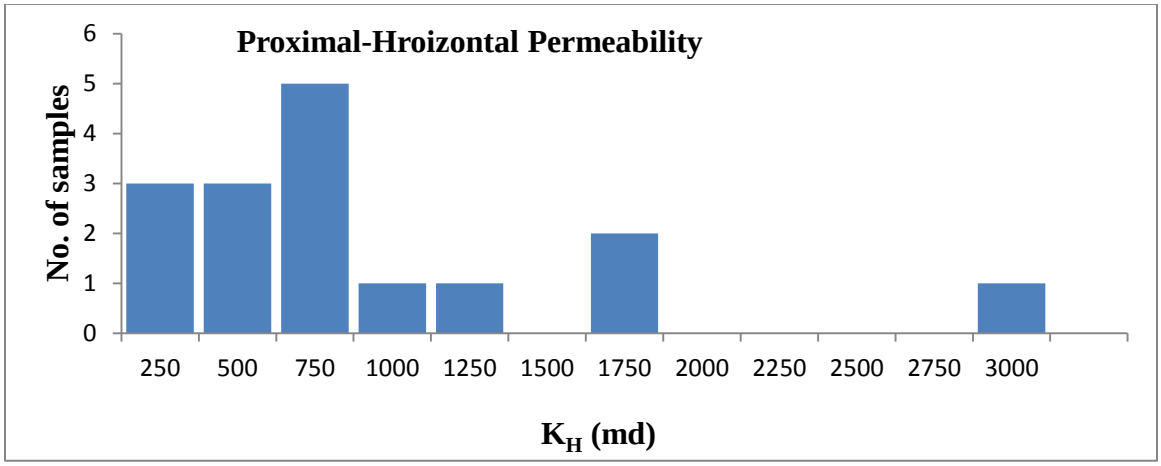


Figure 70: Histogram for horizontal permeability representing the proximal part of Al-Ilb paleochannel.

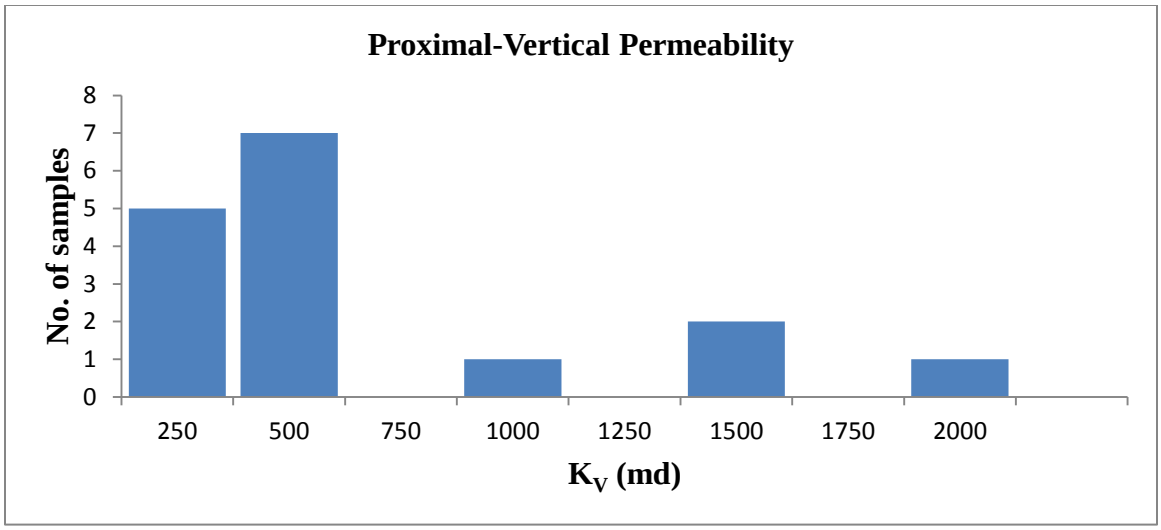


Figure 71: Histogram for vertical permeability representing the proximal part of Al-Ilb paleochannel.

## 6.4 Statistical Analysis of Medial Part of Al-Ilb Paleochannel

### 6.4.1 Porosity

The medial part of Al-Ilb paleochannel is represented by S10 with only six samples. The descriptive statistics and histograms of porosity and permeability measurements are discussed in the following paragraph. The porosity histogram of medial part is normally distributed. Most of the data is clustered between 19% to 23%.

The descriptive statistics of porosity measurements at distal part is listed in Table 14. The equal mean and median show that values are normally distributed. The coefficient of variation for porosity values is less than 0.5, (i.e. 0.08), indicating the homogeneity of

porosity distribution. The kurtosis is less the 3, representing that the distribution is leptokurtic.

### 6.4.2 Permeability

The permeability measurements of medial part are listed in Table 3. The histogram and descriptive statistics of permeability are discussed in the following paragraphs. The permeability histogram shows that the data is positively skewed and most of the values are less than 200 mD. The highest number of data is clustered at 150 mD. The descriptive statistics of permeability is listed in Table 14. There is appreciable difference between mean and median values. The coefficient of variation is just above 0.5; representing homogeneity with slight variability in permeability measurements.

Table 13: Porosity and permeability measurements of Sarah Formation samples, representing the distal part of Al Ilb paleochannel.

| **Sample No.** | **K(md)** | **Porosity (%)** |
|---|---|---|
| **S10-7-H1** | 143 | 19.34 |
| **S10-7-V1** | 110.6 | 19.37 |
| **S10-5-V1** | 311.6 | 17.62 |
| **S10-6-V1** | 158.1 | 19.01 |
| **S10-1-V1** | 100.7 | 21.39 |
| **S10-1-V2** | 92.14 | 22.04 |

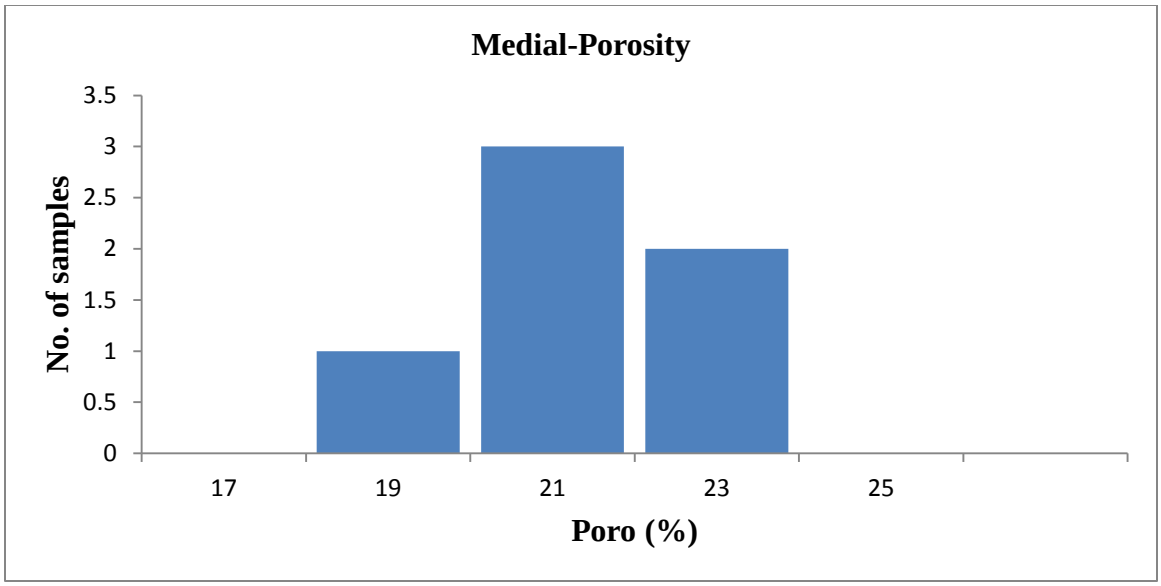


Figure 72: Histogram of porosity representing medial part of Al-Ilb paleochannel.

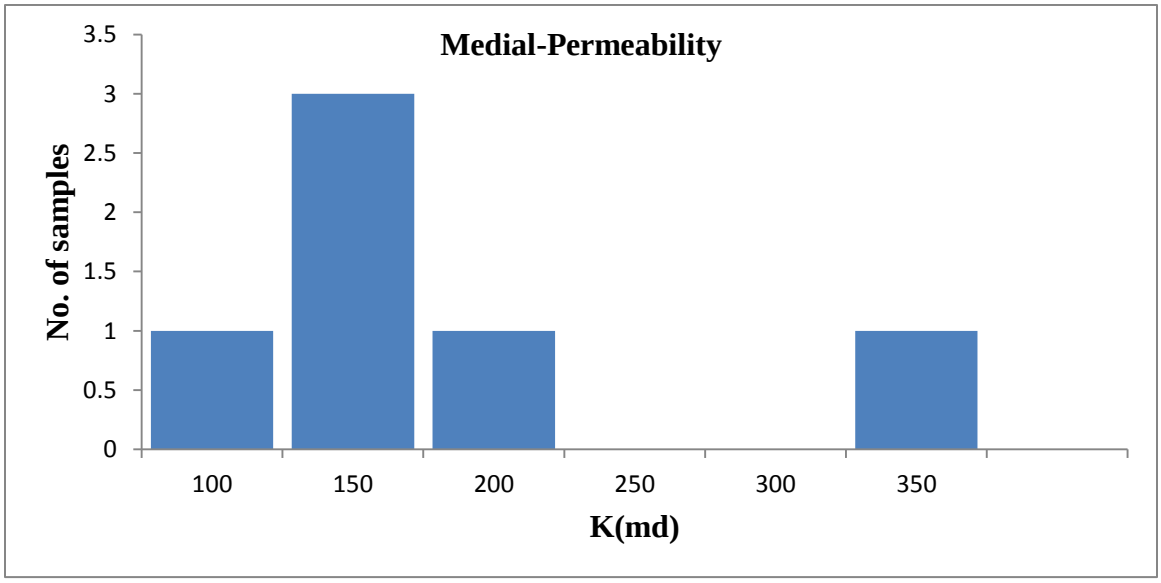


Figure 73: Histogram of permeability representing medial part of Al-Ilb paleochannel

Table 14: Statistical parameters of porosity and permeability measurements representing the proximal part of Al Ilb paleochannel**.**

| **Medial-Statistical Parameters** | | |
|---|---|---|
| **Statistical Parameters** | K(md) | ϕ(%) |
| **Mean** | 152.67 | 19.79 |
| **Median** | 126.77 | 19.35 |
| **Standard Deviation** | 81.89 | 1.63 |
| **Sample Variance** | 6706.1 | 2.66 |
| **Kurtosis** | 4.06 | -0.86 |
| **Skewness** | 1.95 | 0.31 |
| **Range** | 219.48 | 4.41 |
| **Minimum** | 92.14 | 17.62 |
| **Maximum** | 311.62 | 22.04 |
| **Sum** | 916.03 | 118.77 |
| **Count** | 6 | 6 |
| **CV** | 0.54 | 0.08 |

## 6.5 Statistical Analysis of Distal Part of Al-Ilb Paleochannel

### 6.5.1 Porosity

The distal part of Al-Ilb paleochannel is represented by S1, S2, S5, S6, S7, S8 and S9. The distributions of outcrops in Al-Ilb paleochannel are shown in Figure 4. The porosity and permeability (horizontal and vertical) values are listed in the Table 10. The porosity histogram of distal part is shown in the Figure 74. The histogram shows that the distribution is slightly skewed to the right, most of the data ranging between 20% to 28%. Some outliers are also observed at both ends of distribution.

The descriptive statistics of porosity measurements are listed in Table 15. The median and mean values are approximately equal, confirming the normal distribution. The coefficient of variation for the porosity values is less than 0.5, indicating homogeneous distribution. The range of the data shows the there is significant difference between lowest and highest values.

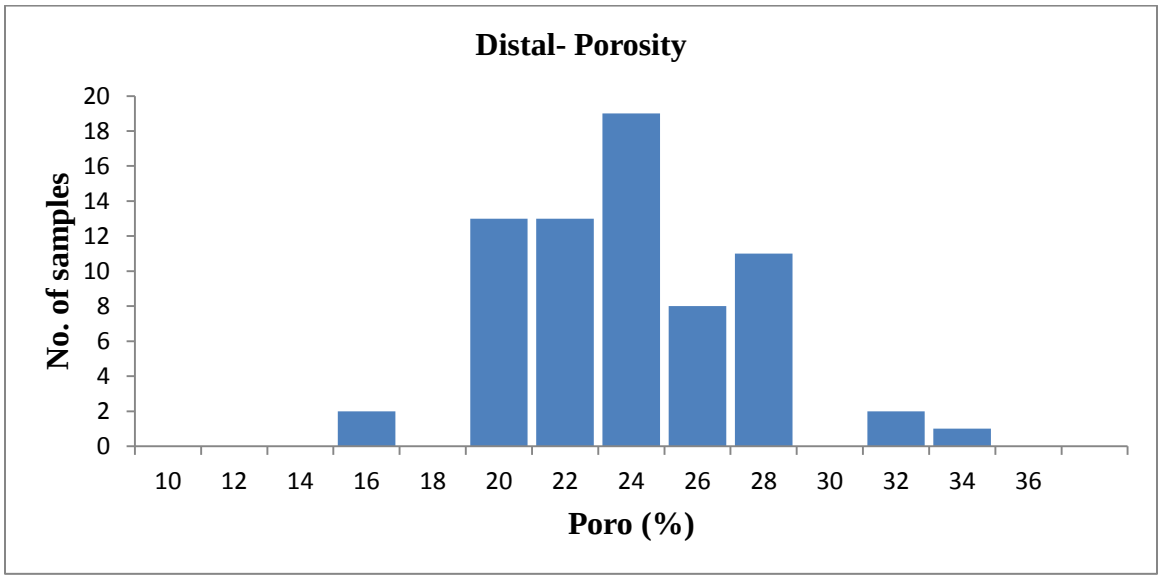


Figure 74: Histogram of porosity representing the distal part of Al-Ilb paleochannel.

### 6.5.2 Permeability

The statistical parameters of vertical and horizontal permeability values in distal part are listed in the Table 15. Histograms for horizontal and vertical permeability measurements are shown in Figure 75, and Figure 76. Both histograms display very high positive skewness. The maximum horizontal permeability value is 4948 mD, while the maximum vertical permeability value is 4316 mD. On the other hand, the minimum horizontal permeability is 53 mD, and minimum vertical permeability is 50 mD. Smaller vertical permeability is due to the presence of bedding planes, bedding creates obstacles for vertical flow. The coefficient of variation for vertical and horizontal permeability is almost the same (0.94 and 0.97), indicating heterogeneity of data. This heterogeneity is also indicated by the large values of range and sample variance values (Table 15).

Table 15: Statistical parameter of porosity and vertical and horizontal permeability of distal part of paleochannel.

| **Distal-Descriptive Statistics** | | | |
|---|---|---|---|
| **Statistical Parameters** | **$K_H$ (md)** | **$K_V$ (md)** | **$\phi$ (%)** |
| **Mean** | 1169.01 | 972.42 | 22.96 |
| **Median** | 780.15 | 730.81 | 22.91 |
| **Standard Deviation** | 1095.76 | 940.52 | 3.53 |
| **Kurtosis** | 2.42 | 3.67 | 0.23 |
| **Skewness** | 1.53 | 1.74 | 0.33 |
| **Range** | 4895.2 | 4266.1 | 18.08 |
| **Minimum** | 53 | 50.4 | 15 |
| **Maximum** | 4948.2 | 4316.5 | 33.08 |
| **Sum** | 80661.54 | 67097.04 | 1584.31 |
| **Count** | 69 | 69 | 69 |
| **CV** | 0.94 | 0.97 | 0.15 |

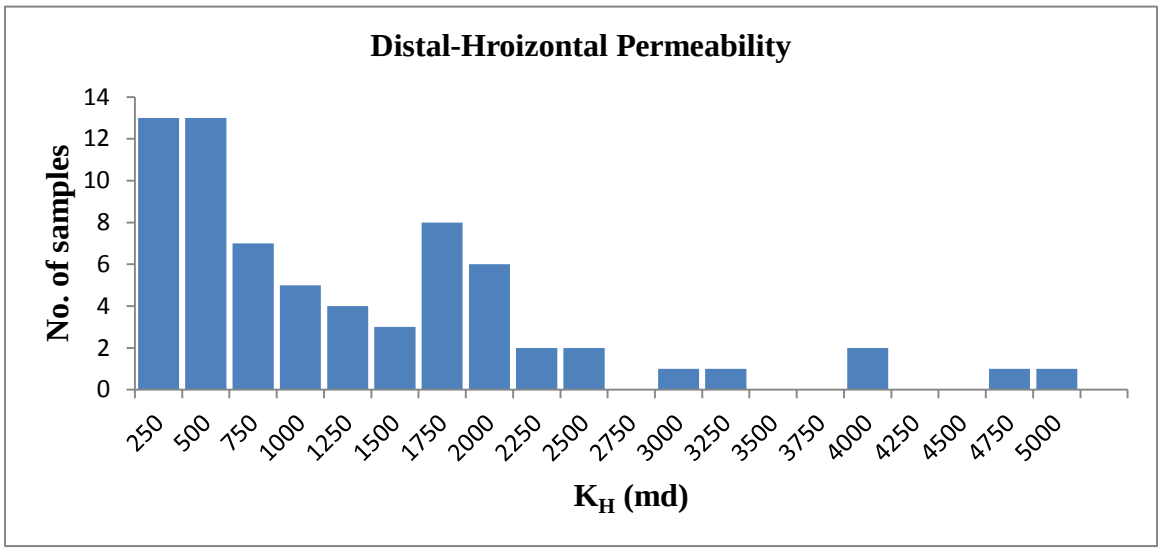


Figure 75: Histogram of horizontal permeability representing the distal part of Al-Ilb paleochannel

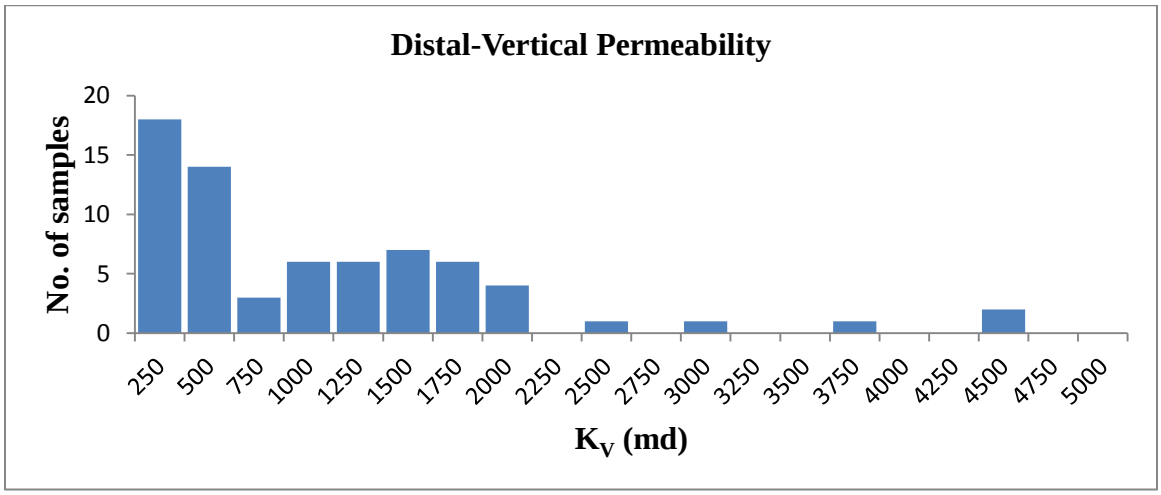


Figure 76: Histogram of vertical permeability representing the distal part of Al-Ilb paleochannel.

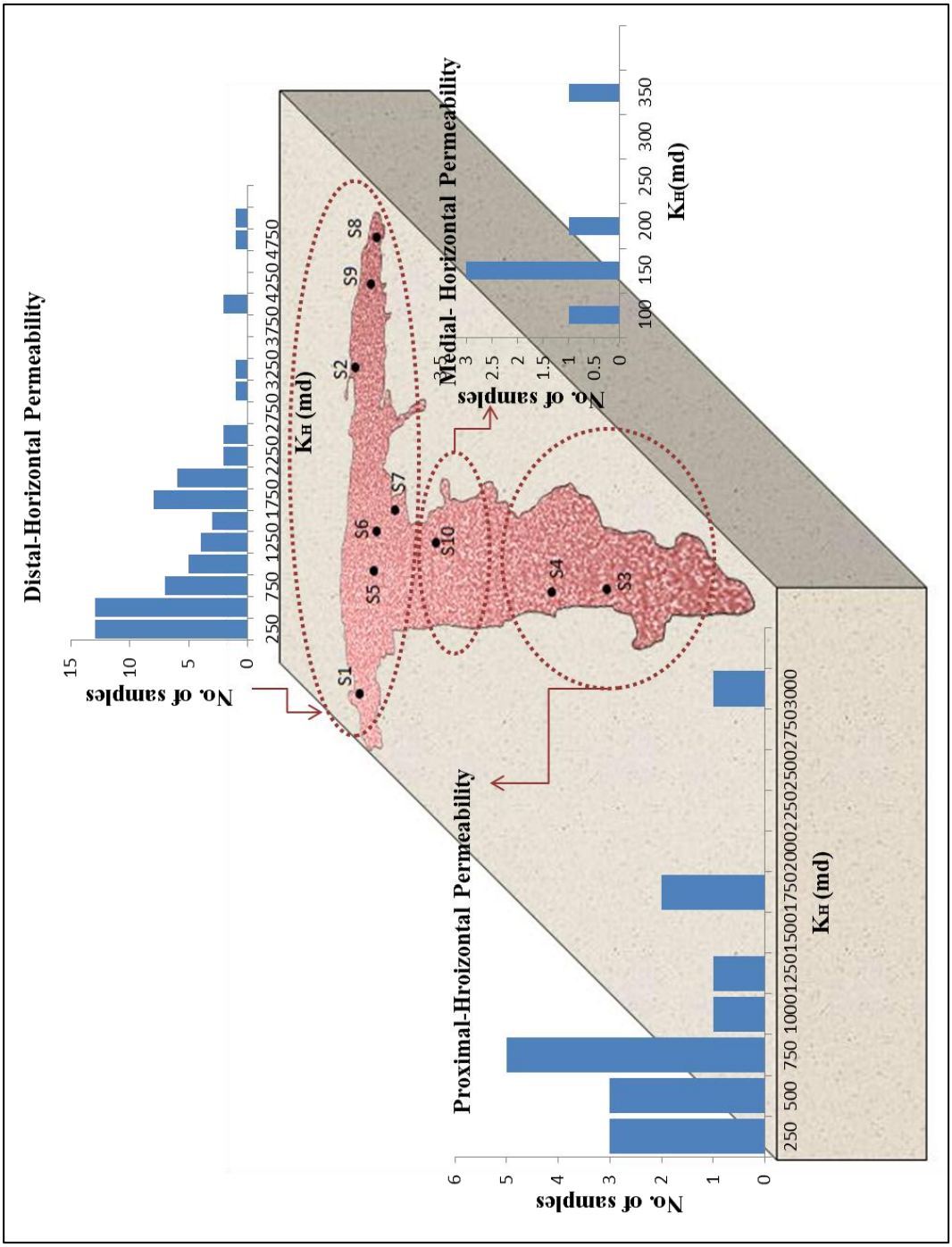


Figure 77: Block diagram showing histogram of horizontal permeability in different part of Al-IIb paleochannel

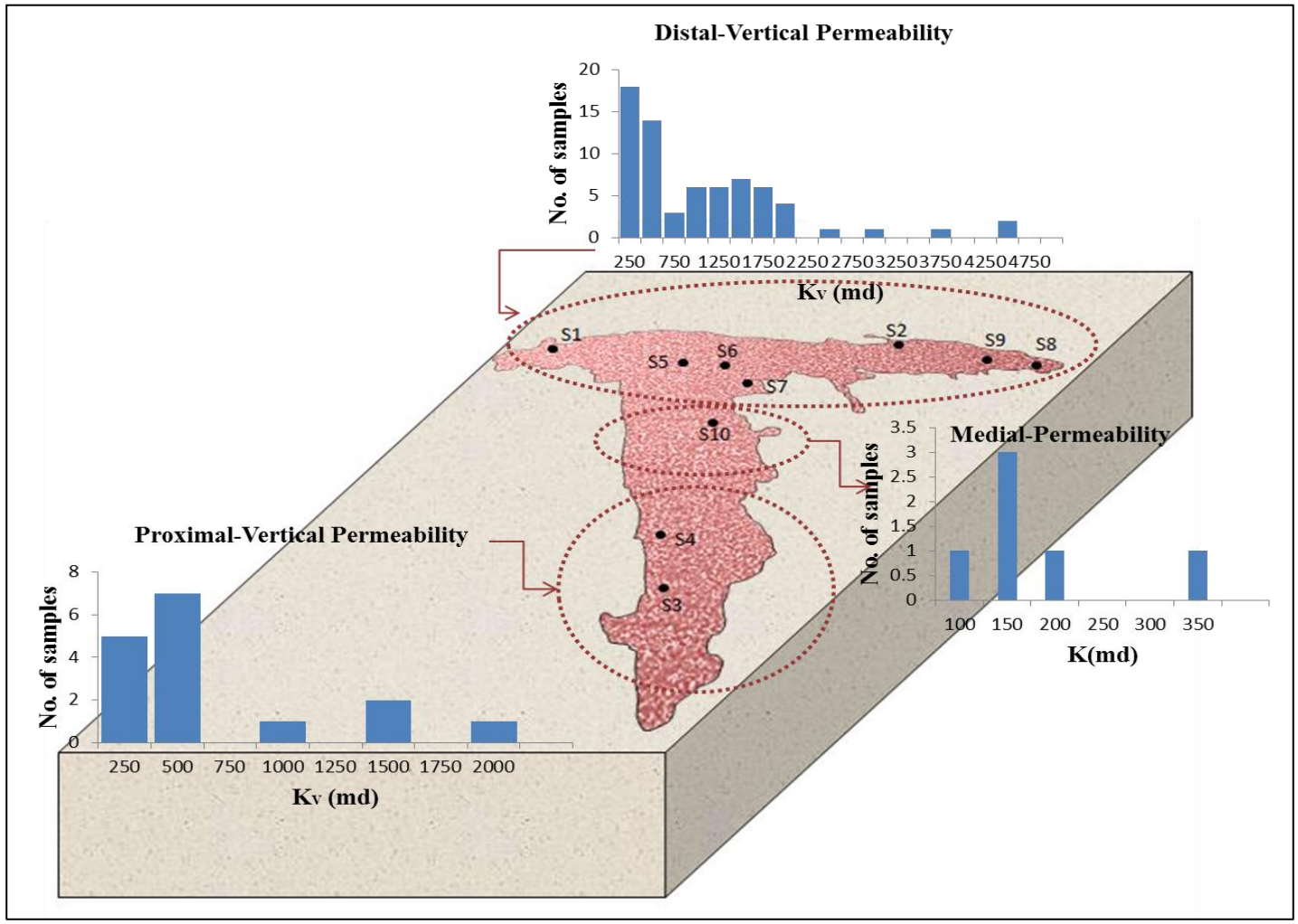


Figure 78: Block diagram showing histograms of vertical permeability in the different parts of Al-Ilb paleochannel

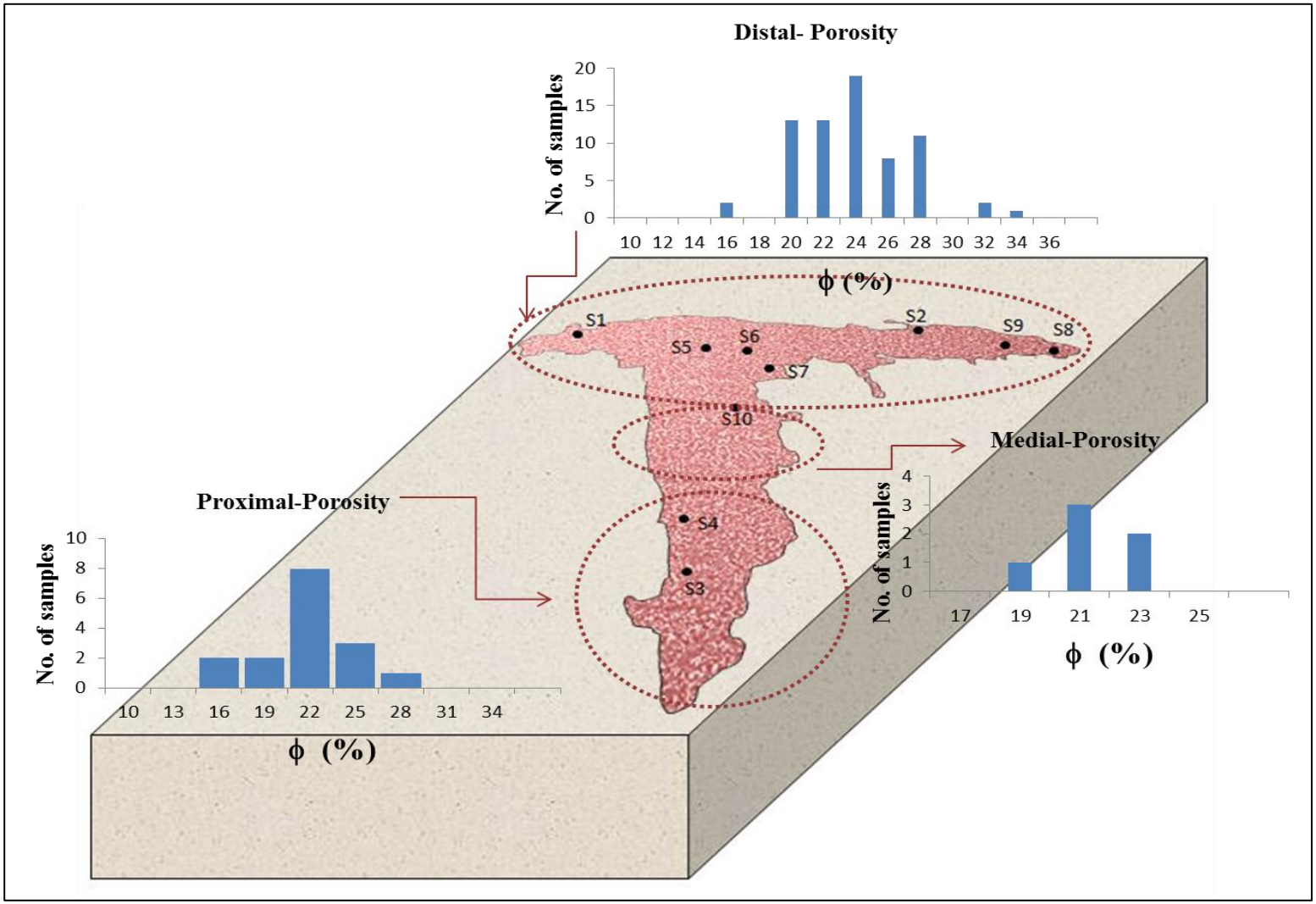


Figure 79: Block diagram showing porosity histogram in different parts of Al-Ilb paleochannel

| Distal-Statistical Parameters | | | |
|---|---|---|---|
| Statistical Parameters | KH(md) | K V(md) | Poro(%) |
| Mean | 1169.01 | 972.42 | 22.96 |
| Median | 780.15 | 730.81 | 22.91 |
| Standard Deviation | 1095.76 | 940.52 | 3.53 |
| Sample Variance | 1200700.69 | 884568.74 | 12.47 |
| Kurtosis | 2.42 | 3.67 | 0.23 |
| Skewness | 1.53 | 1.74 | 0.33 |
| Range | 4895.20 | 4266.10 | 18.08 |
| Minimum | 53.00 | 50.40 | 15.00 |
| Maximum | 4948.20 | 4316.50 | 33.08 |
| Sum | 80661.54 | 67097.04 | 1584.31 |
| Count | 69.00 | 69.00 | 69.00 |
| CV | 0.94 | 0.97 | 0.15 |

| Proximal-Descriptive Statistics | | | |
|---|---|---|---|
| Statistical Parameters | K(md) H | K(md) V | Poro(%) |
| Mean | 793.00 | 584.24 | 20.29 |
| Median | 574.94 | 414.70 | 20.37 |
| Standard Deviation | 722.49 | 519.73 | 2.79 |
| Sample Variance | 521996.39 | 270119.54 | 7.78 |
| Kurtosis | 3.43 | 1.17 | 0.11 |
| Skewness | 1.77 | 1.40 | -0.31 |
| Range | 2792.70 | 1796.66 | 10.08 |
| Minimum | 53.00 | 71.55 | 15.00 |
| Maximum | 2845.70 | 1868.20 | 25.09 |
| Sum | 12687.95 | 9347.77 | 324.61 |
| Count | 16.00 | 16.00 | 16.00 |
| CV | 0.91 | 0.89 | 0.14 |

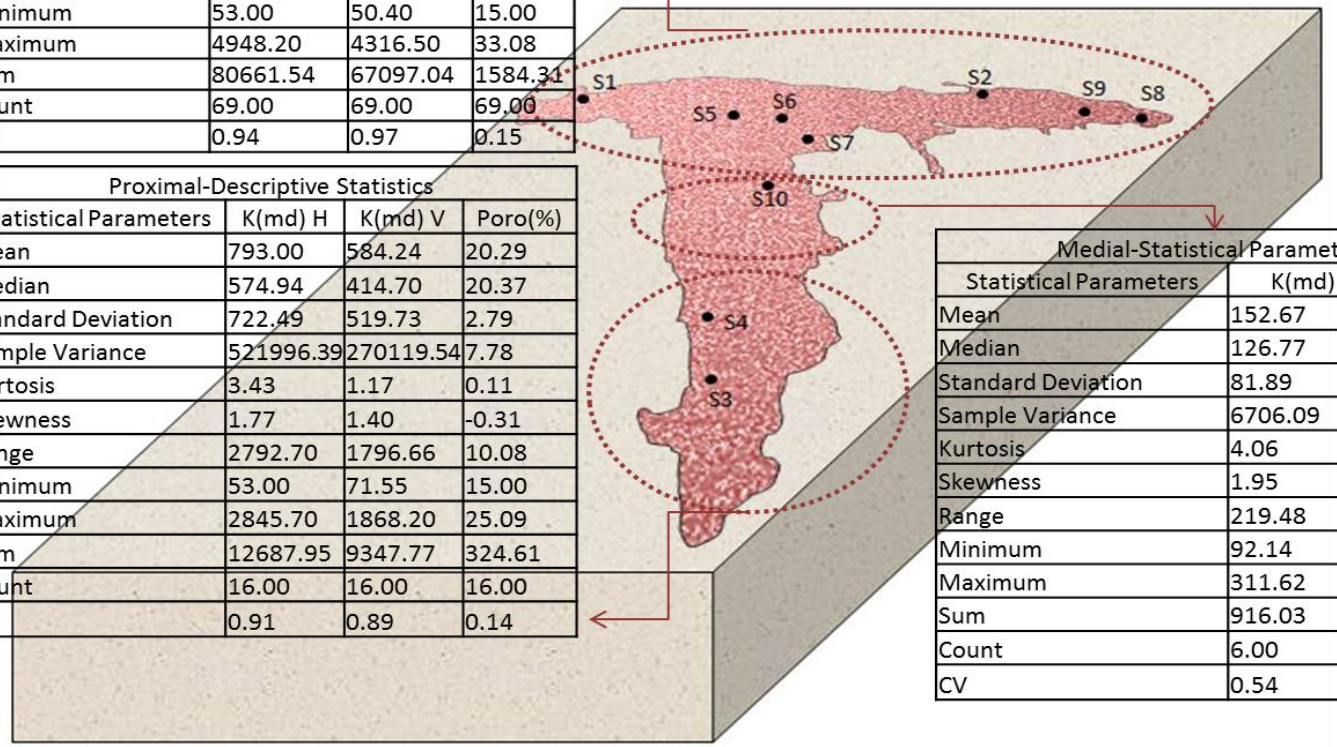


| Medial-Statistical Parameters | | |
|---|---|---|
| Statistical Parameters | K(md) | Poro(%) |
| Mean | 152.67 | 19.79 |
| Median | 126.77 | 19.35 |
| Standard Deviation | 81.89 | 1.63 |
| Sample Variance | 6706.09 | 2.66 |
| Kurtosis | 4.06 | -0.86 |
| Skewness | 1.95 | 0.31 |
| Range | 219.48 | 4.41 |
| Minimum | 92.14 | 17.62 |
| Maximum | 311.62 | 22.04 |
| Sum | 916.03 | 118.77 |
| Count | 6.00 | 6.00 |
| CV | 0.54 | 0.08 |

Figure 80: Block diagram showing statistics of petrophysical parameter in different parts of Al-Ilb paleochannel.

## 6.6 Porosity-Permeability Relationship for Proximal Part

The horizontal and vertical permeability versus porosity for proximal part of Al-Ilb paleochannel are illustrated in Figure 81 and Figure 82. These graphs indicate very low correlation between permeability and porosity. Very poor relationships ($R^2 = 0.34$, and $R^2 = 0.27$ for both horizontal and vertical permeability versus porosity have been observed. The scatter plots indicate that the porosity values for both horizontal and vertical permeability are restricted between 15% to 25%, but permeability values show wide variability.

The poor correlation between variables can be explained by diagenesis. As discussed earlier in the beginning of the Chapter 6, the sample S4-1A, S3-3.5, S4-2 and S4-9 are highly ferruginous and SEM image for sample S3-1A, and S4 shows the presence of kaolinite and smectite. These clays filled the pores and resulting in chocking the pore connectivity phenomena. On the other hand, the samples with high permeability and low porosity indicate that smaller pores are well connected due smaller amount of iron cement. The sample with high porosity and high permeability (S4-3, and S4-4) revealed very low percentage iron leaching and moderately sorting.

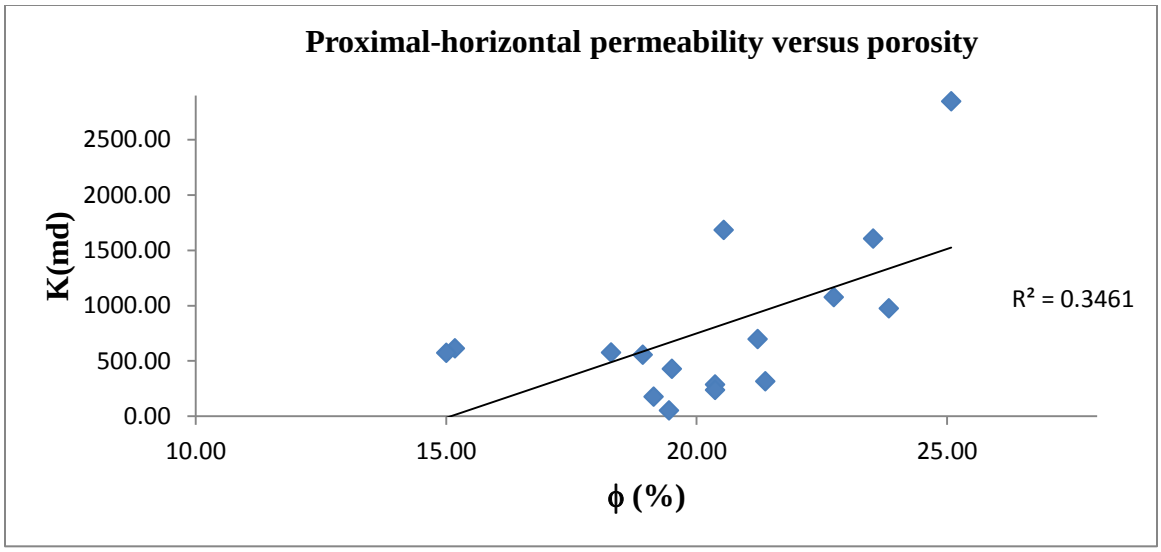


Figure 81: Cross -plot of horizontal permeability versus porosity for proximal part of Al-Ilb paleochannel.

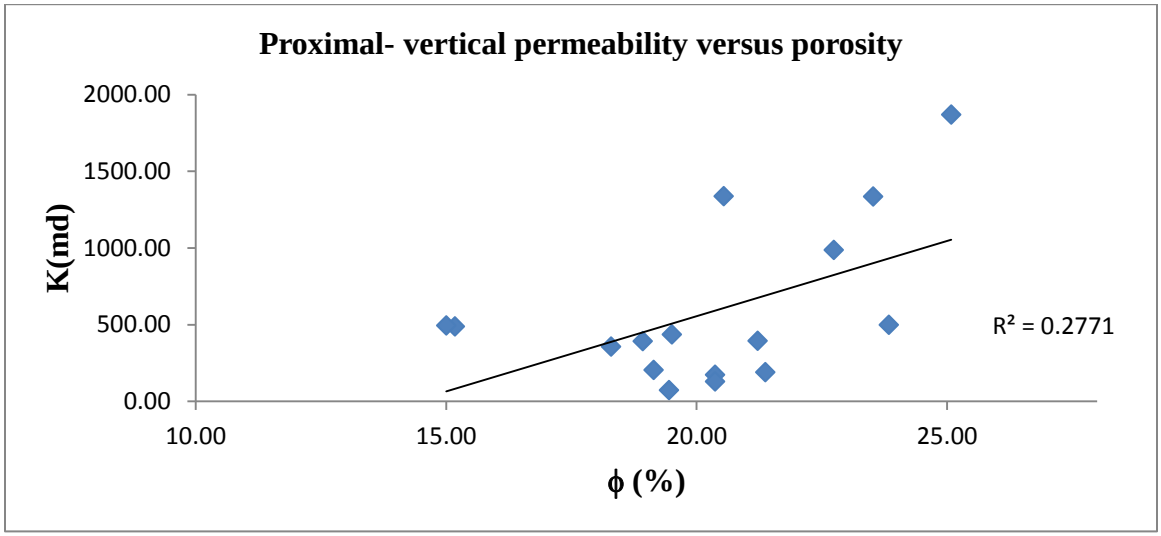


Figure 82: Cross -plot of vertical permeability versus porosity for proximal part of Al-Ilb paleochannel.

## 6.7 Porosity-Permeability Relationship for Medial Part

The porosity versus permeability data for medial part of Al-Ilb paleochannel is illustrated in Figure 83. The graph shows relatively good inverse relationshipship between porosity and permeability. The thin-section and SEM micrograph reveal the reason for this inverse trend. The sample with high porosity and low permeability values is highly leached and ferruginised (S10-1). This iron content block the pore throat reducing the effective permeability. On the other hand, the sample with low porosity shows the partially kaolinites feldspar along with the low percentage of iron oxide. Low percentage of kaolinite increases the permeability acting as bridge between pores.

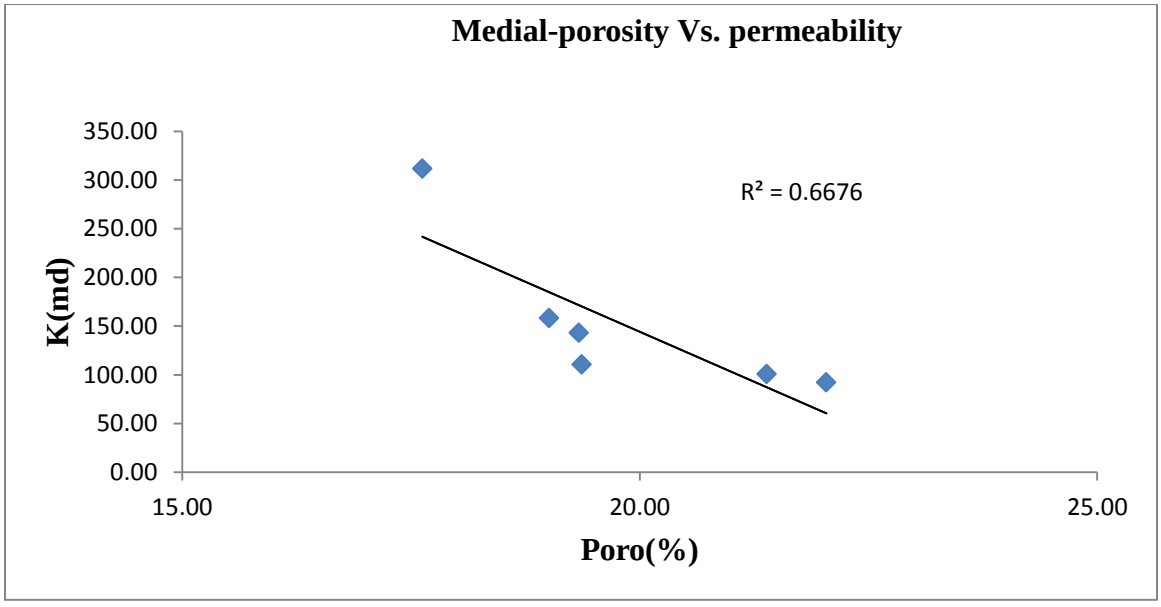


Figure 83: Cross -plot of permeability versus porosity for proximal part of Al-Ilb paleochannel.

## 6.8 Porosity-Permeability Relationship for Distal Part

The horizontal and vertical permeability versus porosity relationships for distal part of Al-Ilb paleochannel are illustrated in Figure 84, Figure 85. These graphs show no correlation between porosity and permeability. The lines of best fit have extremely low coefficient of correlation ($R^2$ = 0.34, and $R^2$ = 0.27 for horizontal permeability versus porosity and vertical permeability versus porosity, respectively).

The distal part of Al-Ilb paleochannel shows different cluster of porosity versus horizontal permeability and vertical permeability, related to depositional and post-depositional changes. On the bases of petrographic and microstructural studies, it can be stated that formation reveals four different categories of cluster in the distal part. These categories include low porosity-low permeability, high porosity-high permeability, low porosity-high permeability and high porosity-low permeability. The samples S1-2A, S6-6, S7-2, and S7-6 represent low porosity and low permeability category with moderate to poorly sorting, highly leached and relatively small grain size. The SEM micrograph clearly shows high quantity of platy kaolinite and iron oxide that fill the pores and reduce the pore throat.

Table 16: Thin-section petrography of Sarah Formation sandstone samples representing proximal, medial and distal parts of Al-Ilb paleochannel

| AL-Ilb Paleochannel | Sec No. | Thin Section ID | Sorting | | ϕ (%) | K (md) | MGS (μ m) | Cement (%) | Matrix (%) | Minerology |
|---|---|---|---|---|---|---|---|---|---|---|
| Proximal | S3 | S3-1A | MS | 0.67 | 20.37 | 285.84 | 186.17 | 6.00 | 3.00 | Quartz Arenite |
| | | S3-3.5 | PS | 1.15 | 19.57 | 514.27 | 394.44 | 5.00 | 1.00 | |
| | | S3-4 | MS | 0.74 | 18.58 | 2202.90 | 233.33 | 3.00 | 1.00 | |
| | S4 | S4-2 | MS | 0.74 | 15.18 | 612.82 | 277.36 | 3.00 | 2.00 | |
| | | S4-3 | MS | 0.74 | 25.09 | 2845.70 | 264.71 | 1.00 | 3.00 | |
| | | S4-4 | MS | 0.74 | 24.53 | 1334.20 | 282.95 | 4.00 | 2.00 | |
| | | S4-9 | PS | 1.15 | 19.63 | 42.68 | 256.25 | 8.00 | 6.00 | |
| Medial | S10 | S10-1 | PS | 1.15 | 22.04 | 92.14 | 227.94 | 5.00 | 5.00 | |
| | | S10-5 | MS | 0.74 | 17.62 | 311.62 | 612.90 | 4.00 | 2.00 | |
| Distal | S1 | S1-2A | MS | 0.74 | 21.12 | 307.23 | 296.43 | 4.00 | 0.50 | |
| | | S1-7 | PS | 1.15 | 19.40 | 3892.20 | 282.61 | 4.00 | 0.50 | |
| | | S1-9 | PS | 1.15 | 19.65 | 2001.50 | 254.72 | 3.00 | 1.00 | |
| | S2 | S2-2 | MS | 0.67 | 23.18 | 3787.90 | 113.16 | 3.00 | 2.00 | |
| | | S2-4 | MS | 0.67 | 22.505 | 138.94 | 100.00 | 6.00 | 6.00 | |
| | | S2-7 | WS | 0.36 | 25.57 | 1696.40 | 104.35 | 3.00 | 0.00 | |
| | S5 | S5-2B | WS | 0.36 | 28.28 | 177.04 | 78.13 | 7.00 | 6.00 | |
| | | S5-9 | MS | 0.74 | 24.83 | 647.69 | 272.64 | 4.00 | 5.00 | |
| | | S5-13B | MS | 0.74 | 27.53 | 1692.30 | 213.41 | 4.00 | 8.00 | |
| | S6 | S6-1 | MS | 0.74 | 24.22 | 52.04 | 151.89 | 8.00 | 10.00 | |
| | | S6-6 | MS | 0.74 | 20.03 | 323.92 | 78.38 | 6.00 | 3.00 | |
| | S7 | S7-2 | PS | 1.15 | 18.44 | 494.90 | 240.00 | 3.00 | 8.00 | |
| | | S7-6 | MS | 0.74 | 22.81 | 152.69 | 181.03 | 5.00 | 8.00 | |
| | S8 | S8-10 | MS | 0.74 | 29.58 | 1741.00 | 315.85 | 3.00 | 3.00 | |
| | | S8-12 | WS | 0.36 | 33.08 | 1585.20 | 104.55 | 4.00 | 2.00 | |
| | | S8-16 | MS | 0.74 | 31.02 | 4010.30 | 229.17 | 2.00 | 4.00 | |
| | S9 | S9-9 | PS | 1.15 | 23.33 | 2970.40 | 483.87 | 4.00 | 2.00 | |
| | | S9-12 | PS | 1.15 | 29.18 | 5768.20 | 394.29 | 2.00 | 3.00 | |

The high porosity-high permeability category is represented by samples S2-2, S2-7, S2-4, S5-13B, S8-10, S8-12, S8-16, S9-9 and S9-12. The thin-section photographs reveal that almost all of these samples are moderately to well-sorted and in some cases poorly-sorted, but the contact is highly leached, and well-defined pores are present. Therefore, good pore throats develop that ultimately leads to development of good permeability. The micrographs for some samples also revealed the presence of special type of clay i.e. palygorskite. The needle like structure of palygorskite acts as bridge resulting in the enhancement of permeability.

The high porosity-low permeability population is represented by S5-2B, S5-9, and S6-1. They exhibit porosity values of 24% and 28%, and permeability values less than 750mD. The high porosity is due to the presence of moderately to sorted grains and low permeability is due to presence of iron staining blocking pores. In addition, sometimes small grains block the pore throat reducing permeability.

The high permeability-low porosity category is due to the presence of comparatively small pores, but these pores are well-connected. The SEM micrographs show presence of iron oxide in some quantity, but micrographs also reveal the clarity of pores.

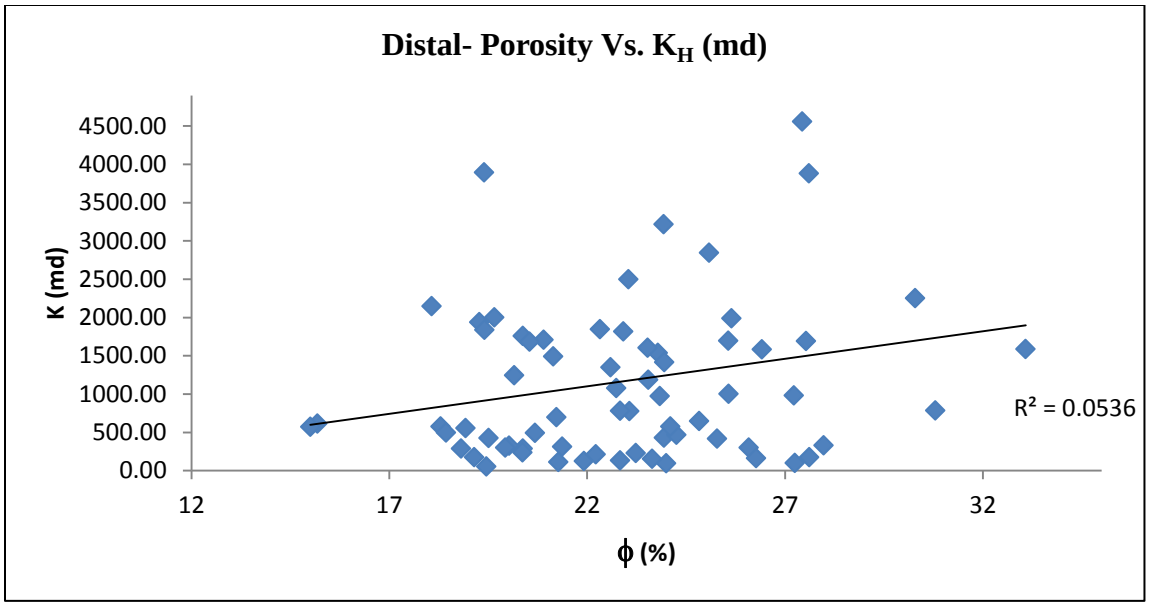


Figure 84: Cross -plot of horizontal permeability versus porosity for distal part of Al-Ilb paleochannel.

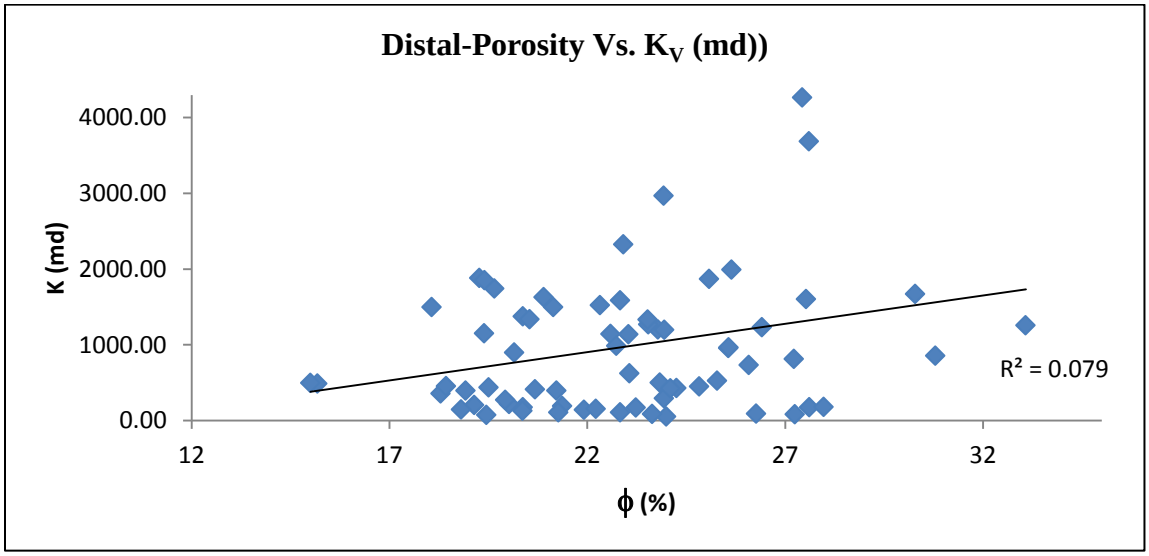


Figure 85: Cross -plot of vertical permeability versus porosity for distal part of Al-Ilb paleochannel.

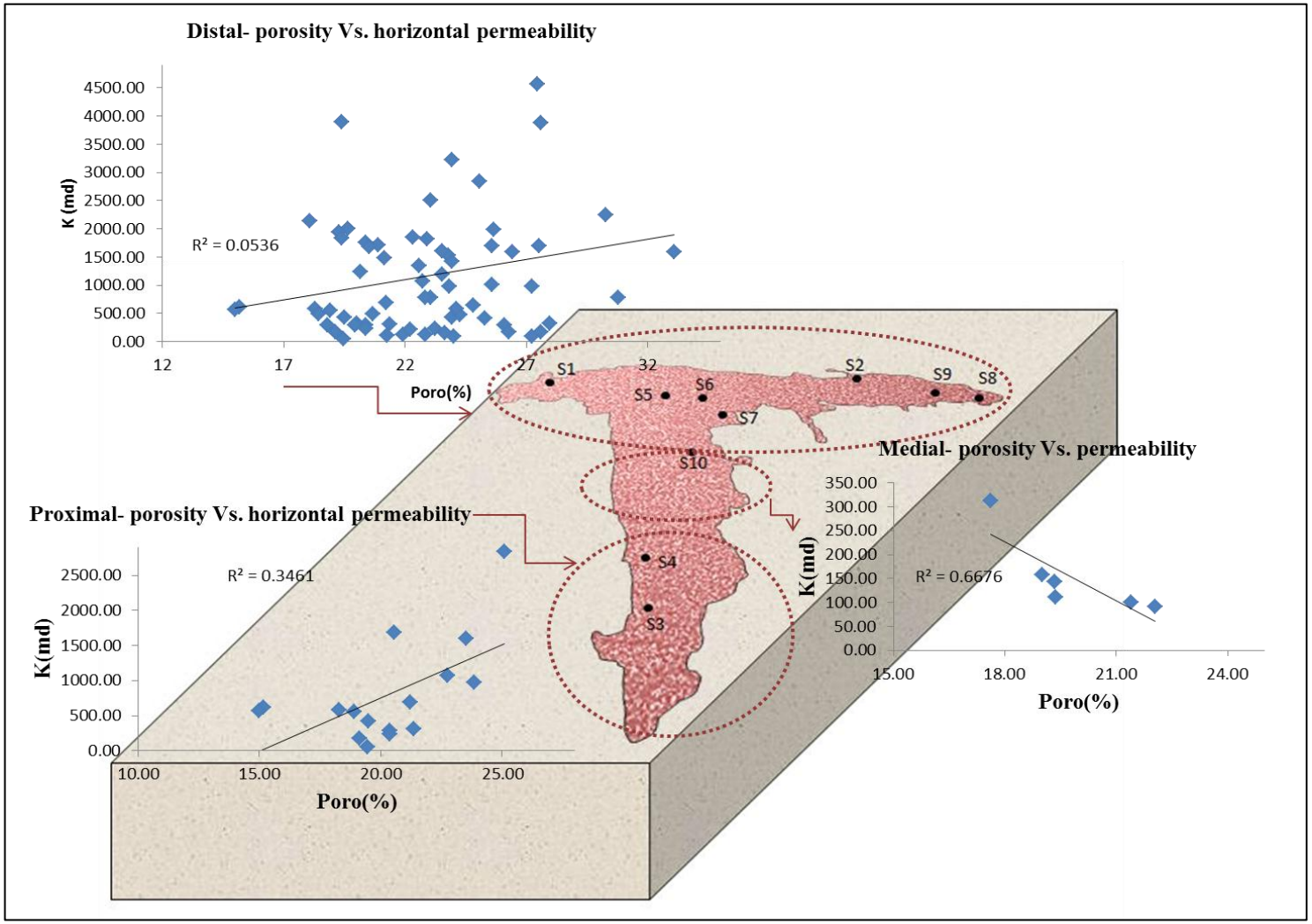


Figure 86: Block diagram showing cross plot of porosity versus permeability values at different part of Al Ilb paleochannel

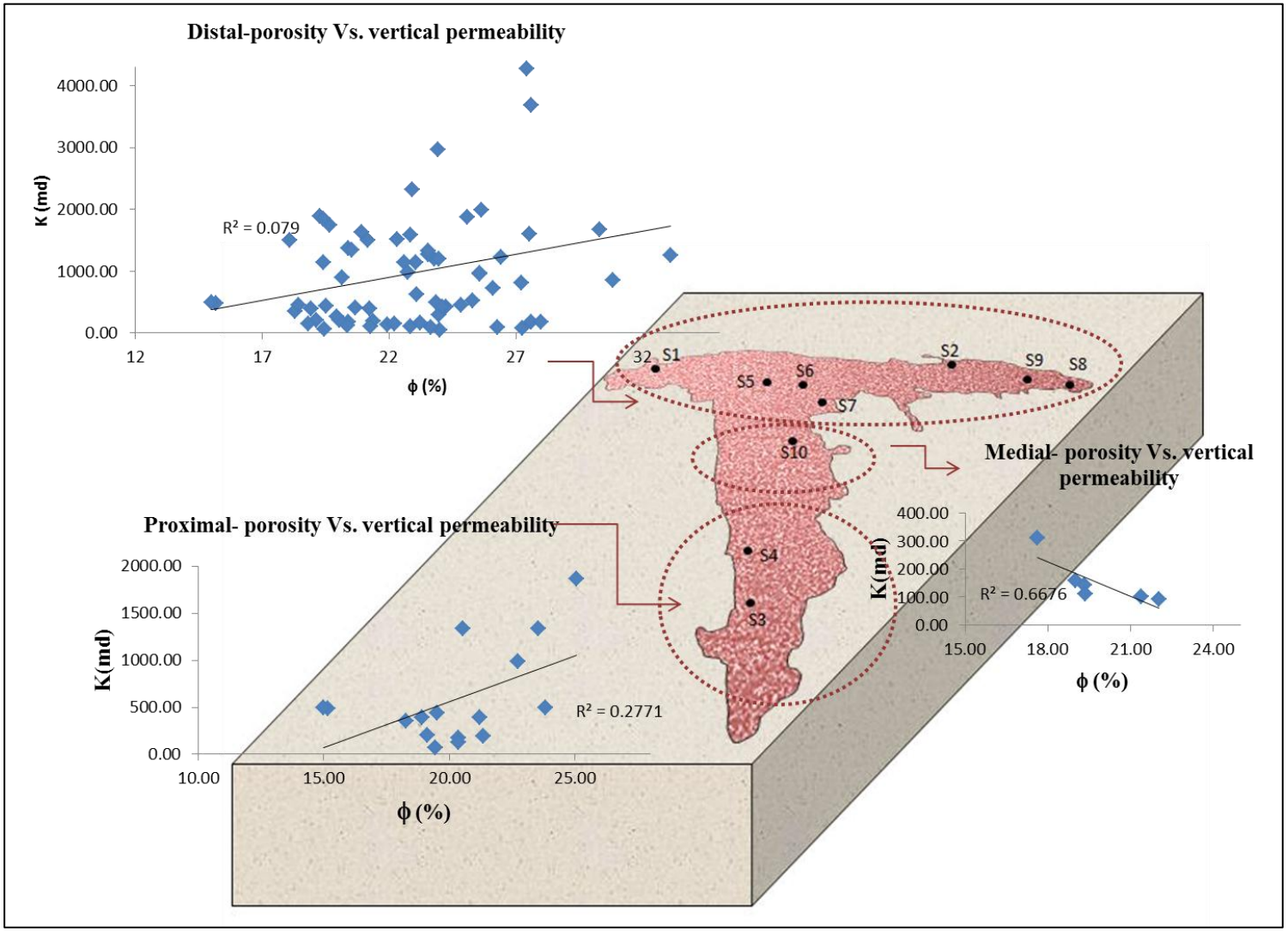


Figure 87: Block diagram showing the scatter plot of porosity and permeability.

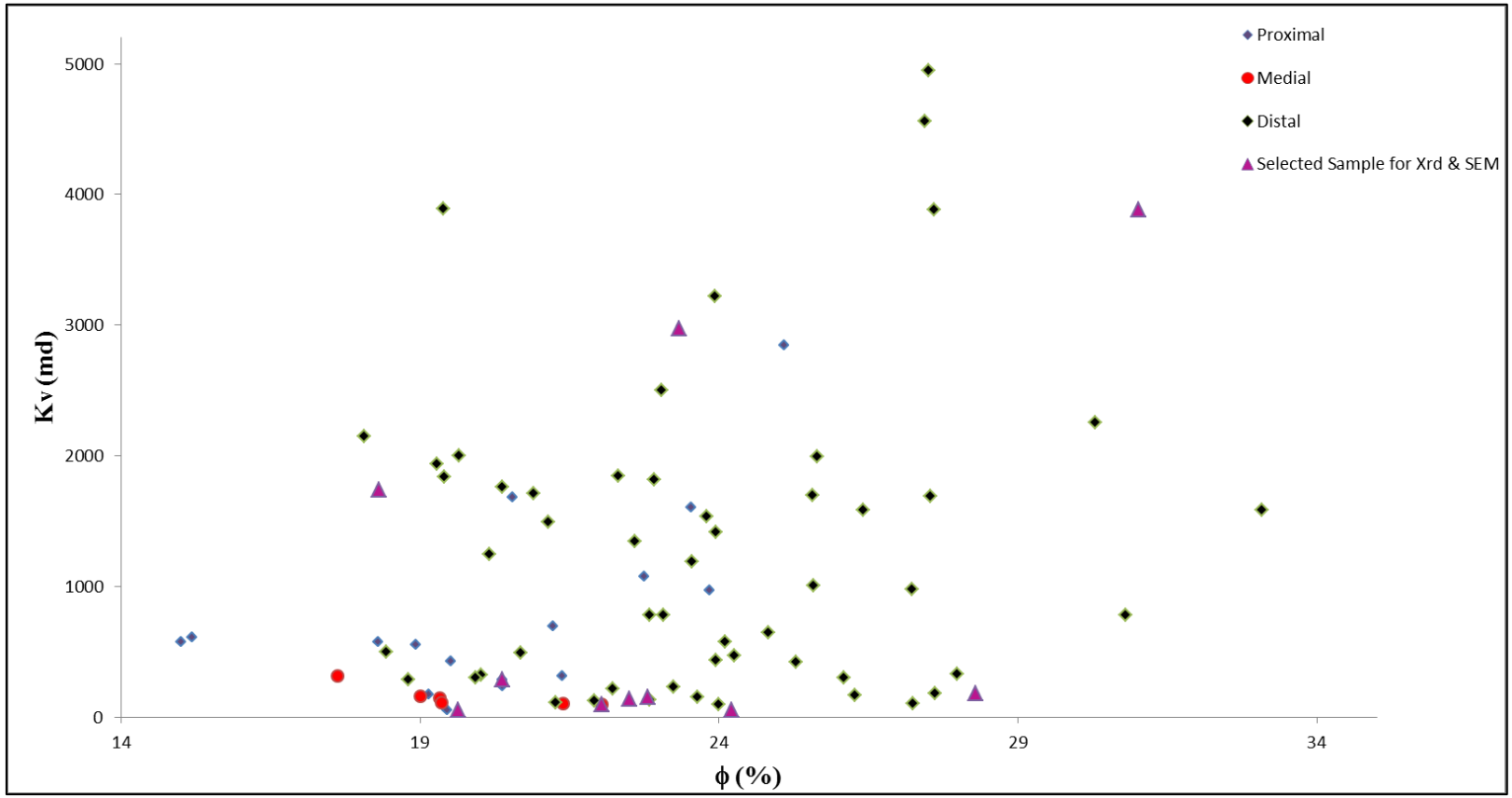


Figure 88: Porosity Vs. Horizontal permeability measurements of proximal, medial and distal part Al Ilb paleochannel.

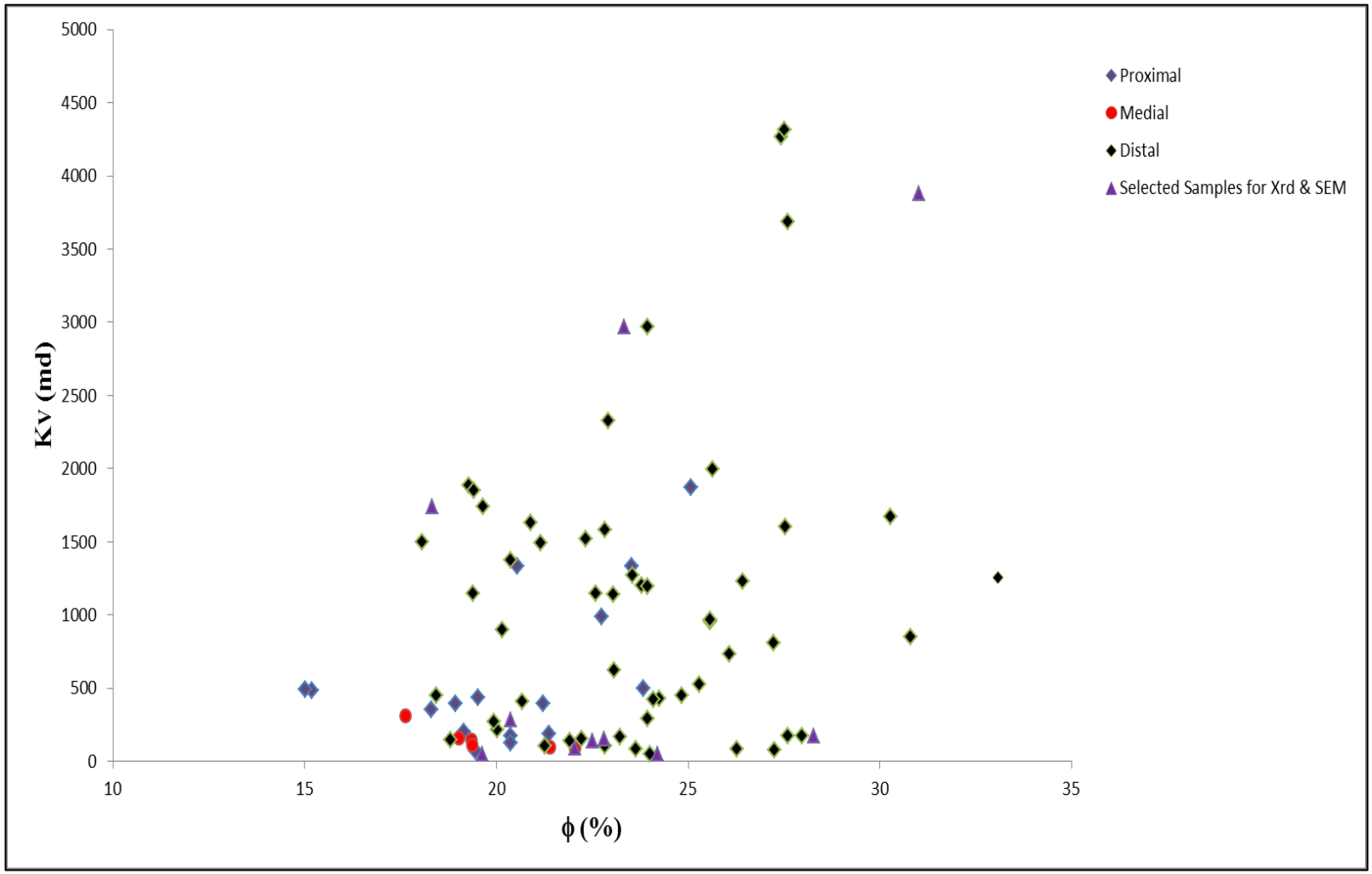


Figure 89: Porosity Vs. Vertical permeability measurements of proximal, medial and distal part Al Ilb paleochannel

# Chapter 7

# GIS Application

## 7.1 Introduction

Geographic information system (GIS) is an emerging technique applied in almost all the fields of geology, earth related sciences, computer and information technology. GIS basically synthesizes the spatial data and then processes and analyzes it with aid of supportive software and hardware. The spatial data management or synthesis is the characteristics of GIS, in which it manages all the existing data scientifically as multi-source, multi-scale data in multiple layers and link stored data with numerical models as data bank or data base (Napieralski et., al. 2007). The data base file is imported as unified reference coordinates system, unified coding, unified standards and organization. So, each point line or polygon (imported as shape file) contained two man information; the attributes and geographic location. The attributes are linked with geographic location and it is in other word unified management of data in integrated GIS environment. Several layers overlaid on one another in the form of multilayers and displayed in the form of thematic map as it is topologically linked with data base. The analysis of statistical data is treated in the form of raster and vector form that includes different tools like 3D analyst. The outstanding ability of GIS is to display the data in the form of maps reports or statistical graph by linking this information to geographic location.

The principal goal of this chapter is to describe and link the sedimentological and petrophysical data of Sarah Formation to geographic location of outcrop in the Al Ilb paleochannel. The sedimentological data consists of thin-section analysis, thin-section photographs and tables that contain all the useful information of studied area. While petrophysical data includes the porosity and permeability distribution within each outcrop (S1 to S10) and within each part of paleochannel i.e. Proximal medial and distal. Moreover, the SEM, XRD and CT scan analyses are also linked in the form of smart maps.

## 7.2 Geological Intelligent Maps

Maps are considered as fundamental tools of understanding the large features of earth and as well as visually representing the area. In addition to that the geological intelligent maps contain all the needed information and geographically linking that information to point line and polygon; that is known as attributes.

### 7.2.1 Methodology

The scanned map of Baqa quadrangle is geo-referenced and the Sarah Formation especially and the nearby exposed formation are digitize using arcGIS9.3. This is carried out by using the following steps:

- Create the shape file in Arc catalogue (for each formation exposed in study area, and uploading the GPS coordinates of outcrops i.e. studied at Al-Il paleochannel.
- Start digitizing the formation by using ‘Edit tool’

- For assigning the attributes to point line and polygon use ‘open attributes’. In this dialogue select the add field and create new field for i.e. Section photographs, SEM, XRD-EDX, and thin-section information.
- The following tools are needed for completing the task:
    - Standard Tool bar
    - Spatial analyst
    - Editor tool
    - Geo referencing tools
    - Layer and attribute data managements
    - Identify tool

### 7.2.2 Sarah Formation Smart Map

Geographic information system (GIS) is a power tool that integrates multisource data and manages multi scale studies. The excellent ability of linking petrographic, petrophysical, and microphotograph data to geographically located geo referenced outcrop sections at Al-Alb paleochannel.

As discussed in previous chapter the detailed field and laboratory investigations of Sarah Formation were performed. All the extracted information to their assigned section as shown in Figure 91, Figure 92,Figure 93,Figure 94 and Figure 95 was linked. The shape file named ‘Data Bank’ contained all the information including that contains field photo, vertical profile, and thin-section, SEM-EDX, and XRD results.

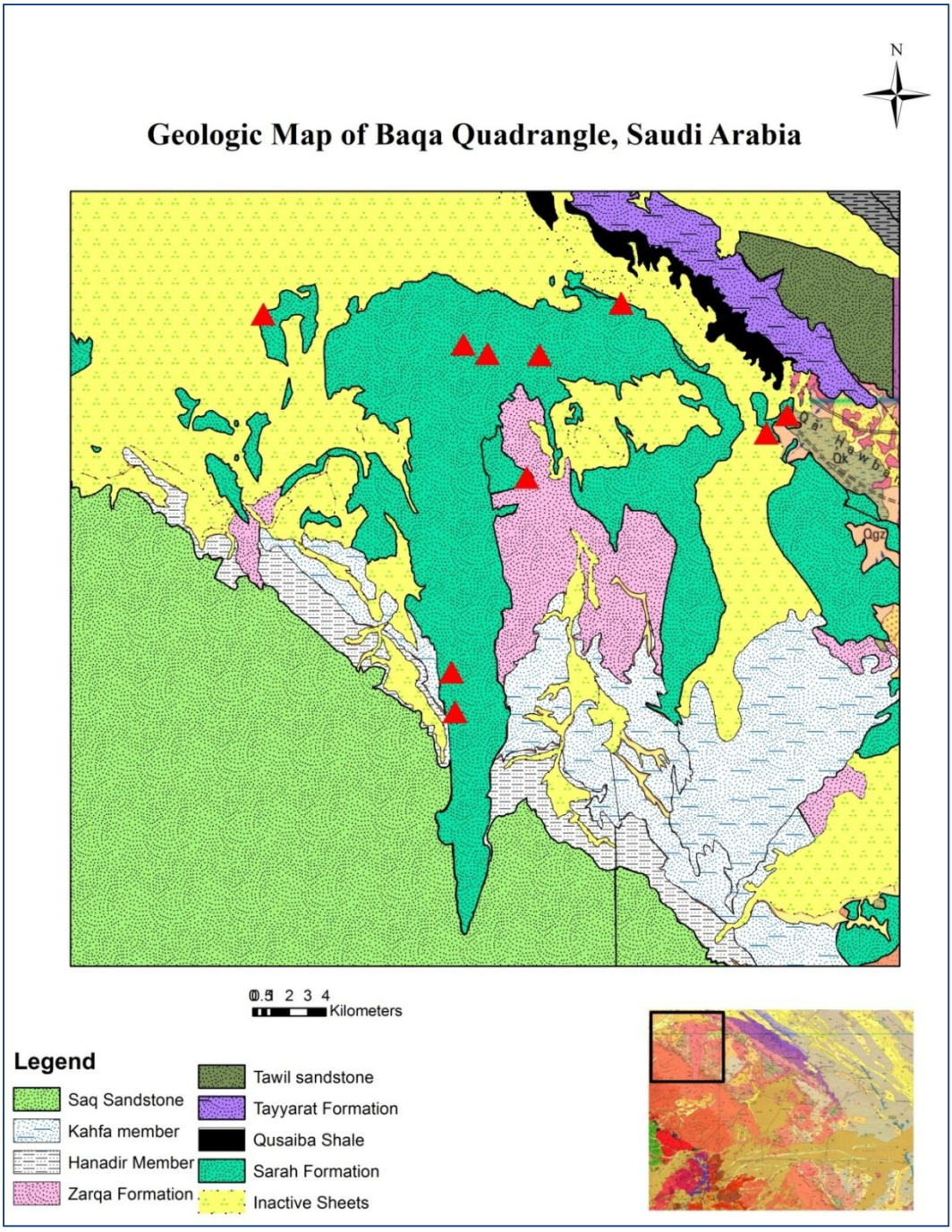


Figure 90: Digitized Sarah Formation and other formation at Baqa, Quadrangle, Al-Il paleochannel

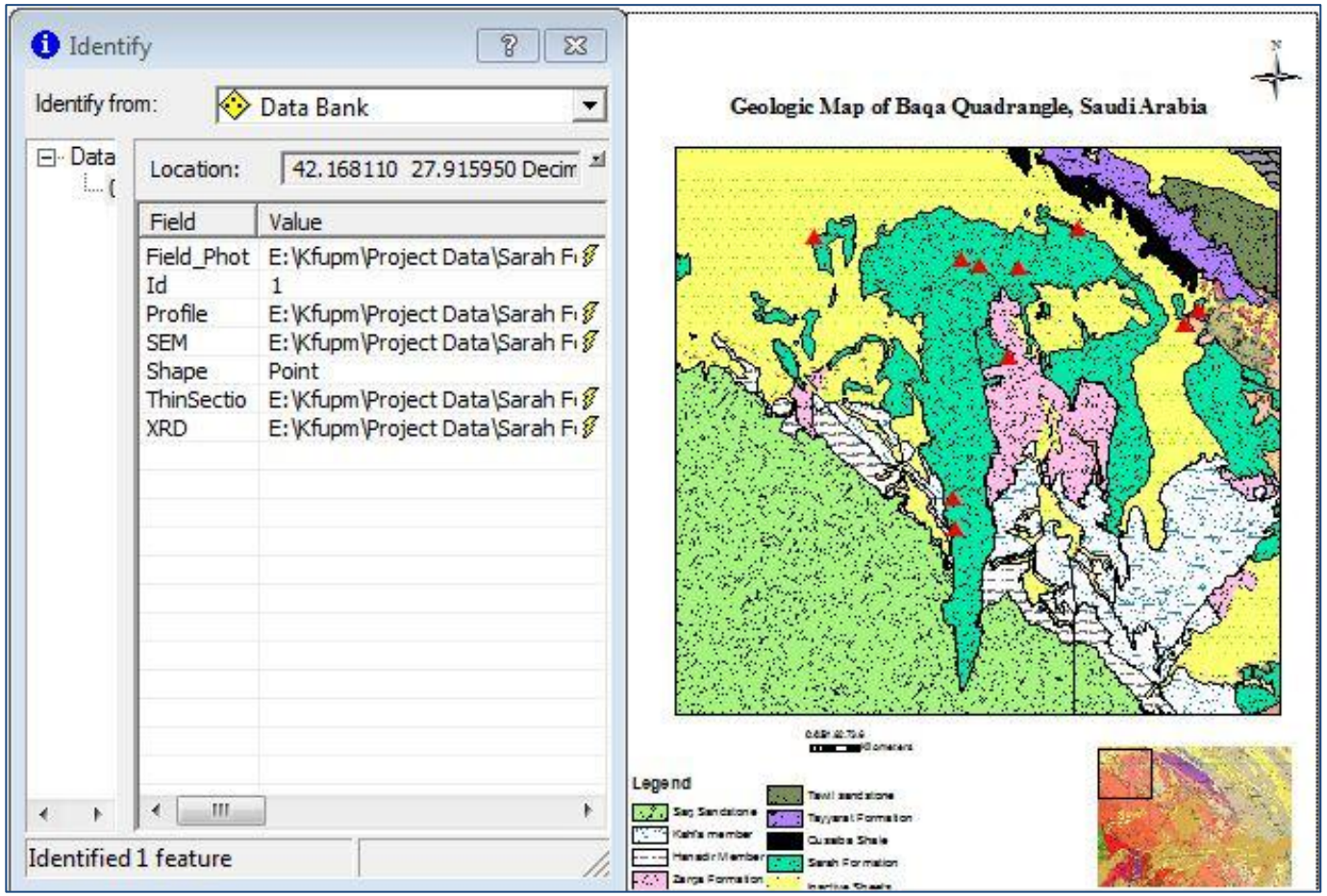


Figure 91: Application Identify tool, showing Data bank

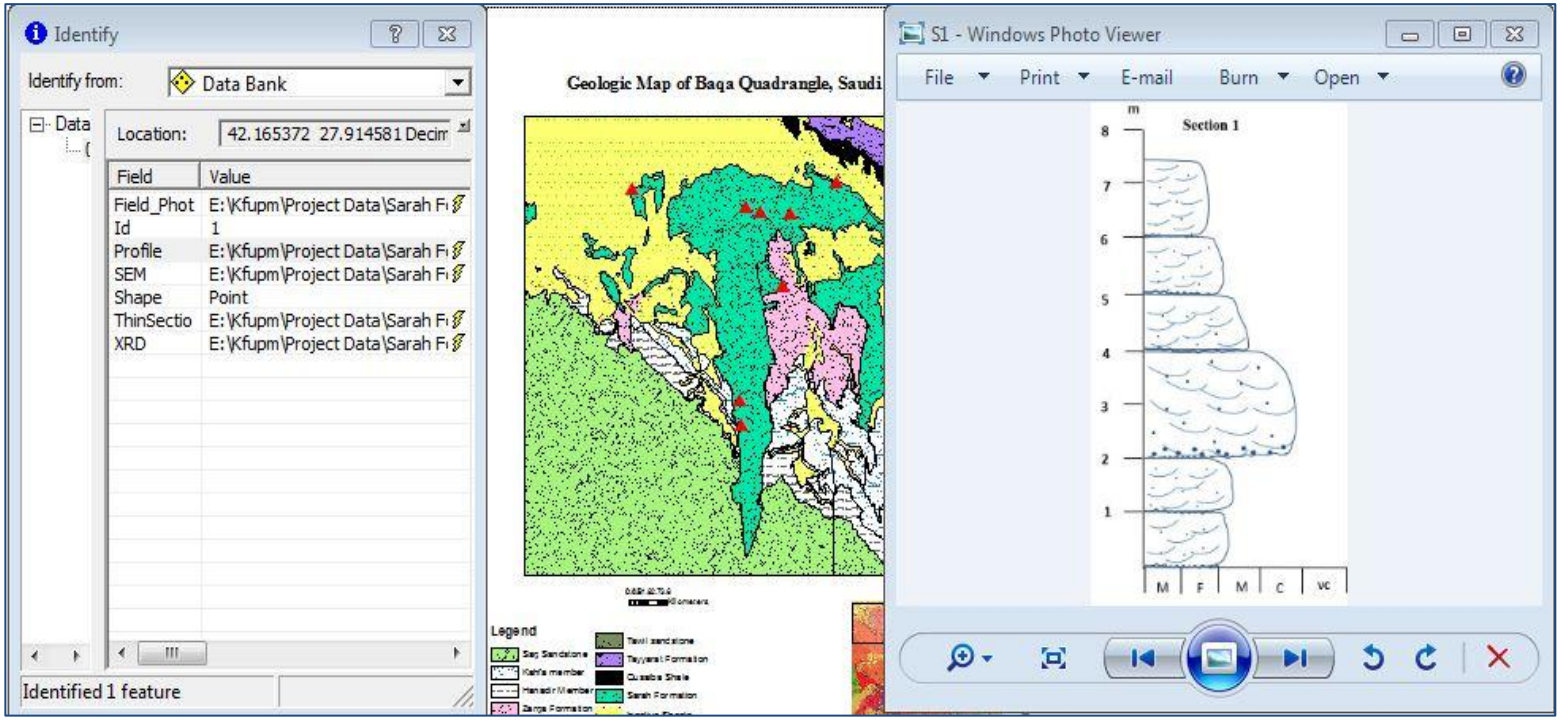


Figure 92: Identify tool showing outcrop of Section 1 as stored in Data bank.

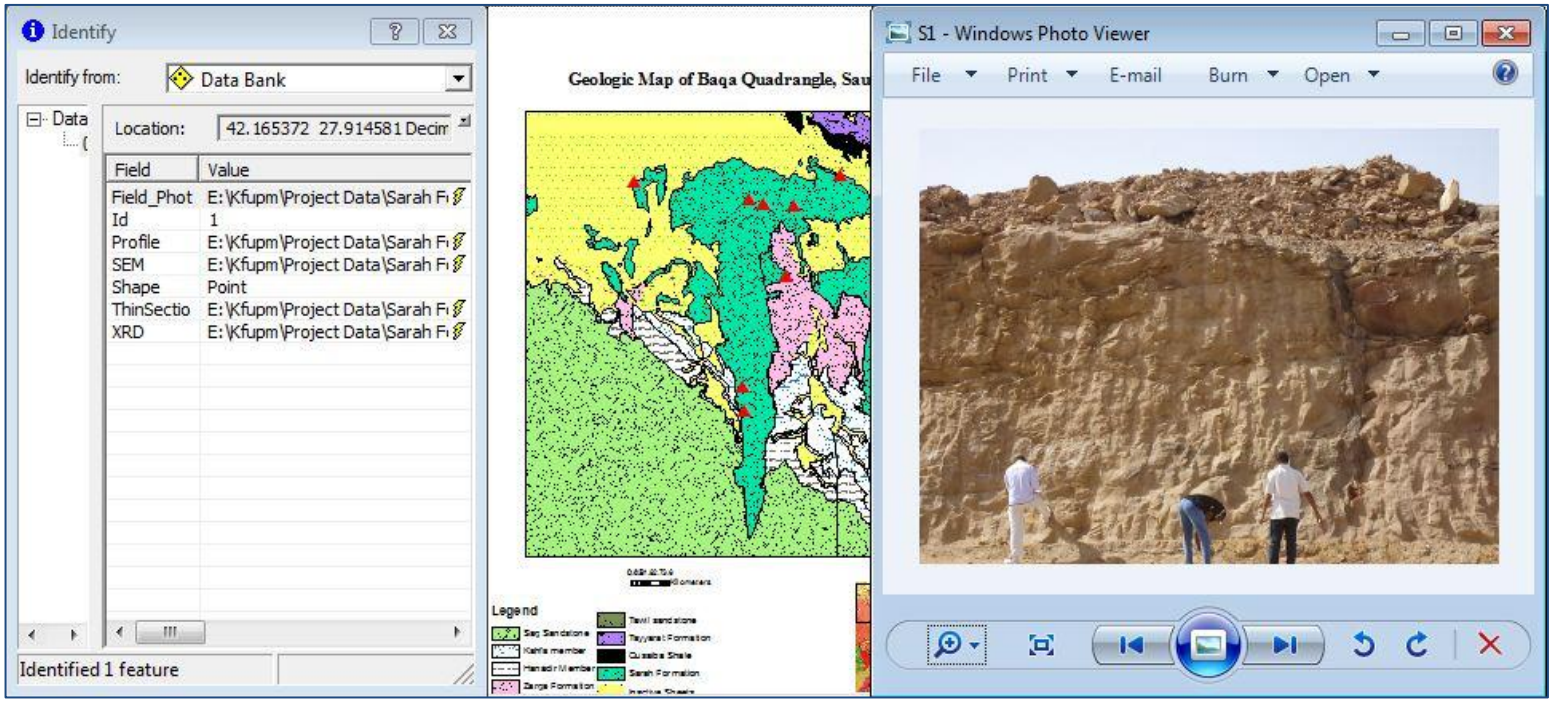


Figure 93: Identify tool showing field photograph of section, Al-Il paleochannel

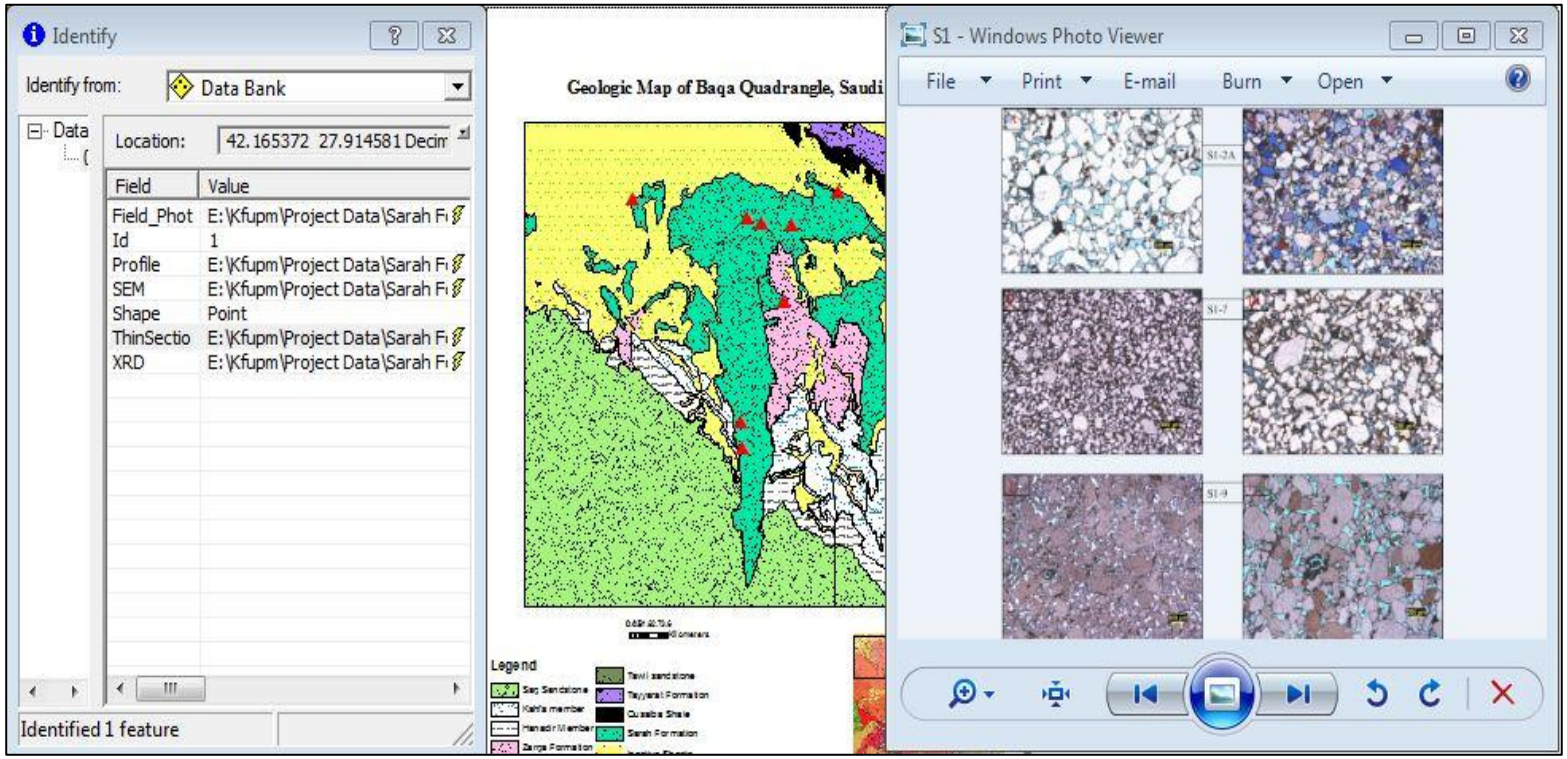


Figure 94: Identify tool showing thin section image of represented samples, Al-Il paleochannel

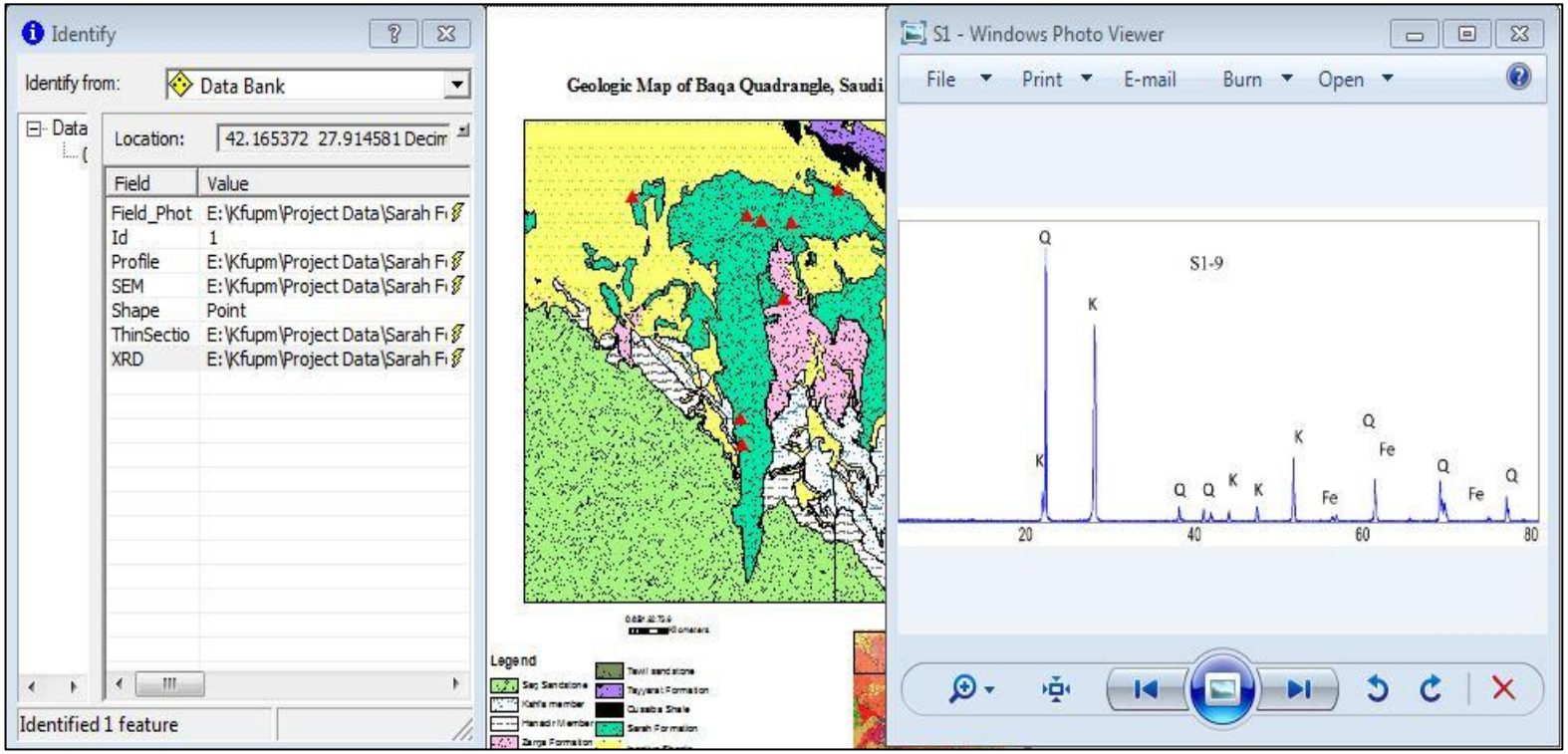


Figure 95: Identify tool showing XRD image of represented samples, Al-Il paleochannel

# Chapter 8

# Conclusions and Recommendations

## 8.1 Conclusions

This research is devoted to investigate the sedimentological and petrophysical heterogeneity of Late Ordovician, glacio-fluvio Sarah Formation. The sedimentological part includes facies analysis and depositional environment and petrophysical part includes porosity and permeability study. The Sarah Formation outcrops in central Arabia parallel to the Arabian Shield. The research area is located in Baqa Quadrangle Sheet 27F. Methods of data analysis include field investigations, facies analysis, thin-section petrography and XRD, SEM-EDX and CT-scan on samples collected from field. The integration of field and laboratory data has led to understanding the distribution of petrophysical parameters (porosity and permeability) in proximal, medial and distal parts of Al-Ilb paleochannel.

The field investigations indicate that the proximal part of Sarah Formation is generally medium to coarse grained, moderately to well-sorted, tough cross bedded sandstone. These beds usually show fining upward sequence with scouring surface at the base. Dominantly trough cross bedding is present and laterally changes to planar and sometime

to crossbedding. The petrographic studies of proximal part shows that it mainly consists of 98% ferruginised quartz. The SEM and XRD results revealed that booklet structure of kaolinite, and grapes cluster of iron oxide are dominantly present is most samples.

The medial part of Al-Ilb paleochannel consists of medium to coarse-grained, moderately to poorly-sorted, and horizontally stratified sandstone. The petrographic studies reveal that dominant composition is quartz (98%), and partially kaolinized feldspar. The SEM micrograph confirms the dissolution of feldspar to kaolinite.

The field investigation indicates that the distal part is highly complex, no specific correlation is made among the sections. In general, the distal part is dominantly composed of fine to medium grained tough cross bedded sandstone, fine to medium horizontally stratified sandstone facies and coarse to very coarse trough cross bedded sandstone. The distal part shows fining upward sequence, beds are thick as much of 3 meters. The thin-section petrography shows that the Sarah Formation at distal part is moderate to poorly and sometime well-sorted sandstone. The SEM micrograph shows the presence of high amount of clays (like kaolinite, smectite, and palygorskite) in some samples and some of the samples are highly leached.

The petrophysical analyses were performed on all the core plugs (226). After removing outliers; 140 core plugs were used for petrophysical analysis. These 140 cores represent the proximal, medial, and distal part of Al-Ilb paleochannel. The proximal, medial and distal part of Al-Ilb paleochannel is represented by very close range of porosity but permeability shows wide range of values.

The porosity and permeability values of Sarah Formation are controlled by both textural and compositional characteristics, cementing material, grain size variation and quartz overgrowth and dominantly by type and amount of clays present. Besides the depositional fabrics and diagenesis controls, the petrophysical property is dominantly affected by pore volume and number of connected pores; ultimately affecting the size of pore throat.

The statistical analysis was conducted on porosity and permeability measurement for proximal medial and distal part of Al-Ilb paleochannel. The statistical analysis proves the homogeneity of porosity distribution among the different of part of channel. The coefficient of variation is 0.1, 0.08, and 0.15 for proximal, medial and distal part respectively. The statistical distributions of horizontal and vertical permeability measurements are positively skewed. The statistical parameters indicate that the horizontal permeability measurements are higher than the vertical permeability. The coefficient of variation (cv) for horizontal and vertical permeability indicates high degree of heterogeneity for each part of paleochannel (cv is greater than 0.5 for each part separately).

The relationships between porosity versus permeability (horizontal and vertical) for all part of Al-Ilb paleochannel reveal very poor correlation. This poor correlation is attributed to several factors, including depositional fabrics, diagenesis, and presence of clays and cementing material, type, size, and number and volume of pore throat.

## 8.2 Recommendations

The following studies are recommended for future work;

1. Detailed outcrop studies of proximal and medial parts are needed to fill the gaps, and to integrate the outcrop data with the subsurface data form South Rub Al-Khali basin for better understanding of geologic units.

2. Sedimentological and petrophysical correlation of Al-Ilb paleochannel with other paleovalleys is needed to understand the spatial distribution of fluvial and glacial-fluvial facies.

3. Geostatistical model is needed for better understanding of reservoir heterogeneity.

4. Detailed mapping of glacial deposits are needed and to cover the all the paleochannels that are bordering the Arabian Shield.

5. Horizontal and vertical heterogeneity within each outcrop and as well as along the whole paleochannel is characterized by using 2d modeling in GIS softwares.

6. CT-scan application can be used for detail study of heterogeneity.

# References


1. Abdullatif, O., & Makkavi, M. 2004. Geological and Geostatistical modeling of Paleozoic sandstone hydrocarbon reservoir of Quwarah Member, Qasim, Saudi Arabia. KFUPM. Dhahran, Saudi Arabia: RI Grant Project

2. Abdullatif, O., & Makkawi, M., 2010. Geological and Geostatistical aquifer characterization of the outcrop analog of Wajid Sandstone in south west Saudi Arabia. KFUPM. Dhahran, Saudi Arabia: KACST Project #25-65

**3.** Al-Hajri, S. 1995. Biostratigraphy of the Ordovician Chitinozoa of Northwestern Saudi Arabia. In Paleozoic Palynostratigraphy of the Kingdom of Saudi Arabia. Special Issue of Review of Palaeobotany and Palynology. v. 89, nos. 1/2 p. 27-48.

4. Al-Harbi, O. A., Khan, M.M., 2011. Source and origin of glacial paleovalley-fill sediments (Upper Ordovician) of Sarah Formation in central Saudi Arabia. Saudi Society for Geosciences. Arab J geoscience 2011. 4:825-835.

5. Al-Laboun, A. 1982. The Subsurface Stratigraphy of the Pre-Khuff Formations in Central and Northwestern Arabia. (PhD thesis); Jiddah, King Abdulaziz University.

6. Al-Laboun, A. 1986. Stratigraphy and Hydrocarbon Potential of the Paleozoic Succession in Both Tabuk and Midyan Basins, Arabia. American Association of Petroleum Geologists Bulletin, v. 40, p. 373-397.

7. Al-Mahmoud and Al-Ghamdi, 2010. Overview of Tight Gas reservoir in Saudi Arabia. 2nd Middle East Tight Gas Workshop, Bahrain. Association, 116, 331-347.

8. Alsharhan, A.S., Nairn, A.E.M., 1997. Sedimentary Basins and Petroleum Geology of the Middle East. Elsevier, Amsterdam.

9. Al-Zayer A., Mesdour R., Al-Faleh K., Basri M., and Utaibi Abdullah 2013. Practical Well Testing Analysis Considerations in Heterogeneous Sandstone. SPE 168092. Presented at the SPE Saudi Arabia section Annual Technical Symposium and Exibition, Khobar, 19-22 May 2013.

10. Bell A, Spaak P (2006) Gondwana glacial events and their influence and petroleum system in Arabia. AAPG International conference and exhibition, Perth, Australia, 5–8 Nov 2006.

11. Beydoun, Z. R., 1985, The geological setting and tectonic framewoor of the Middle East In Proceedings of the seminar in source and habitat of petroleum in the arab sountires OPAEC, Kuwait, p. 5-71.

12. Bigot, M. 1970. Geology of the Tabuk and Jauf Formations in the Wadi alFajr Area, BRGM, 70 Jed 28, Directorate General of Mineral Resources, Ministry of Petroleum and Mineral Resources.

13. Borer, J. M., and P. M. Harris, 1991, Depositional facies and cyclicity in the Yates Formation, Permian Basin Implications for reservoir heterogeneity: AAPG Bulletin, v. 75, p 726-779.

14. Bramkamp, R.A., L.F. Ramirez, G.F. Brown and A.E. Pocock. 1963. Geological Map of the Wadi ar-Rimah Quadrangle, Kingdom of Saudi Arabia. U.S. Geological Survey Miscellaneous Geological Investigations Map I- 206A.

15. Briner et al., 2010. Regional Reservoir Quality Of Tight Gas Plays, the Ordovician Sarah Formation in the Rub al Khali Basin of Southern Arabia. 2nd Middle East Tight Gas workshop, Bahrain.

16. Clark-Lowes 2005, Arabian glacial deposits: recognition of palaeovalleys within the upper Ordovocian Sarah Formation, Al Qasim district, saudi Arabia.Proceedings of the Geologists Association, 116,331-347.

17. Clark-Lowes, D.D. 1980. Sedimentology and Mineralization Potential of the Saq and Tabuk Formations, al-Qasim District. Imperial College of Science and Technology, Cover Rock Contract, Open-File Report CRC/Ic-7, Saudi Arabia, Ministry of Petroleum and Mineral Resources, Deputy Ministry for Mineral Resources, Jiddah, Open File Report DGMR-767, p. 88.

18. Danial Paul le Heron, James Howard 2010. Evidence for late Ordovician glaciation of Al Kufrah Basin, Libya: AES Journal, v. 58, p. 354-364.

19. Al-Dabbagh M. E., 2013 Effect of tectonic prominence and growth of Arabian shield on Paleozoic sandstone succession in Saudi Arabia. Arab Journal of Geoscience. V. 6 p. 835-843.

20. Folks, R. L., 1959, Petrology of sedimentary rocks: Hemphill's Book store, Austin, Texas, 170 p.

21. Ghienne, J, -F., 2003. Lte Ordovicain sedimentary environment, glacial cycles, and Post- glacial transgression in the Taoudeni Basin, West Africa. Palaogeography, Palaeoclimatology, Palaeoecology 189, 117-145.

22. Goldstein, J. I. and Yakowitz, H., 1975, (ed), Practical scanning electron microscopy; electron and microprobe analysis: New York, Plenum Press, 582p.

23. Grant , C. W., D. J. Goggin, and P. M. Harris, 1994, Outcrop analog for cyclic-shelf reservoirs, San Andres Formation of Permian Basin: Stratigraphic framework, Permeability distribution, geostatistics and fluid-flow modeling: AAPG Bulletin, v. 78, p 23-54.

24. Hallett, D., 2004, Petroleum Geology of Libya (second Impression). Elsevier, Amsterdam. 503p.

25. Haq, B.U. and A.M. Al-Qahtani 2005. Phanerozoic cycle chart of sea-level changes for the Arabian Platform. GeoArabia, v. 10, no. 2, p. 127-160.

26. Hardy, R., Tucker, M., 1988, Techniques in sedimentology,-Blackwell Publications.

27. Holdich A. 2006.Tight gas sands. SPE Texas A & M University

28. Krumbein, W. C., and Pettijhon, F. J., 1961, Manual of sedimentary Petrology: New York, Appleton-century-Crofts, 549 p.

29. Le Heron, D., Sutcliffe, O., Bourgig, K., Craig, J., Visentin, C., Whittington, R., 2004. Sedimentary architecture of Upper Ordovician tunnel valleys, Gargaf Arch, Libya: implications for the genesis of a hydrocarbon reservoir. GeoArabia 9, 137-160.

30. Le Heron, D.P., Gienne, J.-F., El Houicha, M., Khoukhi, Y., Rubino, J.-L. 2007. Maximum extent of ice sheets in Morocco during the late Ordovican glaciation. Palaeogeography, Palaeoclimatology, Palaeoecology 245, 200-226.

31. Le Heron, Jonathan C., James L. Etienne 2009. Ancient glaciation and hydrocarbon accumulation in North Africa and the Middle East: ESR, v. 93. P. 47-76.

32. McClure, H.A. 1978. Early Paleozoic Glaciation in Arabia, Paleogeography, Paleoclimatology, Paleoecology, v. 26, P. 315-326.

33. McClure, H.A. 1978. Early Paleozoic Glaciation in Arabia, Paleogeography, Paleoclimatology, Paleoecology, v. 26, P. 315-326.

34. McGillivray, J. G. and M. I. Husseini, 1992, AAPG Bulletin, 76 (10): 1473-1490.

35. Miall, A. D,. 1985. Architectural element analysis: a new method for facies analysis applied to flufial deposits: Earth Sci Rev 22: 261-308.

36. Millson, J. A., Mercadier, C.G.L., Livera, S. E. and Perters, J. 1996. The lower Paleozoic of Oman and its context in the Evolution of a Gondana continental margin. Journal of Geological Society V. 153, no. 2, p. 213-230.

37. Moscariello, A., Spaal, P., Jourdan, A., & Azzouni, A. H. 2009. The Ordovician Glaciation in Saudi Arabia – exploration challenges part 1. Geology outcrop, Subsurface, analogues), search and Discovery article # 50175

38. O.M. Abdullatif 2011. Facies, Depositional Environment and Sandstone Composition of the Late Ordovician Glacio-fluvio Sanamah Member, Wajid Formation, South West Saudi Arabia. EGU poster presentation.

39. Pettijhon, F J., 1987, Persistence of heavy Minerals and Geological age: Geology vol. 46, p. 610-625.

40. Pocock, A.F., R.W. and R.P. Koop. 1949. Geology of the Wadi Atj, Buraida, Hail Area, North Central Nejd, Saudi Arabia. Saudi Aramco Unpublished Geological Report G-41, 66p.

41. Sahin A. aand Hassan H., M. 1998. Enhancement of Permeability Variograms using Outcrop Data. The Arabian Journal for science and Engineering. V. 23, No. 1C.

42. Saner , S., and Sahin, A., 1999, Lithological and zonal porosity-permeability distribution in the Arab-D reservoir, Uthmaniyah field, Saudi Arabia: AAPG Bull., vol. 83, no. 2, p. 230-243.

43. Sahin, A., and Saner, S. 2001. Statistical distribution and correlation of petrophysical parameters in the Arab-D reservoir oilfield, Eastern Saudi Arabia. Journal of Petroleum Geology, 24(1), 101-114.

44. Schenk, C.J. and Pllastro, R. M., 2000. Assessment of undiscovered oil and gas resources of the Great Rub al khali basin by application of the total petroleum system conept- part 11, the Qusiba Paleozoic Petroleum System Geoarabia V.5, p. 175.

45. Schenk, C.J. and Pllastro, R. M., 2000. Assessment of undiscovered oil and gas resources of the Great Rub al khali basin by application of the total petroleum system conept- part 11, the Qusiba Paleozoic Petroleum System Geoarabia V.5, p. 175.

46. Scholle, P. A., 1979. A color illustrate guide to constituents, texture, cements and porosities of sandstone and associated rocks: AAPG Bulletine, 2nd ed., memoir 28, Tusla, Oklahoma, USA.

47. Senalp M 2006. Sedimentology of the incised valleys and their associated low stand Deltic sequence in the Ash-Shiqqah Formation of the Unayzah reservoir, Saudi Arabia. GEO 2006 Middle East conference and exhibition, 27–29 March, Manama, Bahrain.

48. Senalp, M., and A. Al- Laboun., 2000. New Evidence on Late Ordovician Glaciation in Central Saudi Arabia. Saudi Aramco Journal of Technology. Spring 2000.

49. Solomon, M. and Green, R., 1966. A chart for designing modal analysis by point counting: Geol Rundschan, vol. 55, p. 844848.

50. Tyler, N., and R. Finley, 1991, Architectural controls on the recovery of hydrocarbons from sandstone reservoirs, in A. D. Miall and N. Tyler, eds., The three-dimensional facies architecture of terrigenous clastic sediments and its implications for hydrocarbon discovery and recovery: Concepts in Sedimentology and Paleontology 3, SEPM, Tulsa, Oklahoma,p.1–5.

51. Vaslet, D. 1990. Upper Ordovician Glacial Deposits in Saudi Arabia. Episodes v. 13, p. 147-161.

52. Vaslet, D. 1990. Upper Ordovician Glacial Deposits in Saudi Arabia. Episodes v. 13, p. 147-161.

53. Vaslet, D., 2009, Regional geology and stratigraphy of Paleozoic rocks of Arabian Peninsula, Paleozoic clastic Reservoir of the Gulf, Workshop abstract, 14-15.

54. Vaslet, D., K.S. Kellog, A. Berthiaux, P. Le Strat and P.L. Vincent. 1987. Geologic Map of the Baq'a Quadrangle. Sheet 27F, Saudi Arabia, Ministry of Petroleum and Mineral Resources, Deputy Ministry for Mineral Resources, Jiddah.

55. Weibel R., Kristensen L., Olivarius M., Hjuler M., Mathiesen A. and Nielsen L. 2012, Investigating Deviations from Overall Porosity-Permeability Trends. Thirty-Sixth Workshops on Geothermal Reservoir Engineering, Stanford University, California.

56. Willis B. J. and C. D. White, 2000, Quantitative outcrop data for flow simulation: Journal of sedimentary Research, v. 70, p. 788-802.

57. Willis, B., and S. Gabel, 2001, Sharp-based, tide–dominated deltas of the Sego sandstone, Book Cliffs, Utah, U.S.A.: Sedimentology, v. 48, p. 479-406.

58. Young, G.M. 1981. Early Paleozoic Tillites of the Northern Arabian Peninsula. In Hambrey, M.J., and W.B. Harland, eds. Earth's pre-Pleistocene glacial record: Cambridge University Press, Paper C19, p. 338-340.

59. Zatz, L.M., 1981. Basic principles of computed tomography scanning. In: T.H. Newton, D.G. Potts, (Eds.), and Technical Aspects of Computed Tomography. Mosby, St. Louis, pp. 3853-3876.

60. Zhang S., Zhou J., Gas Reservoir of the Gulf, Workshop Abstract, 41-42

# Vitae

**Name**: Waseem Razzaq

**Nationality**: Pakistani

**Date of Birth**: 1st April 1988

**Email**: Wasim@geologist.com

**Academic Background:** Bachelor of Science in Applied Geology (Hons.), March 2010 from University of Azad Jammu and Kashmir, Muzaffarabad, Pakistan

Master of Science in Geology, Dec 2013 fromKing Fahd University of Petroleum & Minerals, KSA